ADSORPTION AND ACTIVATED CARBON

by

Richard L. Boor

A thesis submitted in partial fulfillment of

the requirements for the degree of

MASTER OF SCIENCE

(Mechanical Engineering)

at the

UNIVERSITY OF WISCONSIN-MADISON

1992

Abstract

Gas chromatography is used to investigate the adsorption of acetone, propane and toluene onto various types of activated carbon. The concentrations of the volatile organic compounds range between 1 and 55 parts per million. The activated carbon samples have surface areas ranging from 1000 - 1350 m^2/g and carbon tetrachloride test values ranging from 60 - 100%. Materials for the activated carbon included: coconut shell, coal and wood.

The equilibrium adsorption capacity for each type of carbon is found for all of the contaminants. The estimates of error in adsorption capacity, contaminant concentration and partial pressure are determined by considering the system, experimental procedure and data analysis techniques. Isotherms involving a single type of activated carbon are found using the propane and toluene contaminants. Four propane isotherms are found over a temperature range of 35 - 100°C. Three toluene isotherms are found over a temperature range of 100 - 140°C. The isotherm behavior is modeled using Henry, Langmuir, Freundlich and Dubinin-Astakhov equations. From the isotherm data, heats of adsorption are calculated.

Kinetic information is available for the propane and toluene tests in the form of frontal chromatograms. These chromatograms are modeled using a modified version of the homogeneous-solid diffusion model. The effect that the interstitial flow velocity and the contaminant concentration has on the diffusion coefficient is investigated

ii

ACKNOWLEDGMENTS

iii

TABLE OF CONTENTS

List of Figures

List of Tables

Nomenclature

Presented below is a partial listing of the nomenclature used. Variables which have not been listed are described in the text.

A   adsorption potential, [J/gmole]; area of frontal chromatogram used to calculate q, [volt s] or [ppm s]; cross sectional area of column, $[m^2]$

B   bias error

b   value used to adjust the quantity adsorbed q, to the desired units

C   concentration of contaminant, [ppm]

C_0 initial concentration of contaminant reaching the packed bed, [ppm]

D_L longitudinal diffusion coefficient, $[m^2/s]$

D_s intraparticle diffusion coefficient

E   characteristic energy of adsorption, [J/gmole]

F, F_1, F_2 gas flowrate, [ml/min]

G   Gibbs free energy

H   enthalpy

I   area under the frontal chromatogram (used in the uncertainty analysis, [volt s]

k   Henry constant

k_1 Langmuir constant

k_2	Freundlich constant
m	mass of adsorbent, [m]
n	Freundlich constant dependent on temperature, [unitless]; Dubinin-Astakhov constant signifying the number of degrees of freedom lost of an adsorbate molecule, [unitless]
n	number of moles adsorbed
q	quantity of contaminant adsorbed, [mg/g]
q_m	maximum quantity of contaminant adsorbed, [mg/g]
P, P_1, P_2	partial pressure, [Pa]; precision error
P_{sat}	saturation pressure of propane or toluene, [Pa] or [mmHg]
Q_{diff}	differential heat of adsorption
Q_{st}	isosteric heat of adsorption, [J/gmole]
R	gas constant, [J/gmole K]
S	entropy
T, T_1, T_2	temperature [°C] or [K]; transmission
t, t_b, t_r	time [seconds]
t_0	time at the start of an equilibrium test, [seconds]
t_p	propagation time [seconds]
t_{end}	length of time for frontal chromatogram to reach equilibrium, [seconds]
U	uncertainty
u	interstitial flow velocity, [m/s]

V, V_1, V_2	volume of gas removed by adsorption from the vapor phase, [m^3_solute/g_carbon]; volume of gas measured in soap film flowmeter, [ml]; voltage signal
V_{max}	maximum voltage signal obtained for a frontal chromatogram, [volts]
$\overline{V}_{max}$	mean voltage calculated that segment of voltage signals greater than $0.99V_{max}$, [volts]
W	volume of the adsorbent micropores which are filled with adsorbate
W_0	total volume of the adsorbent micropores

Greek letters

α	fraction of the surface covered by molecules
Δ	the amount of change in a value; dimensionless dispersion number
ε	void fraction
μ	total number of molecules striking a surface per unit time
ν	rate of desorbing when a monomolecular layer of molecules completely covers the surface in question
ρ_{N_2}	density of nitrogen
σ	number of molecules on a surface at a given time
θ	fraction of the surface covered by adsorbed molecules; fraction of adsorbent pore volume filled with adsorbent

Chapter 1

INTRODUCTION

1.1   MOTIVATION

Ever since the energy crisis of the 1970's, buildings have been fabricated with energy conserving ideas in mind. Two of the most widely used practices were to construct a tighter building envelope and decrease the building ventilation rates. Although these practices reduced the amount of energy required for building operation, unexpected side effects began to appear. Some of the occupants in many of these buildings reported minor ailments ranging from eye irritation to nausea. Because complaints of this type were literally occurring worldwide, the World Health Organization (WHO) took notice and defined what is known as the Sick Building Syndrome (SBS). The ailments resulting from this syndrome are listed in Table 1.1.

Causes of SBS

The causes of SBS are threefold. The first two reasons have already been stated - heavily insulated buildings and lower ventilation rates result in a reduced means for contaminants present in the indoor air to leave the premises. The third cause of SBS is that many new building materials were developed and used during this time which emit contaminants in the form of gases and vapors. The most prominent class of contaminant is the volatile organic compounds (VOC's) and it is the VOC's which are

thought to be the leading cause of Sick Building Syndrome. Indeed, the number of organic compounds present indoors may be as high as 250 but usually ranges between 20 and 150 [Molhave (1986)]. The report by Molhave also lists which organic contaminants are most common indoors. The aliphatic hydrocarbons rank first (those molecules having 6 to 17 carbon atoms) with toluene and three xylenes occurring most frequently in this group. Next are monterpenes ($C_{10}H_{16}$) and halogenated alkanes. Other compounds are said to be only found occasionally. The concentrations of these

Table 1.1 Symptoms of Sick Building Syndrome. From WHO (1983).

- eye, nose and throat irritation
- sensation of dry mucous membrane and skin
- Erytheme (redness of the skin)
- mental fatigue
- headaches, high frequency of airway infections and cough
- hoarseness, wheezing, itching, and unspecific hypersensitivity
- nausea, dizziness

contaminants in many cases exceeds that of the outdoors [Berglund, et al. (1982), Johansson (1978)]. However, even though this may be the case, the concentrations of the VOC's are usually in the low parts per billion range [Johansson (1978)]. At these low levels of pollutants, individual species are thought not to cause the symptoms of SBS, rather it is believed that the combined effect of the large number of VOC's present in the indoor air is the basis of SBS [Molhave (1986)].

Prevention of SBS

The large number of VOC's present in the indoor air needs to be kept at acceptable levels (although these levels are still unknown [Knight (1992)]) if the "sick" buildings are to be "cured". There are several ways in which this can be accomplished. Eliminating the sources of the contaminants would definitely help cure the problem of SBS but it is improbable that this will happen in the near future because of the large costs involved in changing the types of material which currently emit irritating compounds. Other options to obtain acceptable indoor air quality include ventilation and filtering practices. A guideline for ventilation of buildings is given by the American Society of Heating, Refrigerating and Air-Conditioning Engineers, Inc. (ASHRAE) Standard 62-1989, *Ventilation for Acceptable Indoor Air Quality*. In this standard, two options for providing satisfactory indoor air quality are listed. The first method is the *Ventilation Rate Procedure*. This procedure utilizes outdoor air to maintain acceptable indoor air quality. If the outdoor air is unacceptable for indoor use, it must be filtered before entry. Complete details of this procedure are described in Section 6.1 of Standard 62-1989. The alternative to the *Ventilation Rate Procedure* is the *Indoor Air Quality Procedure*. This method of obtaining acceptable indoor air quality "provides a direct solution by restricting the concentration of all known contaminants of concern to some specified levels." The means to accomplish this is left to the person(s) working on a specific project, but it does give the designer alternatives to achieve quality indoor air, one of which is the filtering of air already present in the building. Using air that has already been conditioned will reduce energy costs associated with maintaining the building at acceptable climate levels.

Filter Types

Filters used for particulate entrapment are quite common and will not be discussed here but it is noted that these types of filters have minimal capacity for VOC's. The types of filters generally used to reduce the amount of VOC's present are called adsorbents (Chapter Two). A wide variety of adsorbents exist including activated alumina, activated carbon, carbon molecular sieves and zeolites. Of all of these, none adsorbs a wider range of molecule sizes than activated carbon (Chapter 2) and this feature makes it ideal for use in air filtration applications.

1.2 RESEARCH OBJECTIVE

When designing activated carbon filters for an air filtration system, the performance of the activated carbon needs to be characterized. Two specific pieces of information need to be known.

1. The amount of contaminant that a certain carbon can hold.

2. The time when the carbon is to be replaced.

These parameters will vary depending on the amount and types of pollutants present, but if this information is known (or predicted depending on the building materials, equipment, etc.) proper sizing of the filters and replacement times can be determined using modeling techniques.

It is unfortunate that, at this time, the above process can not be enacted to correctly size a carbon filter and determine when it needs to be replaced because the behavior of activated carbons with low level contaminants (such as those found in "sick" buildings) is not known. Little research has been done with activated carbon at low levels of contaminants (Section 1.3). For these reasons, the focus of this research is on activated carbon and its equilibrium and kinetic behavior with various low level contaminants.

1.3   LITERATURE SEARCH

A search by Knight (1992) yielded only six sources that had tested various contaminants at the low parts per million level. Data from these sources is shown in Figures 1.1 - 1.6. Other searches yielded no further information that applies to the investigation of activated carbons and their behavior with low concentration contaminants in the parts per billion range. The limited amount of information that is available has many shortcomings.

1. Much of the data in Figures 1.1 -1.6 are well into the part per million range - significantly higher than the contaminants found in indoor air. Models from the data then will need to be extrapolated to the low concentrations, thus introducing the potential for large errors.

2. The isotherms from Ramanathan, et al. (1988) consist of two to three data points. This low number is not sufficient to show the profile of the isotherm and any isotherm modeling which would be done using this information could posess large errors. Similarly, Clapman, et al. (1970) has four isotherms constructed of three

data and two contaminants, butyraldehyde and butylamine, with only one piece of data.

3. Some of the low concentration data is also in disagreement. Comparisons of the amounts of benzene adsorbed onto different carbons as reported by Clapman (1970) and Ramanathan (1988) differ by three orders of magnitude. The carbons used in these tests had similar surface areas and CCl_4 values and although the base carbon materials were different, it is not likely that the amount adsorbed would vary by such a large amount.

4. Four of the sources listed, Clapman, et al. (1970), Ramanathan, et al. (1988), Kyle and Eckoff (1974), and Forsythe (1988) have done their testing at temperatures ranging from ambient to 30°C. Models obtained could be used to extrapolate to higher temperatures if necessary but significant deviations from the actual capacity of the activated carbon would probably result.

5. All of the sources except Schaefer (1991) did analysis involving the kinetics of adsorption but again, the deficiencies listed above limit the amount and accuracy of modeling which can be done.

It is clear from these points and the requirements of ASHRAE Standard 62-1989, *Indoor Air Quality Procedure*, that further research is needed to obtain accurate isotherms and kinetic information involving activated carbon adsorbing low concentration contaminants. An adequate base of data will permit the development of both equilibrium and kinetic models.
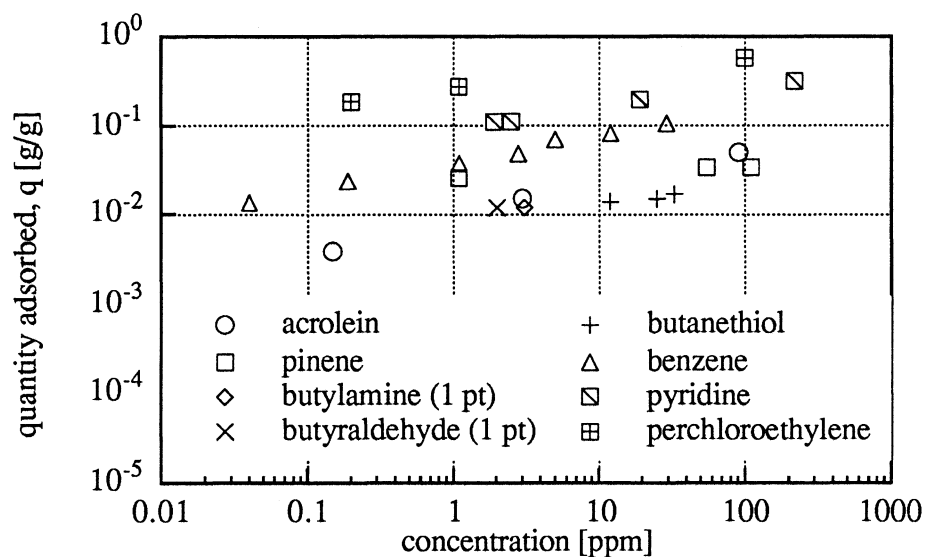
Figure 1.1   Isotherm data replotted from Clapman, et al. (1970). Temperature: 70-75°F; pressure: 1 atm; carbon: Pittsburgh PBL
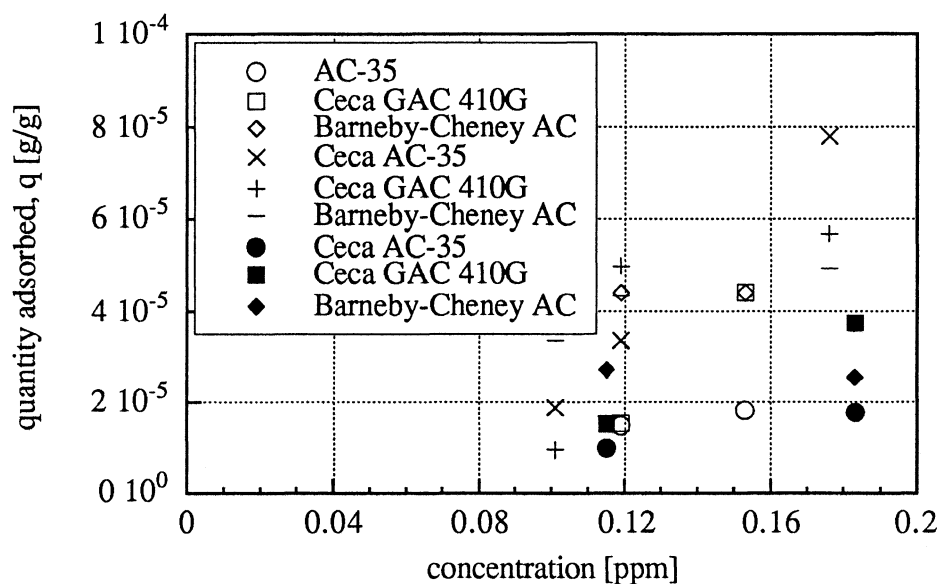
Figure 1.2   Isotherm data replotted from Ramanathan, et al. (1988). Temperature: 30°C; pressure: 1 atm; hollow symbols: acetaldehyde; open symbols: benzene; solid symbols: 1,1,1-trichloroethane.
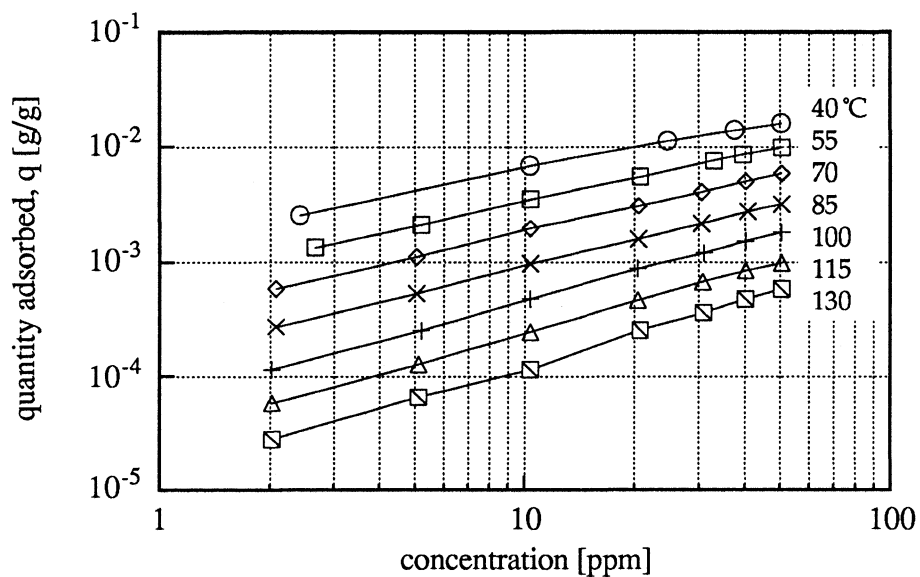
Figure 1.3   Isotherm data replotted from Schaefer (1991). Pressure: 1 atm; contaminant: acetone; carbon: Calgon OL 20x50.
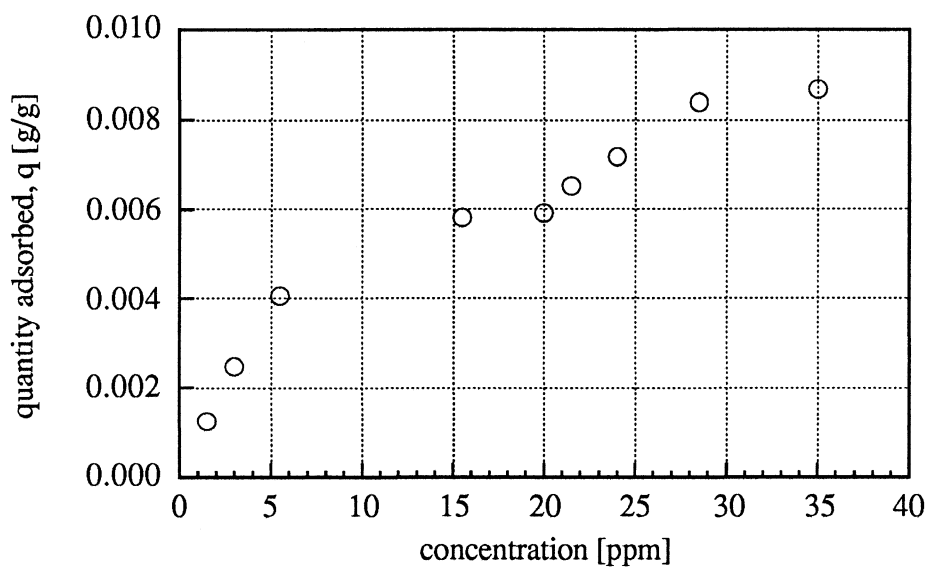
Figure 1.4   Isotherm data replotted from Kyle and Eckhoff (1974). Temperature: 30°C; pressure: 1 atm; contaminant: acetaldehyde; carbon: Pittsburgh PCB.
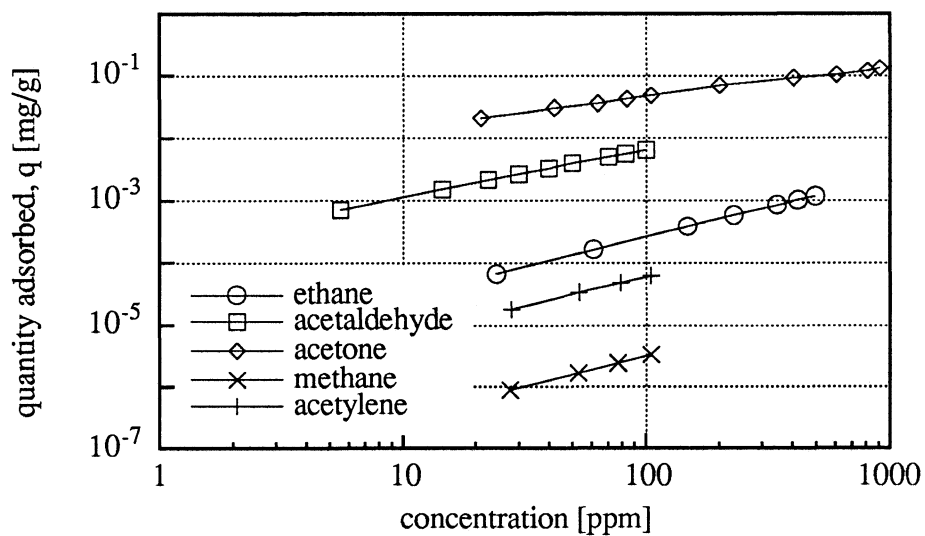
Figure 1.5   Isotherm data replotted from Forsythe (1988). Temperature: 25°C; pressure: 1 atm; carbon: Columbia 4LXC 12/28.
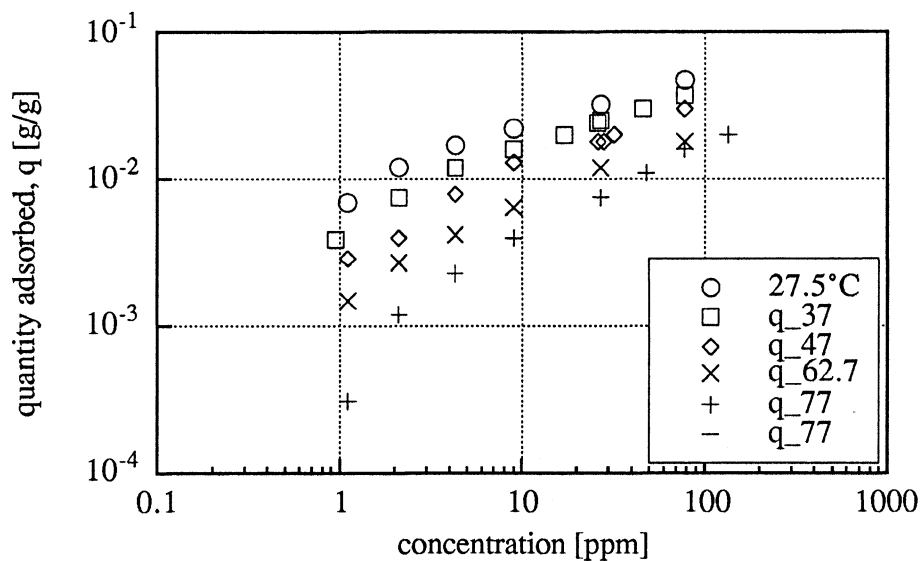
Figure 1.6   Isotherm data replotted from Robell,* et al. (1970). Pressure: 1 atm; contaminant: n-butane; carbon: Barneby-Cheney BD 30x40.

*Note: Not all data from Robell, et al. (1970) was plotted due to transfer difficulties.

REFERENCES

ASHRAE. 1989. ASHRAE Standard 62-1989, *Ventilation for Acceptable Indoor Air Quality*, Atlanta: American Society of Heating, Refrigerating, and Air-Conditioning Engineers, Inc.

Berglund, B., Berglund, U., Lindvall, T., Nicander-Bredberg, H., *Olfactory and Chemical Characterization of Indoor Air.* Towards a Psychophysical Model for Air Quality, Environmental International, **8**, 327-332, 1982.

Clapham, T. M., Junker, T. J., and Tobias, G. S., *Activated Carbon-Odorant Removal from Air Quantified,* ASHRAE Transactions, No. 2145, 75-86, 1970.

Forsythe, R. K., Jr., *Adsorption and Dispersion of Selected Organic Gases Flowing Through Activated Carbon Adsorbent Beds,* Ph.D. Thesis in Physics, Kent State University, 1988.

Johansson, I., *Determination of Organic Compounds in Indoor Air with Potential Reference to Air Quality,* Atmospheric Environment, **12**, 1371-1377, 1978

Knight, K., *Analysis and Design of Adsorptive Processes for Air Quality Control,* Ph.D. Thesis in Mechanical Engineering. University of Wisconsin-Madison, 1992.

Kyle, B. G., and Eckhoff, N. D., *Odor Removal from Air by Adsorption on Charcoal,* EPA-650/2-74-084, PB-236-928, Kansas State University, 1974.

Molhave, L., *Indoor Air Quality in Relation to Sensory Irritation Due to Volatile Organic Compounds,* ASHRAE Transactions, No. 2954, 306-316, 1986.

Ramanathan, K., Debler, V. L., Kosusko, M., and Sparks, L. E., *Evaluation of Control Strategies for Volatile Organic Compounds in Indoor Air,* Environmental Progress, **7**(4), 230-235, 1988.

Robell, A. J., Arnold, C. R., Wheeler, A., Kersels, G. J., and Merrill, R. P., *Trace Contaminant Adsorption and Sorbent Regeneration,* NASA CR-1582, N70-38501, Lockheed Missiles and Space Company, Palo Alto, CA, September, 1970.

Schaefer, M. *Measurements of Adsorption Isotherms by Means of Gas Chromatography,* M.S. Thesis in Chemical Engineering, University of Wisconsin-Madison, 1991.

World Health Organization (WHO). 1983. *Indoor Air Pollutants; Exposure and Health Effects Assessment* (Working Group Report, Nordlingen, Euro reports and studies no. 78, WHO, Copenhagen, Denmark).

Chapter 2

BACKGROUND INFORMATION

In this chapter, background information is presented concerning adsorption, activated carbon and gas chromatography. By covering these topics, the reader will be prepared for the following chapters.

2.1 ADSORPTION

Adsorption is a process in which either atoms or molecules are concentrated at the surface of a solid. This phenomenon differs from absorption, where the substances absorbed actually enter into the crystal lattice of the absorbing material. Figure 2.1 displays adsorption involving various molecules and a typical solid surface. The atoms or molecules being adsorbed are termed adsorbate and the solid on whose surface the adsorbate is condensing is called the adsorbent.

Two types of adsorption exist with various degrees of both occurring in different systems. They are classified as physical adsorption and chemical adsorption (chemisorption). In physical adsorption, the condensating of atoms or molecules on the surface is caused by weak intermolecular (van der Waals) forces. If the adsorbate and adsorbent are nonpolar, bonding between the adsorbate and adsorbent will be caused by dispersion forces. These forces are a result of the temporary dipoles formed in the electron clouds of the molecules. Larger molecules almost always have the outer

electrons located further from the nucleus than small molecules and this results in large molecules having a higher affinity for and stronger bond formation to the adsorbent. If either or both the adsorbate and adsorbent are polar, an additional bonding force is present because of the dipole forces. When chemisorption occurs, the adsorbate and adsorbent share electrons with one another, thus forming a very strong chemical bond at the surface.
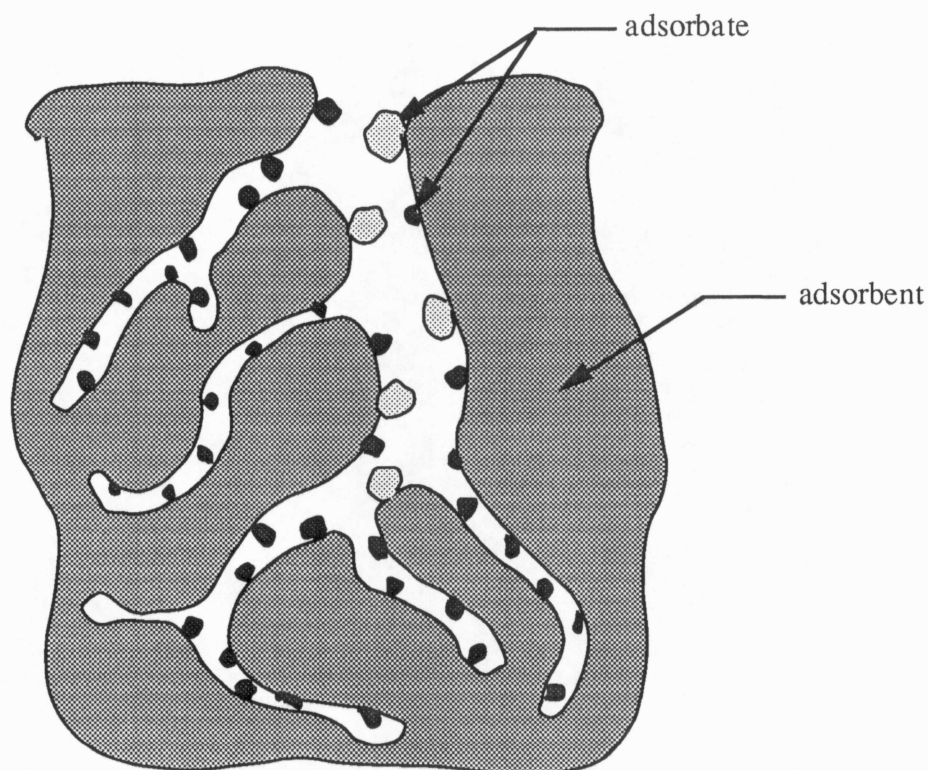
Figure 2.1   Adsorption of particles on a typical adsorbent surface. Adapted from Cheremisinoff and Ellerbusch (1978).

The heat of adsorption is the amount of energy given off when adsorption occurs and indicates the strength of bonding between the adsorbate and adsorbent. It is typical for physical adsorption to have low heats of adsorption because of the weak bonding forces and chemical adsorption to have a high heat of adsorption due the chemical bonding which takes place between the adsorbate and the adsorbent surface.

Physical adsorption is a very common occurrence because no special circumstances need to take place for various species of adsorbate to be bonded to a surface. However, chemisorption does require that the adsorbate and adsorbent be able to form a chemical bond and therefore is not as common. Because the driving force of physical adsorption is van der Waals forces, multiple layers can be formed at the adsorbent surface. Since a chemical bond is formed between the adsorbate and adsorbent, only one layer of molecules can be adsorbed. The speed for physical adsorption is very rapid and is usually limited by the nonuniformity (diffusion controlled) of the adsorbent surface. Chemical adsorption can be slow depending upon the type of reaction taking place. The bonding that occurs with van der Waals forces is relatively weak compared to the bonds formed in chemisorption and for this reason, physical adsorption is generally a reversible process. Chemical adsorption is usually not reversible. When physical adsorption from the gas phase takes place, the adsorbate experiences a reduction in its number of degrees of freedom. When this occurs, the adsorbate undergoes a decrease in entropy. The Gibbs free energy goes down as well. With this information, and knowing that $\Delta G = \Delta H - T\Delta S$, physical adsorption can be shown to be exothermic [Ruthven (1984)]. In contrast to physical adsorption, chemical adsorption is sometimes an endothermic process (even though the number of degrees freedom are reduced), depending upon the type of chemical reaction occurring between the adsorbate and adsorbent. Table 2.1 summarizes the main differences between physical and chemical adsorption.

Table 2.1 Comparison of physical and chemical adsorption. From Ruthven (1984)

	Physical Adsorption	Chemical Adsorption
heat of adsorption	< 2 or 3 times latent heat of evaporation	> 2 or 3 times latent heat of evaporation
frequency of occurrence	readily occurs between various adsorbate and adsorbent	only occurs between select adsorbate and adsorbent
adsorbate thickness	monolayer or multilayer	monolayer only.
speed of adsorption	rapid	may be slow
bond strength	weak	strong
reversibility	generally reversible	generally not reversible
bonding process	exothermic from gas phase	may be endothermic

2.2   ACTIVATED CARBON

History

The use of activated carbon as a filtering agent dates back to centuries B.C. where the Hindus used it to cleanse their water. During the thirteenth century, it was discovered that sugar solutions could be purified using carbon. It was not until the eighteenth century that the applications for activated carbon began to expand rapidly. During this time, Scheel discovered its gas adsorptive properties and Lowitz found it had the capability to eliminate colors from liquid solutions [Cheremisinoff and Ellerbusch (1978)]. Today activated carbon is used extensively in both gas and liquid phase applications. Some examples are gas adsorption, dry cleaning, sugar purification,

organic solvent recovery, purification of water both in residential and industrial applications and air filtration.

Activated Carbon in Air Filtration Applications

Activated carbon is used in air filtration applications because it has several desirable characteristics.

1. High Surface Area. Because adsorption is a surface phenomena, quality adsorbents need to possess a large surface area. The larger the surface area, the more adsorbate that is able to be collected. Activated carbons fulfill this requirement with typical areas ranging from 500 - 1500 m^2/g [Wycherly and Bayati (1991)].

2. Large Pore Diameter Distribution. Activated carbons have pore diameters that range from less than 20 to greater than 5000 angstroms. This wide range of diameters is necessary because there are potentially more than one-hundred contaminants in indoor air where people are located [Knight (1992)]. Each different contaminant varies in size and an adsorbent with a wide diameter range is better able to adsorb a larger number of contaminants than one with a narrow range of pore diameters.

3. Nonpolar Substance. Activated carbon is a nonpolar material. The reason this is desirable is quite simple; nonpolar adsorbents are not as responsive to adsorbate polarity as polar adsorbents are. This property of activated carbon allows it to adsorb a wider variety of contaminants than a polar adsorbent.

Structure

The large surface areas of activated carbon are a result of a very extensive pore structure (shown schematically in Figure 2.2). The pore diameters of activated carbon vary considerably. Because of this, they are usually divided into three groups; macropores, transitional pores and micropores. Figure 2.2 shows the location on the carbon particle where these classifications apply and Table 2.2 gives three author's versions of the diameters of these pores. There are different diameter classes for each pore type, depending on the author. At this time there is no universally accepted pore size classification [Knight (1992)].
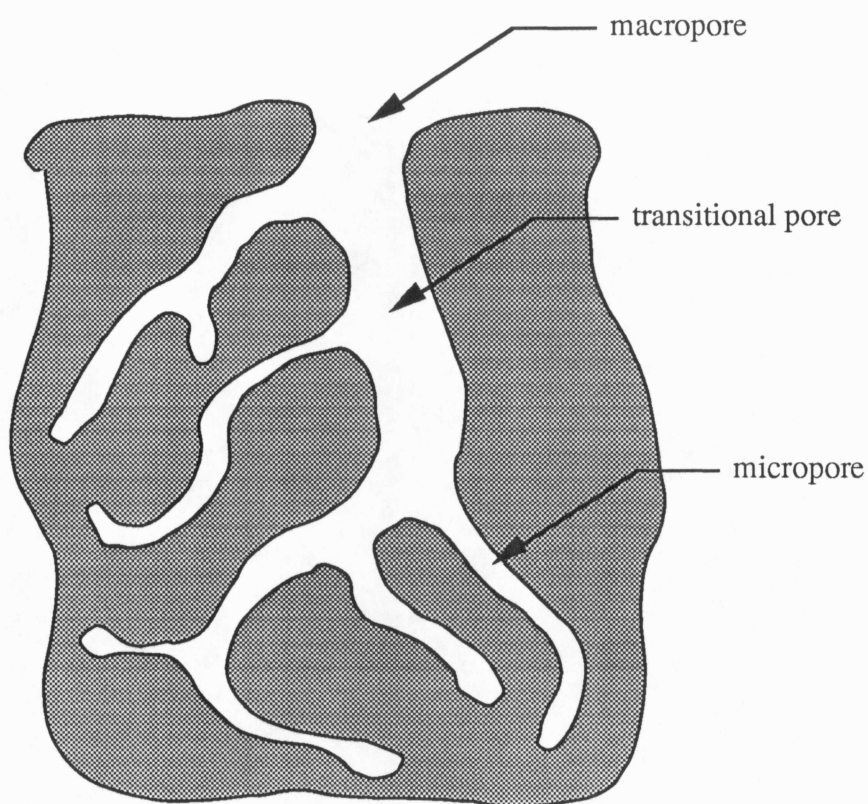
Figure 2.2 Pore structure of activated carbon. Adapted from Cheremisinoff and Ellerbusch (1978).

Table 2.2 Classification of pore diameters.

	Wycherley andBayati (1991)	Ruthven (1984)	Dubinin (1955)
Macropore	> 5000	> 500	>2000
Transitional pore	40 - 5000	20 - 500	40 - 2000
Micropore	< 40	< 20	< 40
pore diameters expressed in Angstroms.			

The pore structure of activated carbon aids in its filtering capacity. An analogous view of this structure is a funnel. Particles to be filtered from solution (liquid or gaseous) enter the large macropores present on the surface of the carbon and pass through the transitional pores to the micropores. Some contaminant also covers the transitional and macropores, but the majority is captured in the micropores because of the large percentage of area (at least 95% of the total surface area per gram of carbon [Dubinin (1955)]). Also, particles and molecules of substantial size that cannot fit into the micropores are then captured by the macro and transitional pores.

Materials

A list of materials used to manufacture activated carbon is given in Table 2.3. Wycherley and Bayati (1991) point out that carbons manufactured from nutshells yield a structure that is highly microporous, whereas carbons from coal have more of a transitional pore structure. Wood or peat base carbons have a large macropore framework.

Table 2.3 Materials used to manufacture activated carbon. From Cheremisinoff and Ellerbusch (1978).

bones	wood
coconut shells	bituminous coal
pecan shells	peat
sugar	fruit stones
pulp mill black ash	wastewater treatment sludges
petroleum-based residues	nutshells

Manufacture

Although material type has a significant effect on the characteristics of the final product, another major factor in determining the qualities of activated carbon is the manufacturing process. Several different methods are used to bring the carbon to its activated state. Smisek and Cerny (1978) list and describe many of these processes. All of the carbon samples used in this study were manufactured using the steam activation process. Because of this, the discussion that follows is limited to this process.

Steam Activation

Depending on whether the final form of the activated carbon is pressed or powder/granular determines the initial preparation of the charcoal (manufactured from any of the raw materials listed in Table 2.3). The charcoal is crushed and ground to a fine

powder if pressed activated carbon is to be the final product but grinding is excluded otherwise.

The first step in the activation process is carbonization of the charcoal. Carbonization is a process in which volatile materials present in the charcoal are driven off and is generally done below 600°C in an oxygen free environment [Cheremisinoff and Ellerbusch (1978)]. The material remaining after carbonization is called char. According to Smisek and Cerny (1970), the char contains about 15% volatile material. At this point in the activation process, the char (although now 85% pure carbon) still has a relatively small surface area due to the lack of a developed pore structure. Activation of the char is achieved using steam as an oxidizing agent. Temperatures for this segment of the process range from 800 - 1000°C [Kovach (1973)]. Smith (1959) states that the mechanism of the reaction for the steam activation process is not completely known but it seems that two intermediate carbon-oxygen surface complexes exist (reactions of the "complex" type are said to occur indirectly and almost always take longer than 5×10^{-12} seconds [Laidler (1987)]). They are designated as the "CO-complex" (CO) and the "CO2-complex" (CO2), respectively. The reactions for the activation process are

$$H_2O + C \rightarrow H_2 + (CO) \qquad (2.1)$$

$$(CO) \rightarrow CO \qquad (2.2)$$

$$H_2O + (CO) \rightarrow H_2 + (CO_2) \qquad (2.3)$$

$$(CO_2) \rightarrow CO_2 \qquad (2.4)$$

$$H_2 + (CO) \rightarrow H_2O \qquad (2.5)$$

The steam not only removes the volatile materials present, but also enlarges the pores, resulting in a developed pore structure. Pore size can be varied by adjusting the time of the reaction.

Carbon Sizing

Carbon to be sold in powder or granular form is run through a final step of grinding and sizing. Sizing is accomplished by passing the carbon through various sizes of mesh. Appendix A gives the classifications of standard mesh sizes along with their corresponding openings in SI and English units.

Regeneration

Many applications require the carbon to be used several times before it is discarded. Reuse of the carbon requires the adsorbate to be removed from the carbon surface. This phenomena is called desorption and upon completion the carbon is said to be regenerated because it possesses nearly the same qualities as virgin carbon. If physical adsorption is the main mechanism in an adsorption process, desorption is relatively easy due to the weak van der Waals forces attaching the particles to the pore walls of the carbon. The bonds between the adsorbate and adsorbent resulting from chemisorption are much more difficult to break. Although many methods of regenerating activated carbon exist, Ruthven (1984) states that only four types are widely used.

1. Thermal Swing. The thermal swing process involves heating the filtering bed using a hot gas stream. The high temperature decreases the amount of contaminant that can be adsorbed, thus driving off most of the impurity.

2. Pressure Swing. Reducing the pressure in a packed bed has the same result as raising the temperature. Less contaminant can be contained in the carbon bed and the excess is driven off. This method is valid only for gases.

3. Purge Gas Stripping. At constant temperature and pressure, regeneration of the bed is accomplished by passing an inert gas stream through the packed bed. Because no contaminant is present in this gas, what is adsorbed on the carbon is removed. This method works well only with pollutants that are weakly bonded to the carbon.

4. Displacement Desorption. Regeneration of the packed bed is obtained by passing a stream (gas or liquid) that adsorbs preferentially to the adsorbate currently on the carbon, thus driving the contaminant from the packed bed.

These methods can be combined in various ways to provide a greater purge in a shorter period of time. Results of regeneration involving activated carbon and ether are given by Kovach (1965) in Table 2.4. Table 2.4 shows that regeneration using steam at high temperatures is the most effective method. Kovach (1973) states, "the only satisfactory means of reactivation is a treatment similar to the activation conditions in a furnace but for a shorter time." About 10% of the carbon is lost during this process due to attrition and burning of the carbon. It is also apparent from Table 2.4 that not all of the adsorbate has been removed and this remainder is typically called the "heel". Kovach (1973) recommends replacing what is lost with virgin carbon to prevent degeneration of the packed bed.

Table 2.4 Comparison of regeneration methods. From Kovach (1965).

method of regeneration	percentage of charge expelled
Heating at 100°C for 20 minutes	15
Vacuum 50 mm Hg at 20°C for 20 minutes	25
Gas circulation at 130°C for 20 minutes	45
Direct steam at 100°C for 20 minutes	98

2.3 GAS CHROMATOGRAPHY AND THE FRONTAL ANALYSIS TECHNIQUE

Chromatography was initially developed by Ramsey (1905). It is a separation process in which mixtures of gases and vapors are passed through a column containing an adsorbent (solid or liquid). The types of gases in the solution have different affinities for the adsorbent and therefore are separated from one another as they proceed through the column. Gases having a stronger attraction towards the adsorbent remain in the column for a longer period of time than gases with lower attraction. A detector at the column exit obtains a signal from the departing gases. The resulting signal generated is called a chromatogram and is used to evaluate the gas mixture which entered the column.

Gluekauf (1947) was the first to indicate that adsorption isotherms could be found using gas chromatography. Chromatograms obtained for this purpose have various profiles, depending upon the method of analysis. The method of analysis used in this

study is called the frontal analysis technique and was introduced by James and Phillips (1954) and Schay and Szekely (1954). The procedure involves a system (Figure 2.3) in which a carrier gas is initially passed through the column. At time t, the carrier gas is replaced with a solute gas mixture of concentration C_o (shown mathematically by Equation 2.6). This step input of contaminant progresses through the column until it reaches the adsorbent at time t_b. It is here the solute is adsorbed until the adsorbent is

$$t \leq 0; \quad C = 0$$

$$t > 0; \quad C = C_o \tag{2.6}$$

saturated. Upon saturation, the adsorbate "breaks through" the adsorbent column and passes to the detector. Ideally, the shape of the contaminant wave exiting the adsorbent
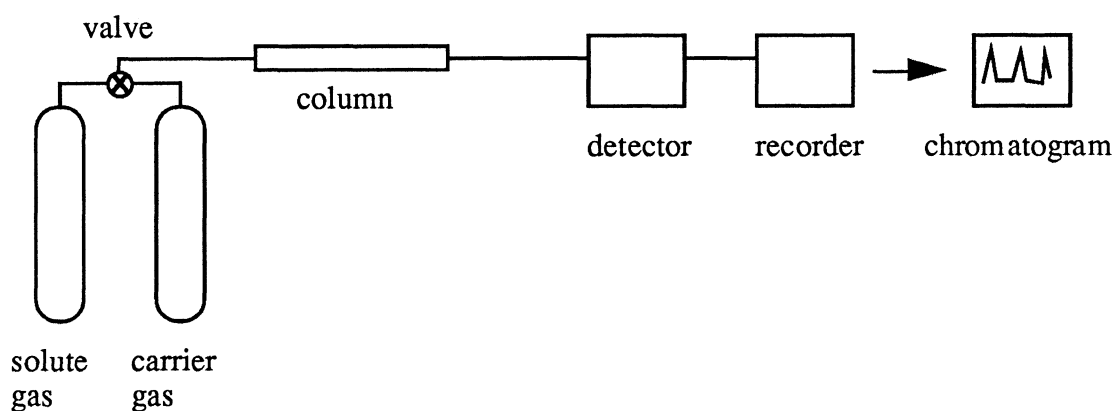
Figure 2.3   Schematic of gas chromatograph system.

bed should be the same as the step function that initially entered the bed (Figure 2.4). However, because of resistance caused by the adsorbent particles, the wave becomes dispersed as it progresses through the bed and typically takes a form similar to Figure 2.5.
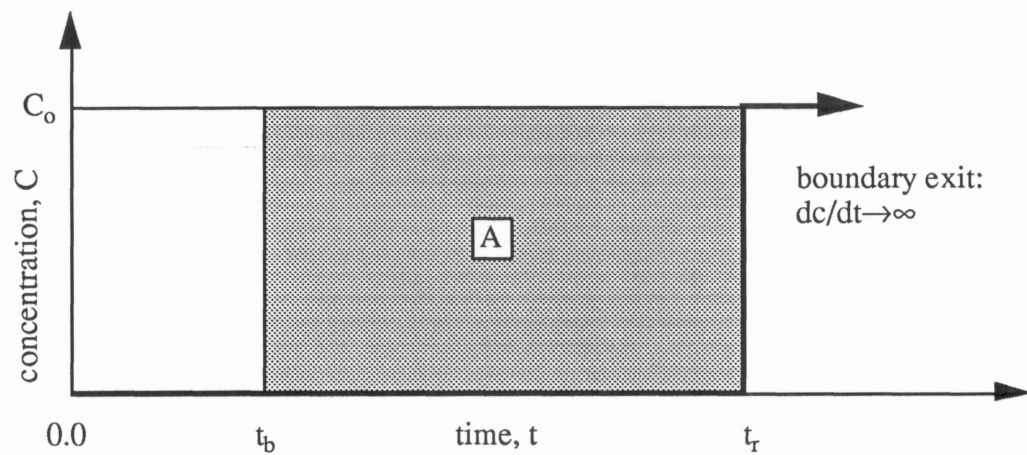
Figure 2.4   Ideal frontal boundary profile.
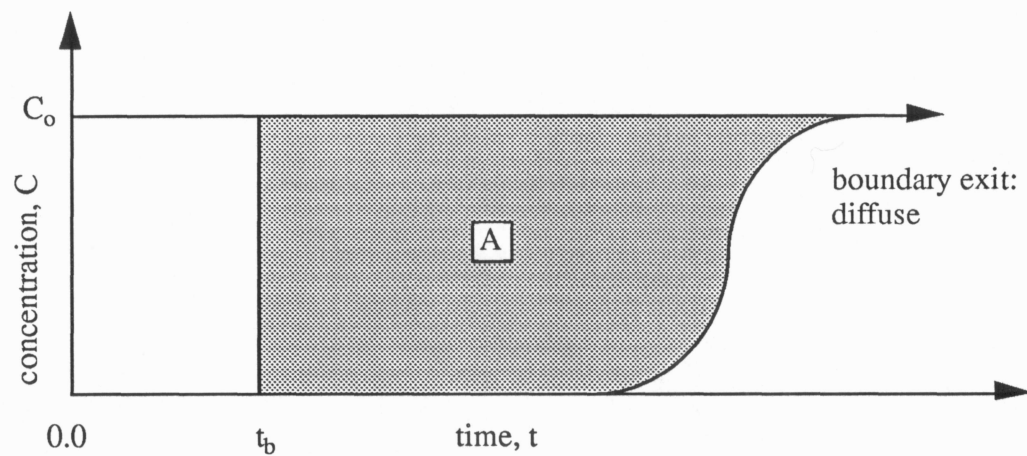
Figure 2.5   Diffuse frontal boundary.

By looking at Figure 2.4 and knowing the solute gas flowrate F, is directly proportional to the quantity adsorbed n (in moles), the equation for n can be determined

$$n = C_o(t_r - t_b)F \tag{2.7}$$

Equation 2.7 can be manipulated by replacing $C_o(t_r - t_b)$ with A, the shaded area in Figure 2.4 and then dividing the amount adsorbed by the adsorbent to obtain a nondimensionalized value of the amount adsorbed q.

$$q = \frac{FA}{m}$$ (2.8)

The value of q can be either determined on a molar or mass basis, depending on the desired units. Although James and Phillips (1954) and Schay and Szekely (1954) developed the frontal analysis method using chromatograms that had approximately the profile as Figure 2.4 (called a self-sharpening boundary) the method also applies to diffuse boundaries like that shown in Figure 2.5. The only thing that has changed here is area determination. Area can be no longer stated as $C_o(t_r - t_b)$ and give an accurate result. Instead, the shaded area A of a diffuse chromatogram is generally determined using integration methods.

2.4 SUMMARY

Both types of adsorption (physical and chemical) were addressed in this chapter, with a summary of their characteristics given in Table 2.1. The next topic was activated carbon. The history was presented, followed by the reasons activated carbon is highly desirable for air filtration purposes. The last portions of this section dealt with the structure, materials used, manufacture, sizing and regeneration of activated carbon. The final section discussed gas chromatography and, more specifically, the frontal analysis technique. This technique is used to calculate the quantity of adsorbate which gathers on the adsorbent surface. Both the ideal (self sharpening) and non-ideal (diffuse) boundaries were covered.

REFERENCES

Cheremininoff, P. N. and Ellerbusch *Carbon Adsorption Handbook*, Ann Arbor Science Publishers, Inc.,1978.

Dubinin, M. M., *Uspekji khim.*, **24** (1955) 3.

Gluekauf, E., J. Chem. Soc. 1302, 1947.

James, D. H. and Phillips, C. S. G., *The Chromatography of Gases and Vapors. Part III. The Determination of Adsorption Isotherms*, J. Chem. Soc., 1066-1070, 1954.

Knight, K., *Analysis and Design of Adsorptive Processes for Air Quality Control*, Ph.D. Thesis in Mechanical Engineering. University of Wisconsin-Madison, 1992.

Kovach, J. L. *Principles of Adsorption,* Director of Research, Barneby-Cheney Company, Columbus, Ohio, 1965.

Kovach, J. L., *Activated Carbon in Air Purification, Part I*, Nuclear Consulting Service Inc., P.O. Box 29151, Columbus, OH 43229, 1973.

Laidler, K.J., *Chemical Kinetics*, Third Edition, Harper Collins Publishers, Inc., 1987

Ramsay, W., Proc. Roy. Soc. **A76** 111 (1905)

Ruthven, D. M., *Principles of Adsorption & Adsorption Processes*, John Wiley and Sons, Inc., New York, NY., 1984.

Schay, G. and Szekely, G., Acta Chim. Hung. **5**, 167, 1954.

Smisek, M. and Cerny, S., *Active Carbon: Manufacture, Properties and Applications,* American Elsevier Publishing Company, Inc., Amsterdam, 1970.

Smith, R.N., *The Chemistry of Carbon-Oxygen Surface Compounds*, Quarterly Reviews (London)., (1959)

Wycherly, D. E. and Bayati, M. A., Information obtained from Barneby and Sutcliffe Corporation, P.O. Box 2526, Columbus, Ohio 43216, 1991.

Chapter 3

EXPERIMENTAL SYSTEM, PROCEDURE AND UNCERTAINTY

In this chapter, the experimental system used to determine the quantity of solute adsorbed q, is shown, with description of the components given in Appendix B. Following this is a description of the experimental procedure. The chapter will close by discussing the results of the uncertainty analysis for the system.

The section containing the experimental procedure discusses the method used to obtain q (shown in Equation 3.1 and previously presented in Chapter 2). A summary at the end of this section gives step by step instructions for the procedure from the beginning of a test to the end.

$$q = \frac{bFA}{m} \tag{3.1}$$

Determining the system uncertainty is an integral part of the experimental process. From an uncertainty analysis, one can learn where the major sources of error are located. This is very important because it may be necessary to either decrease this error through more careful experimental procedure and/or more accurate equipment or (if this is impossible) find the desired result using a completely different system. Section 3.3 contains the uncertainty analysis for the present experimental configuration. The first portion of this section provides definitions of bias and precision errors and general

information concerning the equations involving uncertainty. After this, a complete analysis of the errors in the system is stated. A summary of the errors is presented at the end of the chapter.

3.1 SYSTEM COMPONENTS

The main components of the experimental system are shown in Figure 3.1. A complete description of these components is given in Appendix B.

Figure 3.1   Experimental System. Adapted from Schaefer (1991).

1. compressed air
2. carrier gas
3. nitrogen diluent
4. contaminant-N_2 mix
5. compressed air
6. hydrogen
7. pressure regulator
8. hydrocarbon trap

9. moisture trap
10. chemical trap
11. pressure gauge
12. flow controller
13. on/off valves
14. two-stream selection valve
15. vent to atmosphere

16. glass column and filter
17. flame ionization detector
18. detector exhaust
19. gas chromatograph
20. junction box
21. personal computer
22. electronic integrator

3.2   EXPERIMENTAL DETERMINATION OF THE AMOUNT ADSORBED

When calculating the quantity adsorbed, q, three terms need to be determined.

1.   mass of activated carbon, m

2.   flowrate of solute-nitrogen and diluent nitrogen gas (if necessary), F_1 and F_2

3.   desired area from the frontal chromatogram, A

Each of these components is found by using an experimental procedure. Once known, they are inserted into Equation 3.1 and the quantity of solute adsorbed, q, is calculated.

3.2.1   Mass Measurement

The mass, m, of activated carbon used in each filter is measured using a mass balance. The least significant digit of this balance is 0.0001 gram. Masses of activated carbon used in test filters range from 0.05 - 3.0 grams, depending on the contaminant(s) being run through the system.

The procedure for determining carbon mass is as follows. Powder (weighing) paper is first weighed on the mass balance. An amount of activated carbon is next placed on this paper. The total mass of weighing paper and carbon is then determined. The mass of carbon is found by subtracting the paper mass from the combined mass.

3.2.2 Volumetric Gas Flowrate Measurements

With a new activated carbon filter installed in the HP 5890, the first task before beginning an experiment is to measure the solute-nitrogen flowrate F_1 and if necessary, the diluent flowrate F_2. Diluent is used only when the desired contaminant concentration is less than what is available from the solute-nitrogen source. Flowrates are determined using a soap film flowmeter (shown in Figure 3.2) and a timing device built into the HP 5890.

Setup

All gas flows other than the solute-nitrogen and nitrogen diluent must be turned off using either the valves present on the pressure regulators (7) or the on/off valves (13) to avoid mixing extraneous gases with those that are to be measured. The flexible hose attached to the flowmeter is next inserted into the flame ionization detector [FID (17)] exit. Upon insertion, a seal is formed between the inside diameter of the FID exit and an o-ring located on the adapter, thus preventing any gas from escaping to the atmosphere unmeasured. Before determining the gas flowrates, the inside surface of the soap film flowmeter must be wet. This task is accomplished by sending several soap film bubbles through the meter. Wetting the surface permits the soap film bubbles to flow with minimal friction.

Operation

The soap film flowmeter has a rubber bulb that is partially filled with a water-soap solution (brand name is Snoop®, manufactured by Nupro Company). Squeezing the bulb forces the solution into the glass portion of the meter. If a gas is flowing through

the meter, soap film bubbles will begin to form when the water-soap solution reaches

the meter elbow. These bubbles then flow upward through the meter. Flowrates are
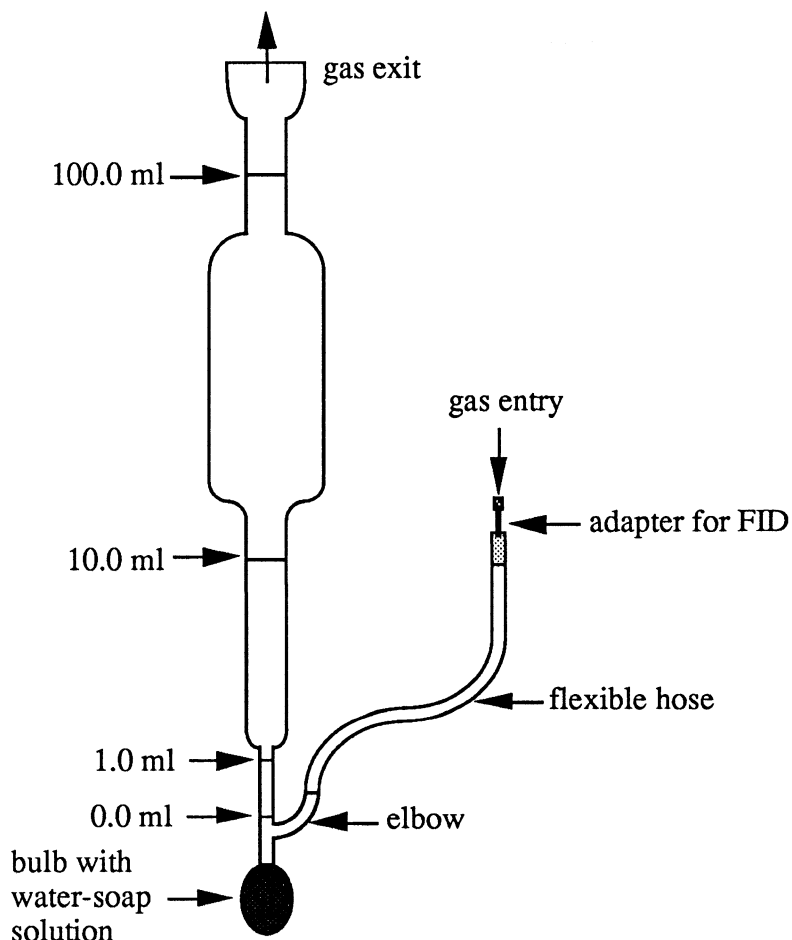
Figure 3.2   Soap film flowmeter.

determined using a timing device to monitor the rate at which a given bubble

progresses up the meter. Timing starts when the bubble is at the 0.0 ml mark and is

stopped either at the 1.0, 10.0 or 100.0 ml mark, depending on the gas flowrate. The

flowrate is then determined from the volume divided by the time necessary for the

bubble to travel from the 0.0 ml mark to the other volumetric mark chosen.

Solute-nitrogen and nitrogen diluent flowrates are measured in the manner stated above. The solute-nitrogen flowrate is measured first. Gas flow is controlled using the flow controllers (12). After adjusting the flowrate, a waiting period of approximately two minutes is permitted before measuring takes place, thus allowing time for the flow in the system to stabilize. After setting the solute-nitrogen flowrate to the desired amount, nitrogen diluent is added (if necessary) to make up the total flowrate. Total contaminant flowrates for this system range from 50.0 to 60.0 ml/min. Too low of a flowrate has a detrimental effect on the FID sensitivity while flowrates greater than 60.0 ml/min pose a risk of blowing out the flame located in the FID.

3.2.3   Area Determination

The area, A, is obtained from a frontal chromatogram previously explained in Chapter One. Data for the chromatogram is acquired using the system shown in Figure 3.1.

Test Preparations

Before a test is started, five preparatory steps are taken.

1. The solute-nitrogen and diluent (if necessary) flowrates are measured using the soap film flowmeter and the timing device in the HP 5890 (explained in section 2.2.2).

2. Nitrogen carrier gas is passed through the glass column at 175 °C for a specified time period (depending upon the type of contaminant tested) to desorb the activated carbon filter. As mentioned previously, 175 °C is the maximum oven temperature for this system and is used in desorbing contaminants from the

activated carbon because of the high rate of desorption. New filters are desorbed for six hours to remove impurities that may be present as a result of filter manufacture and adsorption of particles from the surroundings. Filters that have been tested are desorbed for a time period of one to twelve hours, depending on the type of contaminant adsorbed.

3. Variables in the data logging program used in the Apple IIe must be set correctly. Generally, the only parameters manipulated in the program are the program clock used for timing the test and the time increment between data logging.

4. Set the oven temperature to the desired test level.

5. Set the RANGE 2↑ ( ) command (explained in Appendix B) to the correct level. If this is not done, the data acquired may be truncated and therefore would be invalid.

3.2.4 Executing a Test

Testing is started by initializing the data logging program of the Apple IIe computer, which takes between 24 and 25 seconds. If the time increment between recording the FID signal has been set at 30 seconds, the first data that will be logged after initializing the program will occur at a time of 54 - 55 seconds. To avoid a time error in the chromatogram, it is necessary that the first information be logged at the time when the solute-nitrogen reaches the filter inlet. The time required for the solute-nitrogen stream to travel from the pneumatic valve to the filter is a function of the HP 5890 oven temperature, filter position in the glass column and flowrate. These factors were investigated within the range in which testing was done and it was found that they had

little effect on the amount of time required for the gas to reach the filter inlet. Estimates for the gas travel time were determined from these tests to be within a range of one to two seconds. Assuming a gas travel time from the pneumatic valve to the filter inlet of 1.5 seconds implies the pneumatic valve should be changed from the carrier gas to the solute-nitrogen stream at the 53 second mark. The plotter is started when the first data point is recorded so that the two chromatograms (one electronic and the other a visual copy) correlate. Originally, all of the contaminant present in the solute-nitrogen gas is adsorbed on the activated carbon and the only signal that is transmitted is that obtained by burning the hydrogen-air flame. After a period of time the solute begins to saturate the activated carbon with the result being that some organic is not adsorbed onto the surface and therefore passes into the FID where it is burned. The signal now begins to increase due to the ions generated from the burning contaminant. Eventually, no more solute is adsorbed and the signal reaches a maximum level. Figure 3.3 shows a typical frontal chromatogram displaying the initial FID signal (start of test) and the maximum signal obtained at breakthrough (horizontal line indicating that saturation is complete). When the test is completed, the data logging program and the plotter are stopped. The pneumatic valve is switched from the solute-nitrogen stream to the carrier gas stream and the oven temperature is raised to 175°C, starting the desorbing process.

Data

Figure 3.3 shows three important points concerning the raw data.

1. The data do not begin at zero time.

2.   The FID signal does not start at zero voltage.

3.   Once breakthrough occurs, the signal output from the gas chromatograph is not constant but fluctuates because of noise in the signal.

The first two points can be corrected by subtracting the amount of time and voltage needed to set the initial values equal to zero. The third point poses a more difficult problem. Because noise present in the data has a direct effect on the area desired for determining the quantity of solute adsorbed q, its effect must be minimized. An analysis method selected to accomplish this task is listed below with a schematic of the area analysis shown in Figure 3.4.
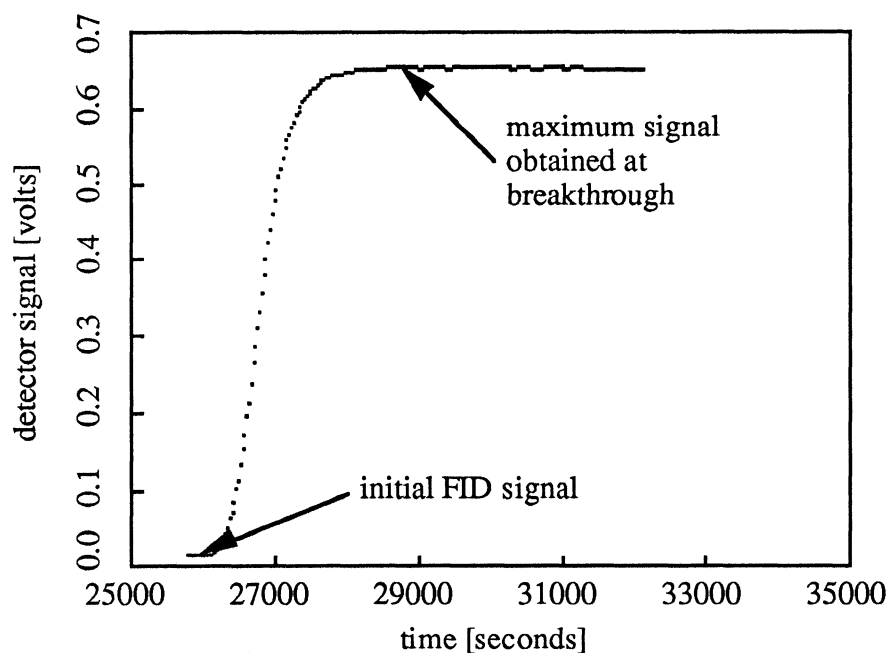
Figure 3.3   Typical frontal chromatogram.

Area Analysis

1. Find the maximum voltage (V_{max}) point of the frontal chromatogram.

2. Find the earliest voltage signal that is approximately 0.99 of the maximum voltage signal. The time of the test run will be from time zero to this point (t_{end}).
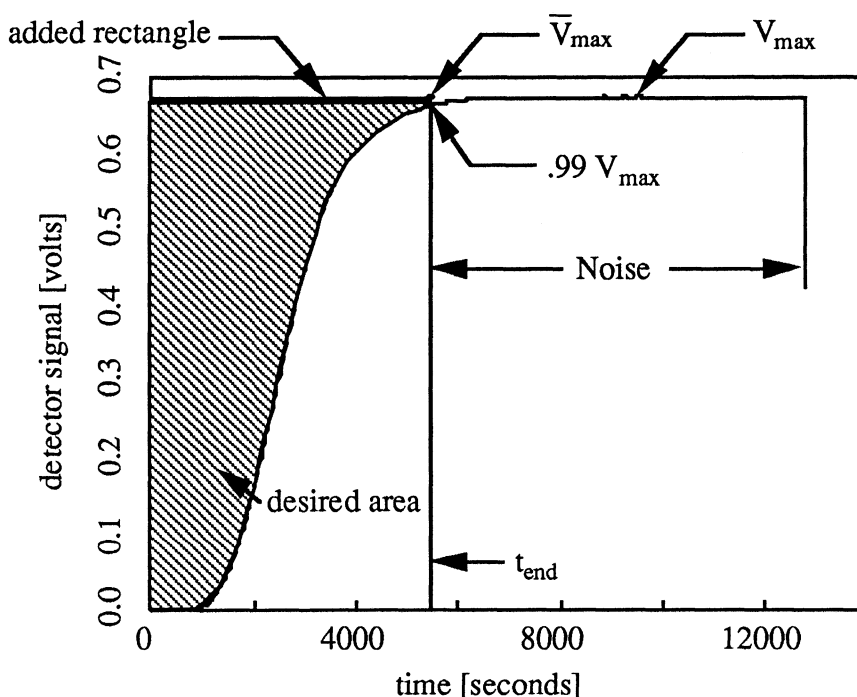
Figure 3.4 Method for area analysis, (not shown to scale).

3. The section of data from 0.99 V_{max} to the time data logging was stopped is used to calculate the mean voltage ($\overline{V}_{max}$) which is then considered to be the maximum voltage of the test run.

4. Replace the voltage value at 0.99 V_{max} with $\overline{V}_{max}$. By doing this, a rectangle of area is added to the total area used to determine the amount adsorbed, q.

Explanation of Area Analysis

The value of 0.99 V_{max} was chosen because voltages greater than this value are located in the noise section of the data as shown in Figure 3.4. These voltage values tend to fluctuate up or down whereas voltages before 0.99 V_{max} are steadily increasing because breakthrough has not yet occurred. If a voltage lower than 0.99 V_{max} were selected as the truncation point of the test, a lesser area would result, thus increasing error in the analysis.

The mean voltage, $\overline{V}_{max}$, is determined using data that has a noise element built into it. It is desired to obtain a $\overline{V}_{max}$ value that will not be affected by using an increased number of data points for its calculation. Therefore, a minimum amount of data is needed to obtain a meaningful $\overline{V}_{max}$ value. The minimum number of data points required for $\overline{V}_{max}$ analysis was found to be 200. This number was determined by investigating the value of $\overline{V}_{max}$ using various numbers of data points. Adding more data to the analysis has a negligible effect on $\overline{V}_{max}$.

Example of Data Manipulation

Table 3.1 shows raw data obtained from a typical chromatogram. A data analysis and graphing program called KaleidaGraph™ for the Macintosh computer is used to manipulate the data. The first step is to zero both the time and voltage signal. Columns two and three of Table 3.2 show this result. The maximum voltage signal is found by using a statistics function built into KaleidaGraph™ and was 0.67657 volts in

Table 3.1 Raw data from a typical test chromatogram.

point #	time [seconds]	signal [volts]
1	20311	0.011262
2	20344	0.011262
3	20369	0.011262
⋮	⋮	⋮
85	22834	0.33536
86	22860	0.34412
87	22895	0.35247
⋮	⋮	⋮
200	28049	0.67907
201	28082	0.67907
202	28108	0.68199
⋮	⋮	⋮
427	33089	0.68783
428	33122	0.68783
429	33147	0.68783

this case. The term $0.99\ V_{max}$ is then 0.66987 volts. A value that is as close to 0.99 V_{max} as possible is then searched for in the voltage column and was found at a time of 6030 seconds to be 0.67073 volts.

Table 3.2 Data of a typical test chromatogram after manipulation.

point #	time [seconds]	signal [volts]	signal [ppm]
1	0.0	0.00000	0.000
2	33.0	0.00000	0.000
3	58.0	0.00000	0.000
⋮	⋮	⋮	⋮
85	2523.0	0.32410	24.180
86	2549.0	0.33286	24.834
87	2584.0	0.34120	25.456
⋮	⋮	⋮	⋮
200	5970.0	0.66781	49.823
201	6002.0	0.66781	49.823
202	6030.0	0.67073 to 0.67554	50.400
⋮	⋮	⋮	
427	12778	0.67657	
428	12811	0.67657	
429	12836	0.67657	

$\overline{V}_{max}$ is found by taking all data past 6030 seconds and using the statistics function to find the mean of this data. $\overline{V}_{max}$ was determined to be 0.67554 volts. As shown in column three of Table 3.2, $\overline{V}_{max}$ replaces the approximate number of 0.99 V_{max}. After $\overline{V}_{max}$ has been inserted, the entire column is converted into contaminant concentration [ppm], with $\overline{V}_{max}$ being the maximum concentration (50.4 ppm for this example, as displayed in column four of Table 3.2). As Figure 3.4 shows, a section of area in the

shape of a rectangle is added to the desired area used to determine the amount of solute adsorbed, q. Once $\overline{V}_{max}$ is inserted into position, the area under the curve (unshaded region) is determined using an integration macro function of KaleidaGraph™. The desired area (shaded region) is then found by subtracting the unshaded area from the total rectangular area (t_{end}*maximum concentration).

3.2.5 Summary of Test Procedure

A summary of the procedure to determine the quantity of contaminant adsorbed, q is given below.

Test Preparations

1. Turn on the pressure regulators for the solute nitrogen and diluent nitrogen (if necessary) to permit flow through the system.

2. Turn on the gas chromatograph, electronic integrator, and data logging computer.

3. Measure solute-nitrogen and (if necessary) diluent flowrates. The total flowrate for this system should range from 54 - 60 ml/min.

4. Adjust the flowrates measured at the set oven temperature to ambient conditions in preparation for data analysis.

5. Turn on the pressure regulators for the nitrogen carrier gas, hydrogen and air.

6. With the valves (Items 13 in Figure 2.1) on, light the flame ionization detector.

7. Switch the position of the pneumatic valve from the "ON" to the "OFF" position via the keyboard on the HP 5890 gas chromatograph. Doing this changes the gas stream passing through the glass column from solute-nitrogen to the nitrogen carrier gas.

8. Desorb the activated carbon filter using the nitrogen carrier gas. Set the oven temperature to 175 °C. New filters are desorbed for six hours to rid them of impurities that may have been acquired during storage and manufacture of the filter. Filters that have been used in tests are desorbed for one to three hours, depending on the type and size of the filter and also the contaminant adsorbed for that particular test.

9. Fix the variables in the data logging program. This usually involves two variables:

    a. set up the clock

    b. adjust the time between data logging to the desired value

10. Adjust the oven temperature of the HP 5890 to that desired for the upcoming test.

11. Set the RANGE 2↑ ( ) command to an appropriate level which ensures that no signal is truncated.

Test execution

12. Start the data logging program.

13. Switch the pneumatic valve from "OFF" to "ON" position via the keyboard on the HP 5890 gas chromatograph to the gas stream passing through the glass column

from nitrogen carrier gas to the solute-nitrogen . Valve switching should be done a determined number of seconds before the first datum is logged (details for calculating this time are given in Section 3.2).

14. Start the plotter when the first data is recorded so the two chromatograms (one electronic and the other a visual copy) correlate.

15. Once breakthrough occurs, a minimum of 200 data points must be taken so an accurate value of $\overline{V}_{max}$ can be calculated. The time needed to accomplish this will vary depending on the time increment between data logging.

16. After the test is completed, turn off the data logging program and plotter.

17. Manipulate the test chromatogram data as previously discussed in section 2.2.3 and then integrate to solve for the desired area.

>**Note:** Nitrogen is passed through the system continuously when testing is not being done to provide a positive pressure inside the system to prevent contaminants in the air from entering the system through the FID exit.

3.3 EXPERIMENTAL UNCERTAINTY

3.3.1 General Information

Uncertainty error is of two types

1. Bias, represented as U_{Br}

2. Precision, represented as U_{Pr}

Bias and precision errors are defined by Coleman and Steele (1989) as follows

"The bias error (U_{Br}) is the fixed, systematic, or constant component of the total error and is sometimes referred to simply as the bias. The precision error (U_{Pr}) is the random component of the total error and is sometimes called the repeatability or repeatability error." Each of these error types will be estimated for this system and then will be combined to yield an estimation of the total error of the experimental layout.

Before determining the overall uncertainty for the system, analysis techniques will be discussed. There are two ways in which uncertainty can be evaluated and this can best be displayed by listing the respective equations.

$$1.\ U_{r_{RSS}}^2 = (U_{Br})^2 + (U_{Pr})^2 \tag{3.2}$$

$$2.\ U_{r_{ADD}} = U_{Br} + U_{Pr} \tag{3.3}$$

Equation 3.2 expresses the root-sum-square uncertainty, $U_{r_{RSS}}$. Coleman and Steele (1989) state this equation yields approximately a 95% confidence interval for the total error. Equation 3.3 expresses the additive uncertainty, $U_{r_{ADD}}$. This equation has

approximately 99% confidence if the bias and precision errors are of the same order and 95% confidence if one of the errors is small relative to the other. The additive uncertainty equation generally yields a significantly larger total error than the root-sum-square uncertainty. The root-sum-square uncertainty method will be used in this analysis.

In Appendix B of Coleman and Steele (1989), an uncertainty equation is derived for an experimental result that is a function of two variables

$$r = r(x,y) \tag{3.4}$$

The initial step is to approximate the function in Equation 3.4 using a multivariable Taylor series expansion that is based around the mean values of x and y.

$$r(x_i,y_i) = r(\mu_x,\mu_y\ ) + \frac{\partial r}{\partial x}(x_i - \mu_x) + \frac{\partial r}{\partial y}(y_i - \mu_y) + R_2 \tag{3.5}$$

The term R_2 is the sum of the remaining terms of the Taylor series which is either zero if the data reduction equation is linear or assumed to be negligible if the function is nonlinear. After some manipulation, the general uncertainty equation for the experimental value, r, is

$$U_r^2 = \left(\frac{\partial r}{\partial x}U_x\right)^2 + \left(\frac{\partial r}{\partial y}U_y\right)^2 + 2\left(\frac{\partial r}{\partial x}\right)\left(\frac{\partial r}{\partial y}\right)\rho_{xy}U_xU_y \tag{3.6}$$

The last term of Equation 3.6 is non-zero when variables x and y are correlated. If the variables are independent, then the coefficient of correlation, $\rho_{xy} = 0.0$ and the equation for uncertainty reduces to

$$U_r^2 = \left(\frac{\partial r}{\partial x}U_x\right)^2 + \left(\frac{\partial r}{\partial y}U_y\right)^2 \qquad (3.7)$$

Although this brief explanation of the derivation of the uncertainty equation involved a function with two variables, it can be easily adapted to accommodate as many variables as necessary.

Uncertainty equations involving precision errors will have the form of Equation 3.7 for this analysis. The reason is "since the precision limits are statistical measures of the effect of random errors and variations on a measurement, the assumption of independent precision limits in the individual measurements seems justified." [Coleman and Steele (1989)].

In some cases, the bias error is known to be either greater or less than the true value being investigated. To simplify this analysis, all bias errors will be assumed to be ± some actual value. As a result of making this assumption, the uncertainty analysis will be more conservative.

When beginning an uncertainty analysis, two rules from Coleman and Steele (1989) should be adhered to.

Rule 1 states that the term whose uncertainty is being determined must be explicitly solved for (if the equation can not be explicitly solved for, the differentiation can be

done implicitly or the error can be found numerically using a jitter program). An example of this is the equation for flowrate

$$F = V/t \qquad (3.8)$$

If the uncertainty for the flowrate is desired, then the equation as written is correct. However, if the uncertainty for volume is to be solved for, then the equation is written as

$$V = F\,t \qquad (3.9)$$

Rule 2 states that the uncertainty analysis expression for a given data reduction equation should be divided by the experimental result (note this can only be done when the equation is in product form such as Equation 3.8). Upon doing this, each term in the uncertainty equation reverts into a percentage. As an example, again refer to the flowrate equation, 3.8. Assuming the volume and time variables to be independent and referring to Equation 3.7 yields an uncertainty equation for the flowrate

$$U_{BF}^2 = \left(\frac{\partial F}{\partial V}U_{BV}\right)^2 + \left(\frac{\partial F}{\partial t}U_{Bt}\right)^2 \qquad (3.10)$$

After taking partial derivatives of Equation 3.8 and dividing by the flowrate, F, the final form of Equation 3.10 is

$$\left(\frac{U_{BF}}{F}\right)^2 = \left(\frac{U_{BV}}{V}\right)^2 + \left(\frac{-U_{Bt}}{t}\right)^2 \qquad (3.11)$$

These rules are utilized in the uncertainty analysis below.

3.3.2 Evaluation of Experimental Error

The first step in the uncertainty analysis is to solve the data reduction equation for the amount of contaminant adsorbed, q, (see Chapter 1 for explanation). This quantity is the term for which the total uncertainty will be calculated. Solving the data reduction equation for q yields

$$q = b\frac{FA\rho_{N_2}}{m} \qquad \left(\frac{mg\ contaminant}{g\ carbon}\right) \tag{3.12}$$

Stated in another way

$$q = q(F, A, \rho_{N_2}, m) \tag{3.13}$$

The value b is a conversion factor and contains no uncertainty. The variables in Equation 3.12 are independent so this allows the following equation to be used in determining the uncertainty of the system

$$U_q^2 = \left(\frac{\partial q}{\partial F}U_F\right)^2 + \left(\frac{\partial q}{\partial A}U_A\right)^2 + \left(\frac{\partial q}{\partial \rho_{N_2}}U_{\rho_{N_2}}\right)^2 + \left(\frac{\partial q}{\partial m}U_m\right)^2 \tag{3.14}$$

Since both bias and precision errors are being analyzed, more specific equations for this analysis are

$$U_{Bq}^2 = \left(\frac{\partial q}{\partial F}U_{BF}\right)^2 + \left(\frac{\partial q}{\partial A}U_{BA}\right)^2 + \left(\frac{\partial q}{\partial \rho_{N_2}}U_{B\rho_{N_2}}\right)^2 + \left(\frac{\partial q}{\partial m}U_{Bm}\right)^2 \quad Bias \tag{3.15}$$

$$U_{Pq}^2 = \left(\frac{\partial q}{\partial F}U_{PF}\right)^2 + \left(\frac{\partial q}{\partial A}U_{PA}\right)^2 + \left(\frac{\partial q}{\partial \rho_{N_2}}U_{P\rho_{N_2}}\right)^2 + \left(\frac{\partial q}{\partial m}U_{Pm}\right)^2 \quad Precision \tag{3.16}$$

Dividing by the experimental result q, yields the following equations for bias and precision.

$$\left(\frac{U_{Bq}}{q}\right)^2 = \left(\frac{U_{BF}}{F}\right)^2 + \left(\frac{U_{BA}}{A}\right)^2 + \left(\frac{U_{B\rho_{N_2}}}{\rho_{N_2}}\right)^2 + \left(\frac{-U_{Bm}}{m}\right)^2 \quad \text{Bias} \qquad (3.17)$$

$$\left(\frac{U_{Pq}}{q}\right)^2 = \left(\frac{U_{PF}}{F}\right)^2 + \left(\frac{U_{PA}}{A}\right)^2 + \left(\frac{U_{P\rho_{N_2}}}{\rho_{N_2}}\right)^2 + \left(\frac{-U_{Pm}}{m}\right)^2 \quad \text{Precision} \qquad (3.18)$$

Once the bias and precision errors are known, the total error in percentage form can be determined from

$$\left(\frac{U_q}{q}\right)^2 = \left(\frac{U_{Bq}}{q}\right)^2 + \left(\frac{U_{Pq}}{q}\right)^2 \qquad (3.19)$$

There are two individual cases for this experimental system. Case 1 involves using a particular contaminant directly from the source and involves no diluting to change the contaminant concentration that is present at the source. In this case, only one flow needs to be measured for the eventual determination of q. Case 2 involves diluting the contaminant concentration to some other desired value. Two gas streams are mixed to accomplish this task, one containing the contaminant and the other to reduce the concentration. The uncertainty analysis for these two cases is different because of the nonindependent flowrates in Case 2. For this reason they are treated separately below.

Case 1: Bias Error (no diluent)

Mass

The mass bias error has one source.

$$U_{Bm} = f(\text{mass balance}) \qquad\qquad (3.20)$$

The bias found in the mass measurement was estimated to be one-half of the last significant digit which could be read from the mass balance, 0.00005 g. However, because two measurements are needed to determine the mass of the activated carbon (first the weighing paper is weighed and then the total mass is weighed) the bias error for the mass is

$$U_{Bm} = [0.00005^2 + 0.00005^2]^{1/2} = 0.00007 \text{ g} \qquad\qquad (3.21)$$

Gas Flow

The gas flow bias error has two sources.

$$U_{BF} = f(\text{flowmeter, time}) \qquad\qquad (3.22)$$

The bias error of the soap film flow meter was found using a static test method. The error was determined by inserting a "known" volume of water into the flow meter and then finding how much more (or less) fluid would be necessary to reach the 1.0 or 10.0 ml mark. A schematic for this test is shown in Figure 3.5.
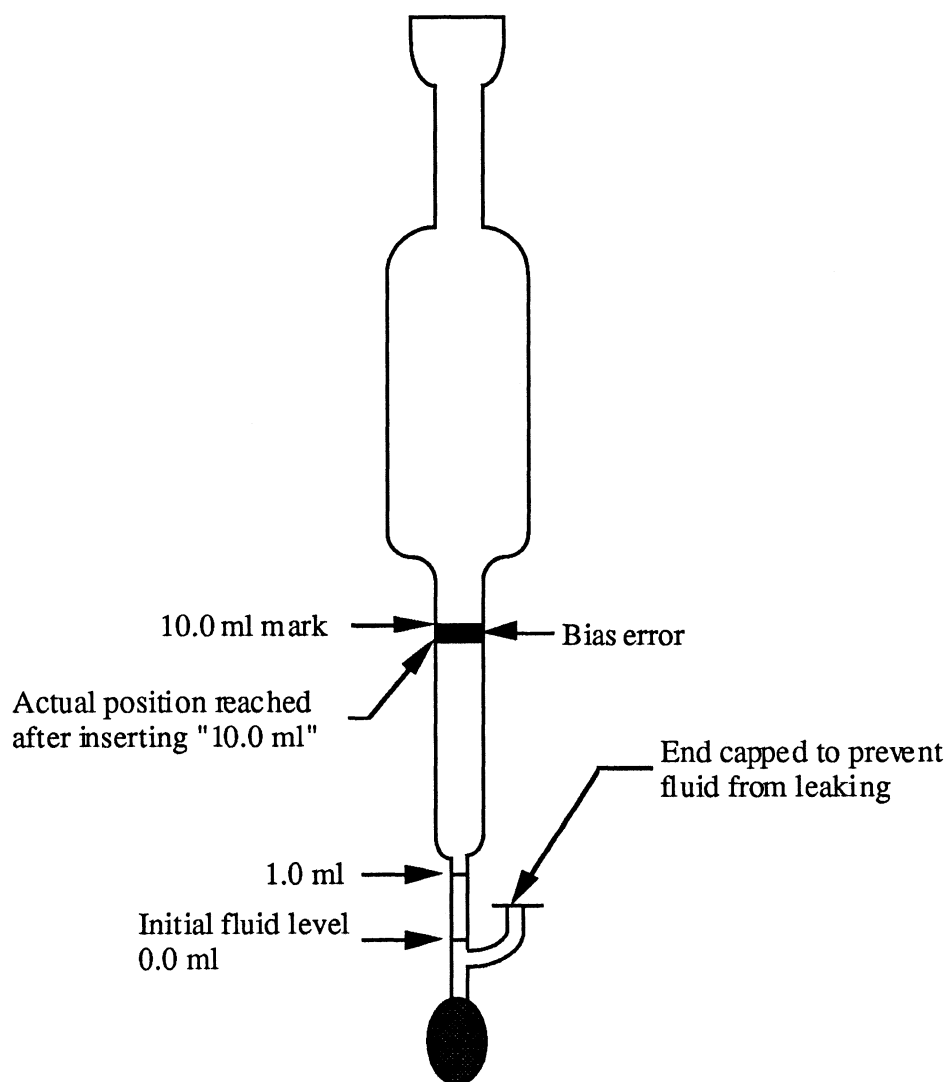
Figure 3.5   Schematic of flowmeter displaying 10.0 ml bias error test.

The uncertainties were found to be ±2.5% for both the 1.0 and 10.0 ml volume. The bias error for time is one-half the last significant digit of the clock being used to measure the flowrate and was found to be 0.05 second. The equation for determining the flow is Equation 3.8 and the resulting uncertainty is represented by Equation 3.10.

After taking partial derivatives of Equation 3.8 and dividing the entire uncertainty equation by the flowrate, the final form of Equation 3.10 is Equation 3.11.

Area

The area that is used to determine the amount of impurity adsorbed onto the activated carbon has several sources of bias error built into it.

$$U_{BA} = f(A/D \text{ converter, FID, contaminant concentration, time}) \qquad (3.23)$$

The analog-to-digital (A/D) converter used in the data acquisition has been programmed to use a 12-bit system, which means the specified voltage range the A/D converter is operating in is divided into 2^{12} segments. The voltage range being used in the A/D converter is 0.0 - 10.0 volts. The bias then present in the converter corresponds to one-half LSB (least significant bit) and is shown by Coleman and Steele (1989) as

$$\frac{\pm \frac{1}{2}(10V)}{2^{12}} = \pm 0.0012 \text{ V} \qquad (3.24)$$

The HP 5890 gas chromatograph is operating with a voltage range of 0.0 - 1.0 volt resulting in a bias error of 0.12%.

The bias error concerning the FID is dependent on its sensitivity. Buffington and Wilson (1991) mention several factors effecting FID sensitivity, some of which are hydrogen and air flowrates, carrier gas flowrate, jet tip inside diameter, and the contaminant being burned. However, no mention is made of the magnitudes of any errors concerning the FID. Because the factors above make determining the FID bias quite difficult, a voltage bias of 0.001 V is assumed. This value was chosen to be

approximately the same magnitude as the A/D bias error and is thought to be conservative .

Combining the two voltage bias errors gives the total bias error for the voltage signal

$$\left[0.0012^2 + 0.001^2\right]^{1/2} = \pm 0.0016 \text{ V} \tag{3.25}$$

The bias error involving the contaminant concentration will vary with different cylinders of gas. However, this information can be found by contacting the company that manufactures the gas products. An example of this is a $\pm 5\%$ bias error in a cylinder containing 50.4 ppm acetone and makeup gas of nitrogen. This information was found in the Matheson Gas Products catalog (1990), supplier of the gas contents.

The bias error for time was determined using a stop watch to investigate the error in the computer clock. Results between the two time measurement devices matched to within one second.

The equation for determining the area is

$$A = C\, t_{end} - \frac{C}{\overline{V}_{max}} \int_{t_0}^{t_{end}} V(t)\, dt \tag{3.26}$$

The bias error is a function of five terms

$$U_{BA} = f(\overline{V}_{max}, V(t), t_{end}, t, C) \tag{3.27}$$

Using Equation 3.6, the uncertainty equation for the area bias error is

$$U_{BA}^2 = \left(\frac{\partial A}{\partial \overline{V}_{max}} U_{B V_{max}}\right)^2 + \left(\frac{\partial A}{\partial V(t)} U_{B V(t)}\right)^2 + \left(\frac{\partial A}{\partial t_{end}} U_{B t_{end}}\right)^2 \qquad (3.28)$$

$$+ \left(\frac{\partial A}{\partial t} U_{Bt}\right)^2 + \left(\frac{\partial A}{\partial C} U_{BC}\right)^2 + 2\left(\frac{\partial A}{\partial \overline{V}_{max}}\right)\left(\frac{\partial A}{\partial V(t)}\right)\rho_{\overline{V}_{max} V(t)} B_{\overline{V}_{max}} B_{V(t)}$$

$$+ 2\left(\frac{\partial A}{\partial t_{end}}\right)\left(\frac{\partial A}{\partial t}\right)\rho_{t_{end} t} B_{t_{end}} B_t$$

The final two terms of Equation 3.28 are present because the voltage values ($\overline{V}_{max}$ and $V(t)$) and the time values (t_{end} and t) are correlated. Because this analysis is quite involved, the partial derivatives are derived for Equation 3.28 and are listed in Appendix C.

After obtaining the partial derivatives from Equation 3.26, the final form of Equation 3.28 is

$$U_{BA}^2 = \left(\frac{C}{\overline{V}_{max}^2}\int_{t_o}^{t_{end}} V(t)dt\, U_{B\overline{V}_{max}}\right)^2 + \left(\frac{-C}{\overline{V}_{max}} t_{end} U_{B V(t)}\right)^2 \qquad (3.29)$$

$$+ (C U_{B t_{end}})^2 + (-C U_{Bt})^2 + \left(\left(t_{end} - \frac{1}{\overline{V}_{max}}\int_{t_o}^{t_{end}} V(t)dt\right) U_{BC}\right)^2$$

$$+ 2\left(\frac{C}{\overline{V}_{max}^2}\int_{t_o}^{t_{end}} V(t)dt\right)\left(\frac{-C\, t_{end}}{\overline{V}_{max}}\right) U_{B\overline{V}_{max}} U_{B V(t)} + 2(C)(-C) U_{B t_{end}} U_{Bt}$$

The correlation coefficients for both voltage and time are 1.0 because they are measured with the same instruments and because they also become the same respective value ($\overline{V}_{max} = V(t)$ and $t_{end} = t$) upon evaluation of the integral.

Density

The bias error for the determination of the density of nitrogen gas has three sources

$$U_{B\rho_{N_2}} = f(\text{amb. temperature, atm. pressure, gas constant, R}) \qquad (3.30)$$

The error for the temperature is one-half of the least significant digit present on the thermometer used, (±0.5 K). Barometric pressure data was obtained from NOAA (1989-1991). A population of 36 monthly average pressure readings were used to calculate the average atmospheric pressure for Madison, (98,508 Pa). The bias error for these readings is one-half the last readable digit and is .0005 in Hg (1.7 Pa). The gas constant, R, obtained from Myers (1989) has a value of 8.3143 J/gmole K. Errors are present in all property values. For this uncertainty analysis, it is assumed this error is $\pm2.0\%$.

The equation used to determine the density is the ideal gas law.

$$\rho_{N_2} = \frac{P}{RT} \qquad (3.31)$$

This equation is assumed applicable because the temperature and pressure are at ambient conditions. An uncertainty equation for the density can be determined by referring back to Equation 3.7.

$$U_{B\rho_{N_2}}^2 = \left(\frac{\partial \rho_{N_2}}{\partial P}U_{BP}\right)^2 + \left(\frac{\partial \rho_{N_2}}{\partial R}U_R\right)^2 + \left(\frac{\partial \rho_{N_2}}{\partial T}U_T\right)^2 \qquad (3.32)$$

Upon entering the partial derivatives obtained from Equation 3.31 into Equation 3.32 and then dividing by the experimental result, ρ_{N_2}, yields the final form of the density bias error

$$\left(\frac{U_{B\rho_{N_2}}}{\rho_{N_2}}\right)^2 = \left(\frac{U_{BP}}{P}\right)^2 + \left(\frac{-U_{BR}}{R}\right)^2 + \left(\frac{-U_{BT}}{T}\right)^2 \tag{3.33}$$

The uncertainty terms that have been calculated can now be substituted into Equation 3.15 to yield the bias uncertainty for the system.

Case 1: Precision Error (diluent present)

Mass

The mass precision error has two sources.

$$U_{Pm} = f(\text{mass balance, transfer losses}) \tag{3.34}$$

The precision error has two sources which cannot be separated from one another. They involve the precision error in weighing the activated carbon and losses of mass due to transfer of the activated carbon from the scale to the glass column in which the filter is to be located. Mass is lost because some of the very small particles of activated carbon adhere to the weighing paper and also to the funnel used to guide the carbon into the glass column. Twenty data sets (one data set is comprised of four mass measurements) were obtained to determine the combined error which was found to be 0.0005 g. Precision error for the weighing process alone was determined from ten mass measurements and was found to be one-half of the last significant digit which could be read from the mass balance, 0.00005 g.

Gas Flow

The gas flow precision error is a result of flowrate measurements.

$$U_{Pf} = f(\text{high and or low flowrate}) \qquad (3.35)$$

The precision uncertainty for high flowrates (> 20.0 ml/min) was determined by taking 30 consecutive flow measurements and then finding the standard deviation of these values. From Figure 3.7 it looks as though the data are Gaussian and the standard deviation was multiplied by two to obtain a 95% confidence interval. A histogram of the data taken is shown in Figure 3.6.
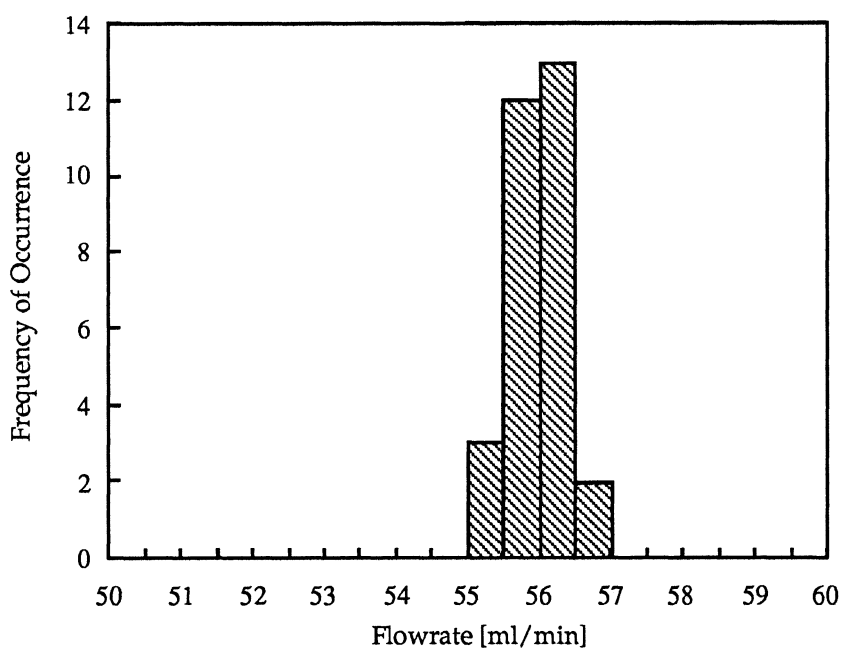
Figure 3.6 Distribution of flowrate measurements. The precision uncertainty was determined to be ±0.8 ml / min.

The precision uncertainty for low flowrates was found in the same manner as the high flowrate uncertainty, except that 40 consecutive flow measurements were taken. The uncertainty was determined to be ± 0.5 ml/min.

Area

The sources of precision error present are

$$A = f(t_{end}, \overline{V}_{max}, \int_{t_o}^{t_{end}} V(t)dt) \tag{3.36}$$

The error for t_{end} is 0.5 second and is found by taking one-half the least significant digit of the timing device. The 0.5 second error is the minimum possible for this timing device and was determined after running thirty tests. Coleman and Steele (1989) state that the precision error for $\overline{V}_{max}$ is generally found by taking one-half the flicker of the noise. However, the mean value of the noise is not at the midpoint of $\overline{V}_{max} - 0.99V_{max}$ so a more conservative approach was taken. Approximately the total amount of $\overline{V}_{max} - 0.99V_{max}$ was used and is found to be 0.005 V.

Integrating the chromatogram results in a precision error caused by numerical integration. Trapezoidal integration was the method used in this study. It is known from Cheney and Kincaid (1985) that the error involved when using this type of numerical integration can be determined from the formula

$$E = -\frac{1}{12}(b-a)h^2f''(\zeta) \quad \text{where} \quad |f''(\zeta)| \leq M_{max} \tag{3.37}$$

for the interval in question.

The interval has been described fully in Section 3.2. In order for the error to be determined, the data had to be curve fit and the obtained equation had to have a second derivative. Figure 3.7 shows a typical curve fit. Five chromatograms were analyzed and fit to a sixth order polynomial. All regression values were very near one. The polynomials of the data were then imported into a math program which was used to differentiate the equations analytically. After differentiating, the value M_{max} was able to be determined. Figure 3.8 displays a curve of a second derivative used in this analysis. Depending on the total integrated area, the mean error determined from the five chromatograms ranged from 0.02 - 0.2 % of the desired area. Because the integral term has its own precision error, this term will be called "I". The equation for the area is then

$$A = C\,t_{end} - \frac{C}{\overline{V}_{max}}\,I \tag{3.38}$$

The resulting uncertainty equation for the area precision error is (from Equation 3.7)

$$U_{PA}^2 = \left(\frac{\partial A}{\partial C}U_{PC}\right)^2 + \left(\frac{\partial A}{\partial t_{end}}U_{Pt_{end}}\right)^2 + \left(\frac{\partial A}{\partial \overline{V}_{max}}U_{P\overline{V}_{max}}\right)^2 + \left(\frac{\partial A}{\partial I}U_{PI}\right)^2 \tag{3.39}$$

The precision error of the contaminant concentration taken directly from the source is zero, resulting in the first term of Equation 3.39 to be zero. Taking partial derivatives of Equation 3.38 and applying them to Equation 3.39 yields the final result for area precision error

$$U_{PA}^2 = \left(CU_{Pt_{end}}\right)^2 + \left(\frac{C}{\overline{V}_{max}^2}I\,U_{P\overline{V}_{max}}\right)^2 + \left(\frac{-C}{\overline{V}_{max}}U_{PI}\right)^2 \tag{3.40}$$
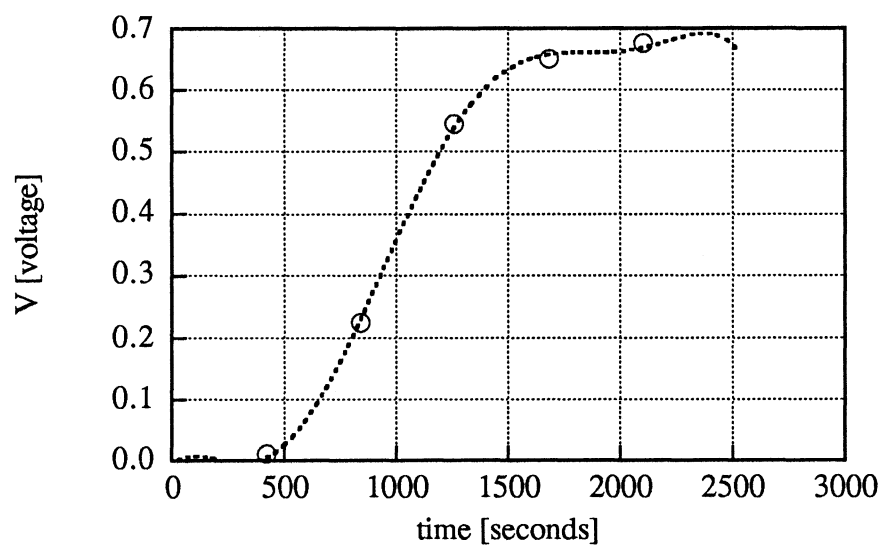
Figure 3.7   Typical curve fit of frontal chromatogram with sixth order polynomial.
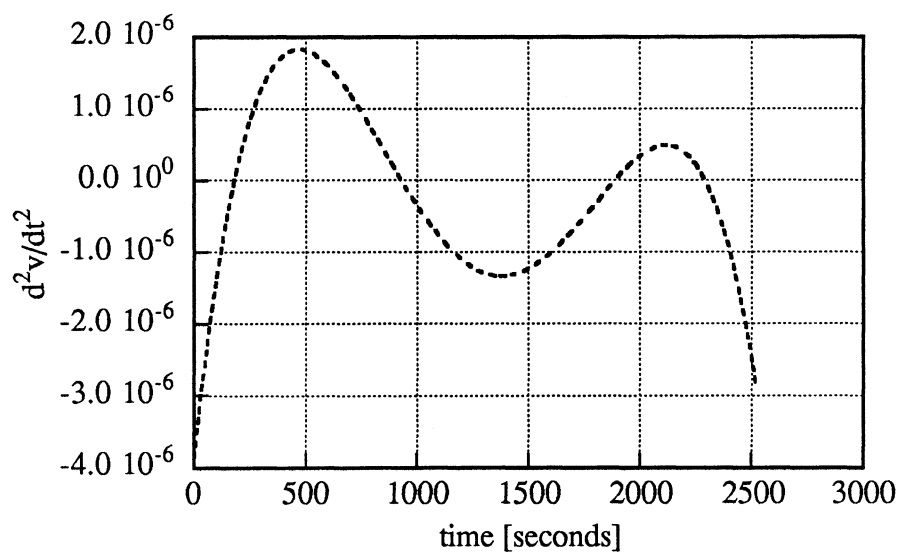
Figure 3.8   Second derivative of frontal chromatogram.

Density

The density precision error has two sources.

$$U_{P_{\rho_{N_2}}} = f(\text{amb. temperature, atm. pressure}) \tag{3.40}$$

The precision uncertainty for the temperature was determined by obtaining 23 temperature measurements over a period of months. The data were assumed to be Gaussian and the standard deviation of 0.7 K was multiplied by two to obtain a 95% confidence interval. The precision error for the pressure was estimated by finding the high and low average daily pressure values for a period from 1989 - 1991. The largest difference from the average was 2.7% and although conservative, is used in this analysis. Equation 3.31 displays the density equation. By taking a partial derivative with respect to pressure and temperature and then dividing by ρ_{N_2}, the final form of the density precision error is

$$\left(\frac{U_{P_{\rho_{N_2}}}}{\rho_{N_2}}\right)^2 = \left(\frac{U_{PP}}{P}\right)^2 + \left(\frac{-U_{PT}}{T}\right)^2 \tag{3.42}$$

The uncertainty terms that have been determined can now be substituted into Equation 3.16 to yield the precision error for the system.

The total uncertainty can then be calculated by inserting the bias and precision values into Equation 3.19.

Case 2: Bias Error

Much of the analysis that was done for Case 1 also applies to Case 2. Related items will be mentioned in this section but will not be dealt with in an in depth manner. Explanations of the error sources are also the same as was previously discussed.

Mass

The mass bias error is unchanged from the previous analysis.

Gas Flow

The bias error for the gas flow is now a function of two flowrates, one that contains the contaminant being tested and the other gas that is used to dilute the concentration to some desired value. The equation for the total flow is

$$F_{tot} = \frac{V_1}{t_1} + \frac{V_2}{t_2} \tag{3.43}$$

The uncertainty equation for total flow is (from Equation 3.6)

$$U_{BF}^2 = \left(\frac{\partial F}{\partial V_1}U_{BV_1}\right)^2 + \left(\frac{\partial F}{\partial t_1}U_{Bt_1}\right)^2 + \left(\frac{\partial F}{\partial V_2}U_{BV_2}\right)^2 + \left(\frac{\partial F}{\partial t_2}U_{Bt_2}\right)^2 \tag{3.44}$$

$$+ 2\left(\frac{\partial F}{\partial V_1}\right)\left(\frac{\partial F}{\partial V_2}\right)\rho_{V_1V_2}U_{BV_1}U_{BV_2} + 2\left(\frac{\partial F}{\partial t_1}\right)\left(\frac{\partial F}{\partial t_2}\right)\rho_{t_1t_2}U_{Bt_1}U_{Bt_2}$$

After taking partial derivatives of Equation 3.43 and implementing them into Equation 3.44, the final form of the bias uncertainty is

$$U_{BF}^2 = \left(\frac{1}{t_1}U_{BV_1}\right)^2 + \left(\frac{-V_1}{t_1^2}U_{Bt_1}\right)^2 + \left(\frac{1}{t_2}U_{BV_2}\right)^2 + \left(\frac{-V_2}{t_2^2}U_{Bt_2}\right)^2 \tag{3.45}$$

$$+ 2\left(\frac{1}{t_1}\right)\left(\frac{1}{t_2}\right)U_{BV_1}U_{BV_2} + 2\left(\frac{-V_1}{t_1^2}\right)\left(\frac{-V_2}{t_2^2}\right)U_{Bt_1}U_{Bt_2}$$

It can be seen from Equation 3.43 that the correlation coefficients for volume (V_1 and V_2) and time (t_1 and t_2) are 1.0 because each of these respective sets of variables was found using the same measuring device.

Area

As a result of the multiple flowrates, the concentration bias error is now a function of the flowrate bias as well as the tank concentration bias. The equation for concentration is

$$C = C_{tank} \frac{V_1 \, t_{tot}}{t_1 \, V_{tot}} \qquad (3.46)$$

From Equation 3.6, the uncertainty equation for a given concentration is

$$U_{BC}^2 = \left(\frac{\partial C}{\partial C} U_{BC_{tank}}\right)^2 + \left(\frac{\partial C}{\partial V_1} U_{BV_1}\right)^2 + \left(\frac{\partial C}{\partial t_1} U_{Bt_1}\right)^2 + \left(\frac{\partial C}{\partial t_{tot}} U_{Bt_{tot}}\right)^2 \qquad (3.47)$$

$$+ \left(\frac{\partial C}{\partial V_{tot}} U_{BV_{tot}}\right)^2 + 2\left(\frac{\partial C}{\partial V_1}\right)\left(\frac{\partial C}{\partial V_{tot}}\right)\rho_{V_1 V_{tot}} U_{BV_1} U_{BV_{tot}}$$

$$+ 2\left(\frac{\partial C}{\partial t_1}\right)\left(\frac{\partial C}{\partial t_{tot}}\right)\rho_{t_1 t_{tot}} U_{Bt_1} U_{Bt_{tot}}$$

Taking partial derivatives of Equation 3.46 and placing them into Equation 3.47 yields the final form of Equation 3.47

$$U_{BC}^2 = \left(\frac{V_1 t_{tot}}{t_1 V_{tot}} U_{BC_{tank}}\right)^2 + \left(\frac{C_{tank} t_{tot}}{t_1 V_{tot}} U_{BV_1}\right)^2 + \left(\frac{-C_{tank} V_1 t_{tot}}{t_1^2 V_{tot}} U_{Bt_1}\right)^2 \qquad (3.48)$$

$$+ \left(\frac{C_{tank} V_1}{t_1 V_{tot}} U_{Bt_{tot}}\right)^2 + \left(\frac{-C_{tank} V_1 t_{tot}}{t_1 V_{tot}^2} U_{BV_{tot}}\right)^2$$

$$+ 2\left(\frac{C_{tank} t_{tot}}{t_1 V_{tot}}\right)\left(\frac{-C_{tank} V_1 t_{tot}}{t_1 V_{tot}^2}\right) U_{BV_1} U_{BV_{tot}}$$

$$+ 2\left(\frac{-C_{tank} V_1 t_{tot}}{t_1^2 V_{tot}}\right)\left(\frac{C_{tank} V_1}{t_1 V_{tot}}\right) U_{Bt_1} U_{Bt_{tot}}$$

The rest of the analysis for determining the area bias error, U_{BA} has been done previously, with the final result being Equation 3.29.

Density

The density bias error is unchanged from the previous analysis.

The uncertainty terms that have been determined can now be substituted into Equation 3.15 to yield the bias error for the system.

Case 2: Precision Error

Mass

The mass precision error is unchanged from the previous analysis.

Gas Flow

There are now two gas flows which need to be measured. The equation for the total flow is

$$F_{tot} = \frac{V_1}{t_1} + \frac{V_2}{t_2} = F_1 + F_2 \tag{3.49}$$

Since the partial derivatives of F_1 and F_2 are 1.0, the flowrate precision uncertainty equation is

$$U_{PF}^2 = (U_{PF_1})^2 + (U_{PF_2})^2 \tag{3.50}$$

Area

The equation for contaminant concentration is a function of two flowrates and can be written in the following form

$$C = \frac{C_{tank}F_1}{F_{tot}} \tag{3.51}$$

The uncertainty equation for the contaminant concentration is (from Equation 3.7)

$$U_{PC}^2 = \left(\frac{\partial C}{\partial C_{tank}}U_{PC_{tank}}\right)^2 + \left(\frac{\partial C}{\partial F_1}U_{PF_1}\right)^2 + \left(\frac{\partial C}{\partial F_{tot}}U_{PF_{tot}}\right)^2 \tag{3.52}$$

Once the partial derivatives of Equation 3.51 are taken, they can be put into Equation 3.52 and the final form for the concentration precision error is

$$U_{PC}^2 = \left(\frac{F_1}{F_{tot}}U_{PC_{tank}}\right)^2 + \left(\frac{C_{tank}}{F_{tot}}U_{PF_1}\right)^2 + \left(\frac{-C_{tank}}{F_{tot}^2}U_{PF_{tot}}\right)^2 \tag{3.53}$$

The rest of the analysis for determining the area precision error, U_{PA} has been done previously, except that multiple flowrates yield a concentration precision error. The final form of the area precision error equation is

$$U_{PA}^2 = \left(t_{end} - \frac{I}{\overline{V}_{max}}U_{PC}\right)^2 + (CU_{Pt_{end}})^2 + \left(\frac{C}{\overline{V}_{max}^2}I\, U_{P\overline{V}_{max}}\right)^2 + \left(\frac{-C}{\overline{V}_{max}}U_{PI}\right)^2 \tag{3.54}$$

Density

The density precision error is unchanged from the previous analysis.

The uncertainty terms that have been determined can now be substituted into Equation 3.15 to yield the precision error for the system.

Both the bias and precision uncertainty values can be placed into Equation 3.16 and the total uncertainty can now be determined for the system.

3.3.3 Results

Case 1 (no diluent)

Final results for the system uncertainty yielded total error values for q ranging between 6 - 8% for Case 1. The bias error is nearly two times larger than the precision error for this case and is caused by the bias error of the contaminant concentration (±5.0%). The second largest error is the precision error for the atmospheric pressure at ±2.7%. Although this error could be reduced by taking measurements on a daily basis and statistically determining the precision error resulting from the human measurements, it is unnecessary at this time because the contaminant concentration error is the driving factor in the system. The third and final major source of error is the flow measuring system. The flow errors for the single flow case were: bias error of ±2.5% and precision error of ±.8 ml/min.

Case 2 (diluent present)

The results for the Case 2 analysis give a range of errors for q spanning from 7 to 15%. The low errors are dominated by the concentration bias error in the same manner as the single flow case. The larger errors are brought about by diminishing solute flowrates as the concentration becomes more and more dilute. At present, the high flowrate measurements are set at ±0.8 ml/min and the low flowrates are set at ±0.5 ml/min. As the measured solute flowrates become smaller, the percent error increases and hence

the results listed. Other errors present in this system are the same as Case 1 and will not be mentioned here.

Bias errors and sources

U_{Bm} :bias uncertainty caused by mass balance, ±0.00007 gram

U_{BF} : bias uncertainty for flowrate, (ml/min)

flowmeter: ±2.5% for both 1.0 and 10.0 ml volumes

time: one-half least significant digit of clock, ±0.05 second

U_{BA} : bias uncertainty for area, (ppm s)

A/D converter: ±0.0012 volt

FID: ±0.001 volt (assumed)

total voltage error is .0016 volt (applies to $\overline{V}_{max}$ and V(t))

contaminant conc.: ±5.0% for all contaminant types used in this system

time: ±1.0 second (applies to t_{end} and t)

$U_{B\rho_{N_2}}$: bias uncertainty for density, (gmole/m³)

temperature: one-half least significant digit of thermometer, ±0.5 K

gas constant, R : property value assumed to have an error of ±2.0%

pressure: ±1.7 pa, negligible relative to the avg. total pressure of 98,508 pa.

Precision errors and sources

U_{Pm} : precision uncertainty caused by mass balance and transfer losses (combined), ± 0.0005 gram

U_{PF} : precision uncertainty for flowrate, (ml/min)

high flowrate: ± 0.8 ml/min

low flowrate: ± 0.5 ml/min

U_{PA} : precision uncertainty for area, (ppm s)

t_{end} : error for time at end of test; 0.5 second

$\overline{V}_{max}$: error caused by noise in signal; 0.005 volts

I: integration error caused by trapezoidal integration; variable

$U_{P\rho_{N_2}}$: precision uncertainty for density,(gmole/m^3)

temperature: ± 1.4 K

pressure: $\pm 2.7\%$

REFERENCES

Alltech Catalog #200, address: Alltech Associates Inc. 2051 Waukegan Road, Deerfield IL 60015, 1989.

Buffington, R. and Wilson, M. K., *Detectors for Gas Chromatography - A Practical Primer*, Hewlett Packard part number 5958-9433, Printed in U.S.A., 1991.

Cheney, W. and Kincaid, D., *Numerical Mathematics and Computing, Second Edition*, Brooks/Cole Publishing Company, Monterey, California, 1985.

Coleman, H. W., and Steele, W. G., *Experimentation and Uncertainty Analysis for Engineers*, Wiley-Interscience, 1989.

Hewlett-Packard 5890 Series II Reference Manual, Third Edition, Printed in U.S.A., 1990.

Hewlett Packard 1992 Chromatography Users Catalog, Printed in U.S.A., 1992.

Kyle, B. G., *Odor Removal from Air by Adsorption on Charcoal*, Distributed by: National Technical Information Service, 1974.

KaleidaGraph™ data analysis/graphics program. Synergy Software (PCS Inc.) 2457 Perkiomen Avenue, Reading PA 19606.

Liquid Carbonic Specialty Gas Corp Catalog, Form 6466 R90, Printed in U.S.A., 1991. address: 640 E. Polk St., Milwaukee, WI 53202.

Matheson Gas Products Catalog, Printed in U.S.A., 1990. address: Matheson Gas Products, Post Office Box 1587, Secaucus, N.J. 07096-9801.

McNair, H. M. and Bonelli, E. J., *Basic Gas Chromatography*, Printed in U.S.A., 1968.

Myers, G. E., *Engineering Thermodynamics*, Prentice-Hall, Inc., 1989.

NOAA, National Oceanic and Atmospheric Administration *Local Climatological Data*; Monthly data from 1989-1991, available from National Climatic Data Center; Asheville, North Carolina.

Schaefer, M. *Measurements of Adsorption Isotherms by Means of Gas Chromatography,* M.S. Thesis in Chemical Engineering, University of Wisconsin-Madison, 1991.

Chapter 4

BEHAVIOR OF ACTIVATED CARBON

Before isotherm data can be obtained, the experimental system and procedure must be able to duplicate the measurements within the expected uncertainty. To ensure that this can be done, an investigation concerning the behavior of the activated carbons and the contaminants used in this study was completed. Three main issues were addressed concerning the activated carbons and the contaminants.

1) The extent of losses in adsorptive capacity when a sample is cycled through several adsorption and desorption runs.

2) The assumption that physical adsorption is the sole type of adsorption occurring (it is possible that chemical adsorption is occurring as well).

3) The ability of data to be duplicated. If this can not be accomplished, then the reason for this needs to be determined.

The answers to these issues will provide the information necessary to determine the methods used in acquiring acceptable data.

4.1   BEHAVIOR OF CALGON CARBON OL 20x50

Carbon OL 20x50 (manufactured by Calgon Carbon Corporation and discussed in Appendix D) was the first carbon to be investigated. It is typically used for water filtration but is studied here because it was used by Schaefer (1991) and follow up work was needed. Technical information concerning this carbon is given in Appendix D. Isotherms were taken by Schaefer (1991) with the adsorbate being acetone. Concentrations ranged from 2.5 to 50.4 ppm (by volume) in nitrogen. Temperatures at which isotherms were obtained varied from 27 to 130°C. These isotherms were taken using one sample of activated carbon. It was assumed at this time that the carbon was not losing adsorptive capacity and that the method of data acquisition was adequate.

In attempting to duplicate the original isotherms, it became apparent that the carbon filter had lost up to 40% of its original adsorptive capacity. Figure 4.1 shows the original isotherms and also the duplication isotherms taken at 40, 55 and 100°C.

After observing the results in Figure 4.1 several problems needed to be addressed: the reason for capacity loss; the rate at which this loss occurred; and whether or not a steady-state adsorptive capacity of the activated carbon is ever reached. To examine these problems, a virgin sample of OL 20x50 was used to prepare a new filter. Forty eight consecutive tests of adsorption at 100°C and desorption at 175°C were then completed. Acetone was the adsorbate with the concentration being 50.4 ppm. The results are shown in Figure 4.2. The data in Figure 4.2 show that the carbon is losing capacity in a gradual manner with a steady-state value apparently reached by test number forty one. The maximum amount of degradation during these trials was 27%.

The next question posed was to determine the cause of the degradation. There are several possibilities why this loss is occurring.
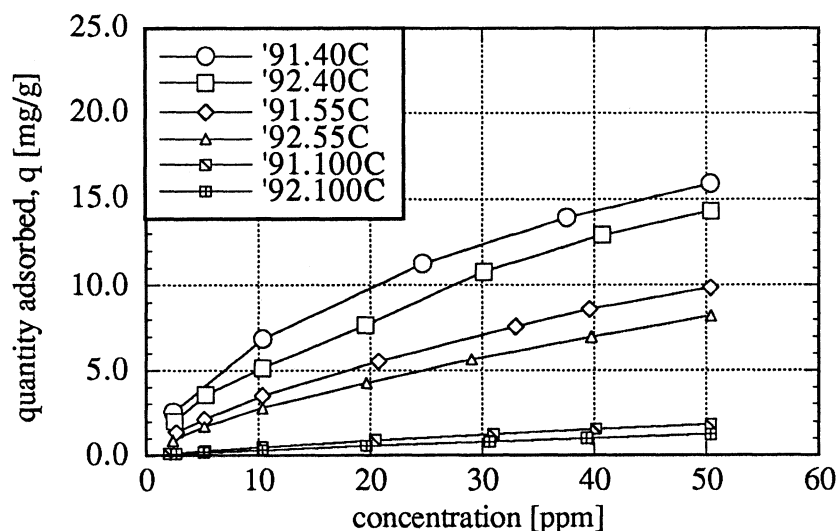
Figure 4.1   Duplication of isotherms with acetone on carbon OL 20x50.

System Uncertainty

The uncertainty analysis in Chapter 3 yielded a system uncertainty which varied from 6 to 8 percent for the single flow case. It is possible that this determination was incorrect and that the error is really much larger. The error could even so great as to make it seem like a large loss in adsorptive capacity occurred, although it really did not. If this were indeed the case, large fluctuations in adsorptive capacity would be seen from test to test in Figure 4.2. This phenomena did not occur, rather, a gradual decrease in capacity is seen. The trend in Figure 4.2 then proves system uncertainty is not the factor causing the large degradation.
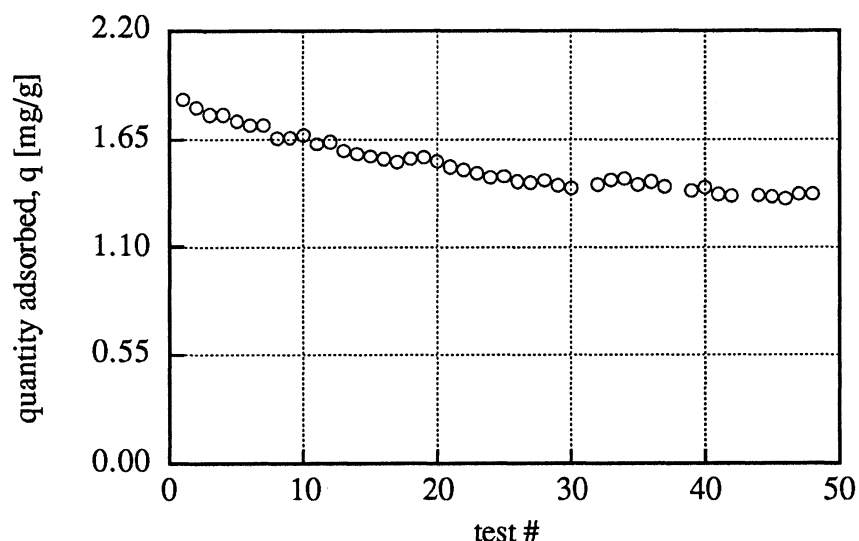
Figure 4.2   Consecutive runs with acetone (50.4 ppm) at 100°C on carbon OL 20x50.

Thermal Cycling

Thermal cycling of the carbon during testing may degrade it in some manner. All desorption was done at 175°C while adsorptive runs were done at various temperatures. This potential cause of degradation was investigated with the results shown in Figure 4.3. A virgin sample of OL 20x50 carbon was used to make a new filter. Acetone was the contaminant with the concentration being 50.4 ppm. Two initial runs were done at 100°C to determine the adsorptive capacity of the activated carbon. Twenty thermal cycles were then completed. A thermal cycle consisted of 45 minutes at 175°C and two hours at 100°C with a pure nitrogen gas stream passing through the system at all times. The amount of time designated at 100°C and 175°C was used to simulate a typical adsorption-desorption test. The gas chromatograph was programmed for this task to permit uniform cycling times. After the twenty thermal cycles, two tests with acetone

at 50.4 ppm at a temperature of 100°C were executed. It is evident that only a small amount of degradation had occurred. When comparing the percent change between the first and twenty-third tests in Figure 4.2 and 4.3, it is seen they are quite different at values of -20.0% and -4.0%, respectively. After the two tests with acetone were finished, sixteen more thermal cycles were done and a final two data points with acetone present (under the same conditions as stated previously) were taken with results showing negligible loss in capacity relative to that experienced in Figure 4.1 (Test 41 in Figure 4.2 is at -26% whereas the corresponding test in Figure 4.3 is at -10%). The conclusion from this series of tests is that thermal cycling has little, if any, effect on the loss of adsorptive capacity of the carbon.
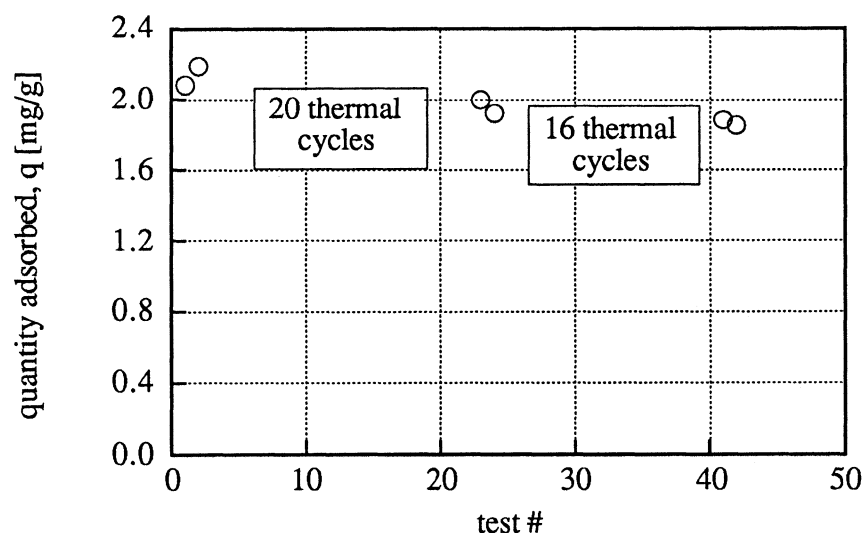
Figure 4.3   Investigation of thermal cycling. Testing was done with acetone (50.4 ppm) at 100°C on carbon OL 20x50.

Physical and Chemical Adsorption

Two other possibilities which may explain the loss of adsorptive capacity are physical adsorption and chemical adsorption. If physical adsorption occurs, the van der Waals forces between the acetone and the surface of the carbon may be too strong to break all of the adsorption sites, resulting in degradation. The other possibility is chemisorption. Acetone has the chemical formula CH_3COCH_3. The oxygen atom present in this molecule is reactive. Upon coming into contact with the surface of the carbon, this oxygen atom has the potential to form a chemical bond.

All of the likely causes for loss in adsorptive capacity of the carbon have been discussed and ruled out, except for strong physical adsorption and chemical adsorption. Either one or a combination of both appears to be present to some degree and therefore prevents complete regeneration of the carbon with the desorption methods currently in use.

Regeneration Methods

The filter was regenerated (desorbed) at 175°C with pure nitrogen gas passing through the column during this period. The time of regeneration is determined from the signal given by the flame ionization detector (FID) located in the gas chromatograph (see Appendix B). When desorption of the contaminant laden carbon filter begins, the signal from the FID reads in the thousands due to the large amount of adsorbate present in the effluent. After a period of time, the signal decreases to a point where it no longer changes a noticeable amount and this is the point where it is assumed the carbon is completely desorbed. The time to desorb acetone from carbon OL 20x50 varied from 45 minutes to 2 hours using this method. Determining the regeneration time in this

manner may be unacceptable because not all of the solute may have been removed. An investigation ensued to find if this was the case. A carbon sample was desorbed for a period of 10 days and 15 hours with the results shown in Figure 4.4 (desorption took place between tests eight and nine) Test number nine shows a 20% improvement in capacity over test number eight. However, when looking at test number ten, it is observed that most of the capacity gained from the long desorption time was negated. Kovach (1973) mentions that in industry the method of regeneration (similar to the activation process) typically destroys 10% of the carbon through burning and attrition. Kovach (1973) recommends that the carbon lost be replaced with virgin carbon to ensure adsorptive capacity of the bed remains at an acceptable level. In this test, the quality of the carbon appears to have gone down, even though a significant improvement in adsorptive capacity was initially seen. Also, the results displayed in Figure 4.4 indicate a very long period of time is necessary for adequate regeneration. This large amount of time is unsuitable due to the limited number of tests which could be completed and therefore indicates that either the method of regeneration must be changed in some manner or different carbons and different contaminants should be tested that are easily desorbed.

Steady-State Adsorptive Capacity

Because the current system is unable to completely regenerate the carbon with acetone as the contaminant, a new method was implemented to try to have the carbon reach steady-state (as was done in Figure 4.2) in a rapid manner. If this could be accomplished , the amount of time saved would be significant and duplication of the isotherm data could then be achieved. The procedure involved saturating the carbon

with liquid acetone, letting it stand for a period of time (sealed from the environment to prevent the acetone from escaping) reinstalling the glass column into the gas chromatograph, desorbing the carbon and then passing acetone at a concentration of 50.4 ppm at a temperature of 100°C to determine if loss in adsorptive capacity took place. Figure 4.5 shows the first attempt to attain constant capacity in rapid fashion. Three runs were initially taken to determine the capacity. Then approximately 100 μL of 99.5 mol % pure acetone was injected into the
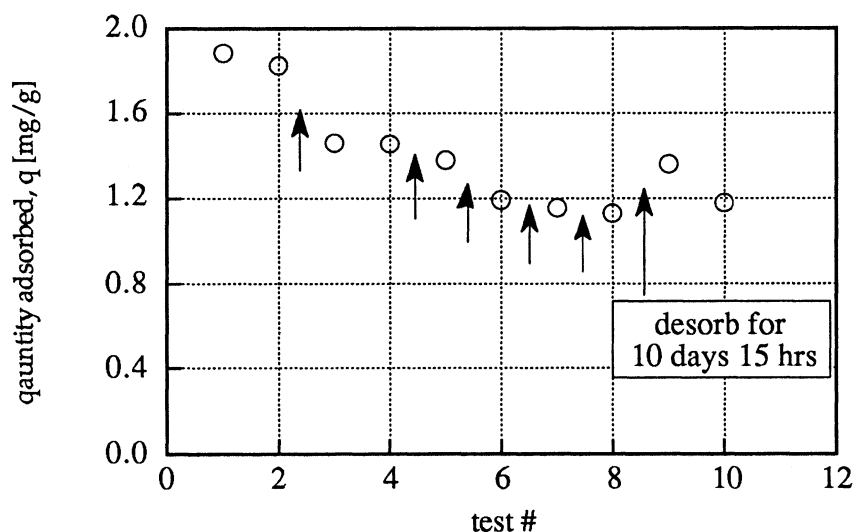
Figure 4.4 Liquid acetone injections done at 100°C. Testing was done with acetone (50.4 ppm) at 100°C on carbon OL 20x50.

packed bed. After a period of 21 hours the column containing the carbon filter was placed into the oven of the gas chromatograph and desorbed. Following this, two tests involving gaseous acetone (50.4 ppm) at 100°C were completed to determine if any large amount of degradation occurred. It did not, so the same procedure was tried again with little success as can be seen by the sixth data point in Figure 4.5. At this time it was thought that placing the saturated filter inside the chromatograph oven

(with both ends of the column sealed to prevent acetone from escaping into the oven) for a period of time might bring about the desired goal of reaching steady-state in a rapid manner. Figure 4.4 displays the results from these trials. Again, initial tests involving gaseous acetone at a concentration of 50.4 ppm at a temperature of 100°C were taken to determine the adsorptive capacity of the new carbon sample. After
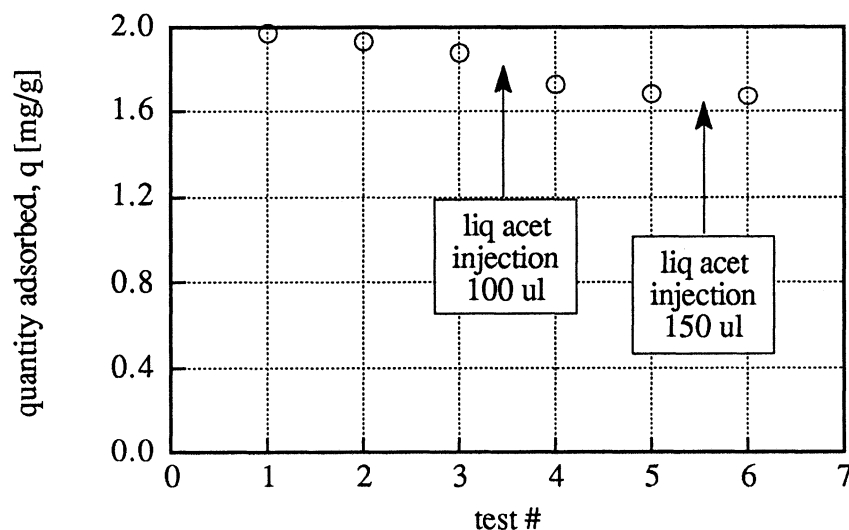
Figure 4.5 Liquid acetone injections done at ambient conditions. Testing was done with acetone (50.4 ppm) at 100°C on carbon OL 20x50.

injecting 200 μL of liquid acetone into the filter, the column containing the filter was placed into the oven at 100°C for a period of 13.5 hours. Tests after the first injection showed a 22.6% reduction in capacity and further tests involving the same amounts of liquid acetone and approximately the same amount of oven time also resulted in a continuing loss of capacity of the carbon. Test number eight is 40% less than the initial adsorptive capacity with no indication that steady-state has yet been reached.

The method to obtain the steady-state adsorptive capacity of the carbon sample was not successful for two reasons. First, there is still no sign of steady-state being reached, and second, the time required to obtain the information in Figure 4.4 spanned over several days, meaning this method of obtaining steady-state (if steady-state could be found) is not rapid enough to warrant its use.

Low Temperature Tests

The liquid acetone injections at ambient temperatures (Figure 4.5) result in approximately no loss in adsorptive capacity of the carbon. Because of this, it was thought the high temperature testing at 100°C (where degradation of the carbon was observed) might not be representative of actual air filtration operations. To see if this was the case, testing was done for twelve cycles with acetone at a concentration of 50.4 ppm at a temperature of 35°C. The temperature for these tests was not ambient because the gas chromatograph is not capable of maintaining a stable temperature at that level since it is not fitted with cooling equipment. The results of these tests illustrate a greater rate of capacity loss than at higher temperatures. This result can be explained by noting that if strong physical or chemical adsorption is occurring, more acetone will adhere to the carbon surface per test because larger amounts of contaminant are adsorbed at lower temperatures. For example, the amount of degradation at run number twelve in Figure 4.6 is -21.5% while in Figure 4.2 the corresponding value was -11.6%. However, in both cases the trend downward in overall adsorption capacity exists. The conclusion can therefore be drawn that the tests at high temperatures are representative of the behavior of the carbon at lower temperatures.
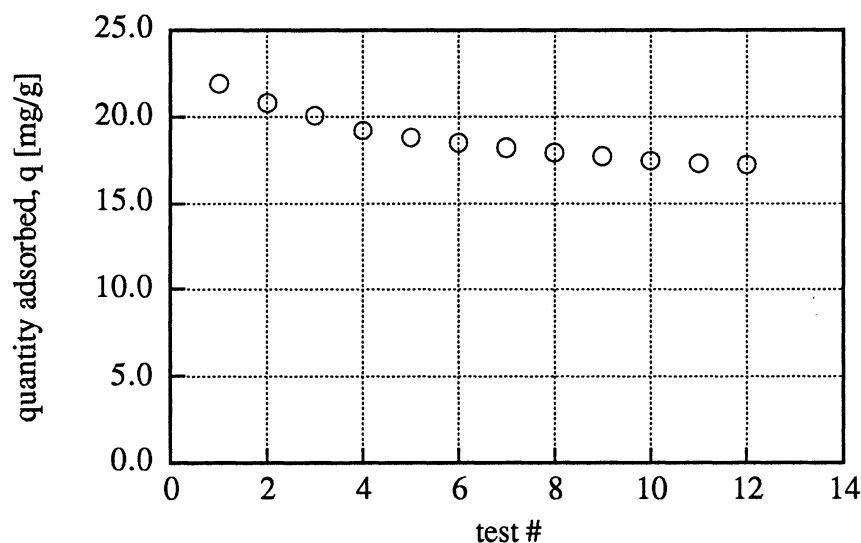
Figure 4.6   Consecutive tests with acetone (50.4 ppm) at 35°C on carbon OL 20x50.

4.2 BEHAVIOR OF OTHER CARBONS

Because the main use of Calgon OL 20x50 is water filtration, its behavior with other contaminants was not pursued. Instead, samples produced for air filtration were investigated. Three such samples were obtained from NUCON International, Inc. Technical information for these carbons is provided in Appendix D. The samples were made from base materials of coal, coconut and wood. All of the samples were manufactured using the steam activation method. Different base material carbons were selected to investigate their adsorptive capacity involving three individual contaminants; acetone, toluene and propane. The contaminants were selected because they represent the ketone, alkane and aromatic groups of organic compounds Also, the experimental system has no hood to vent toxic gases and these contaminants present no direct health threat to other people present in the laboratory. Testing involved a virgin

carbon sample which was subjected to one of the contaminants for a designated number of tests similar to that obtained for Calgon OL 20x50 in Figure 4.2. Once established, this data base provided the information necessary to decide which carbon(s) and contaminant(s) to be used for generating experimental isotherms.

4.2.1 Acetone Tests

The first set of data taken with the three carbons were performed with acetone at a concentration of 50.4 ppm and a temperature of 100°C. Both expected and unexpected results were obtained. Figure 4.7 shows the adsorptive capacity of each of the carbons decreases with the number of tests taken. This result was found previously and is expected but the behavior of Nusorb G65 50x150 (coconut) from test number one to
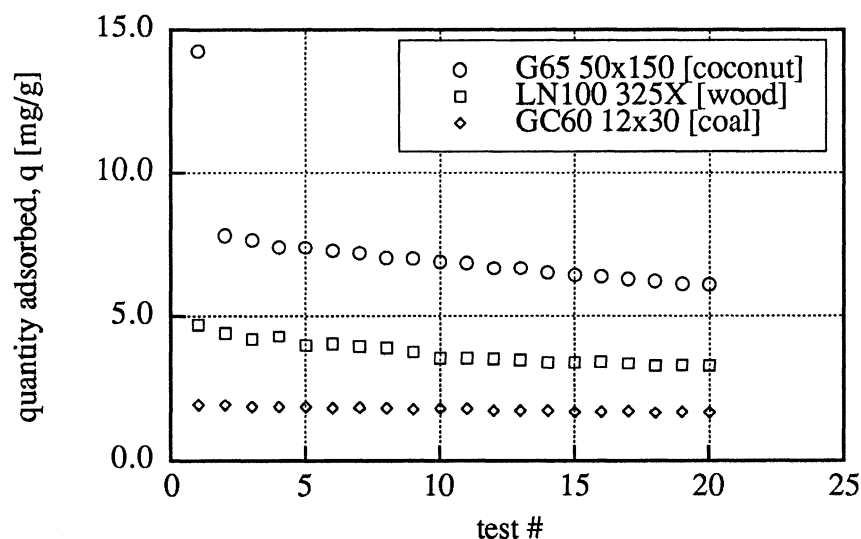
Figure 4.7   Consecutive tests with acetone (50.4 ppm) at 100°C. Carbons tested are from NUCON International, Inc.

test number two was not. A forty-five percent decrease in adsorptive capacity was observed between these two trials. The possibility exists that these data are invalid because of improper test procedure. To ensure that the carbon was indeed behaving as shown, two new samples of G65 50x150 carbon were prepared and tested. Results are shown in Figure 4.8. The duplication data confirmed that this large drop in adsorptive capacity is characteristic behavior of G65 50x150 carbon when exposed to acetone under the stated conditions.

Although the trend involving acetone as the contaminant was confirmed, Figure 4.8 shows a disturbing development. Test number one of Filter 2 is located outside the uncertainty bars. This problem must be examined. First, it should be noted that the uncertainty analysis involved a 95% confidence interval and that a 99% confidence
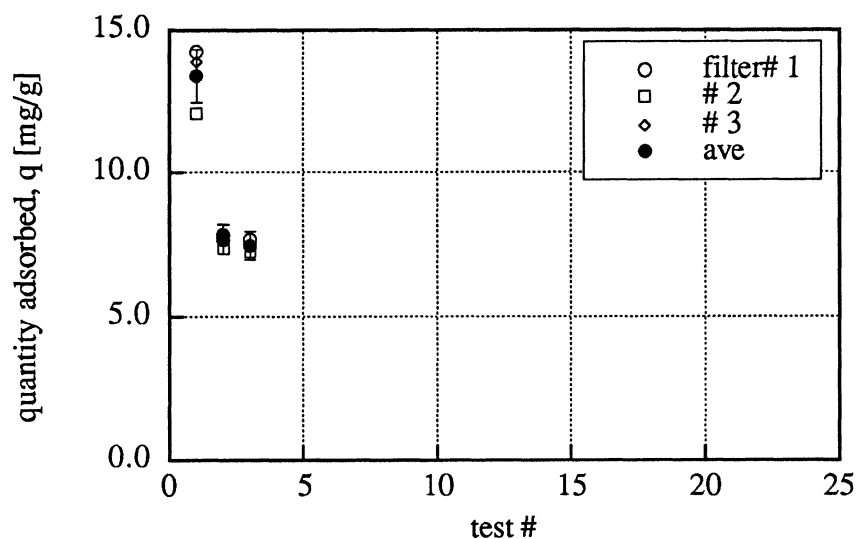
Figure 4.8   Duplication data of G65 50x150 carbon with acetone (50.4 ppm) at 100°C.

interval would contain this point. But, none of the data in Figures 4.3 and 4.7, indicate the type of discrepancy shown in Figure 4.8. It can be concluded from this observation that the outlier is not a result of the system or data acquisition method but rather is a result either of a nonhomogeneous mixture of carbon from which the sample was drawn or the possibility that initial preparations of a new sample involving six hours of desorbing at 175°C with nitrogen passing through the column is inadequate to bring about equal adsorptive capacities.

One other note should be made about the carbons in Figure 4.7. The numbers 65, 100 and 60 present in the identification of the carbons indicates how much carbon tetrachloride CCl_4 can be adsorbed (as a percentage of the carbon weight) under a certain set of conditions (See ASTM D3467-88). Although this value is indicative of the adsorptive performance of the carbons, it does not mean the carbon adsorbing the most CCl_4 will always adsorb the greatest amount of contaminant. The results in Figure 4.7 make this statement clear, where the coconut based carbon, G65 50x150, adsorbed more acetone than the carbon which adsorbed 100% of its own weight of CCl_4.

4.2.2 Toluene Tests

Figure 4.9 displays results involving the three carbons with toluene as the contaminant. Again, the coconut based carbon adsorbs the greatest amount, but this time the coal based carbon adsorbs more toluene than the wood based carbon. After the first two tests, the coconut based carbon experiences a 15.0% decline and for the remaining tests, the capacity remained approximately unchanged. The two other carbons display a small loss in capacity, 5.0% for G60 20x30 and 2.6% for LN100 325X.
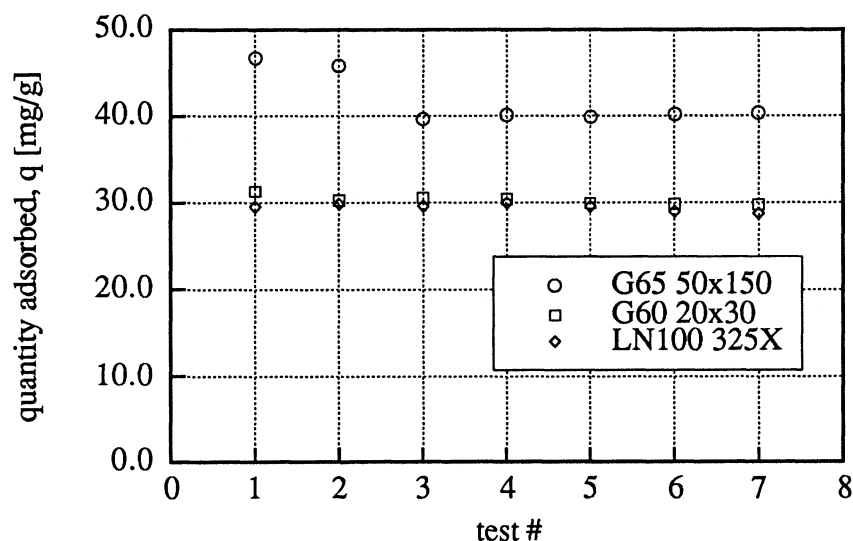
Figure 4.9   Consecutive tests with toluene (10.31 ppm) at 100°C. Carbons tested are from NUCON International, Inc.

Although the amount of toluene adsorbed was much greater than that of acetone, relatively little loss in capacity was noticed. The reason for this may be that little or no chemisorption is taking place. Since toluene has the formula C_7H_8, there are no oxygen atoms present in this molecule (as there is in acetone) to react with the carbon surface.

Because the coconut-based carbon adsorbed the most contaminant and it appears to have reached steady-state quickly, another sample of this carbon was tested with toluene under the same conditions stated previously to see if the results could be duplicated. The data obtained are shown in Figure 4.10. Unlike the acetone duplication data (Figure 4.8) all data points obtained were within the bounds of the uncertainty analysis. Although the mass of carbon in each of these filters was less than

that used for the acetone tests, the data indicates that homogeneity exists between the two samples.
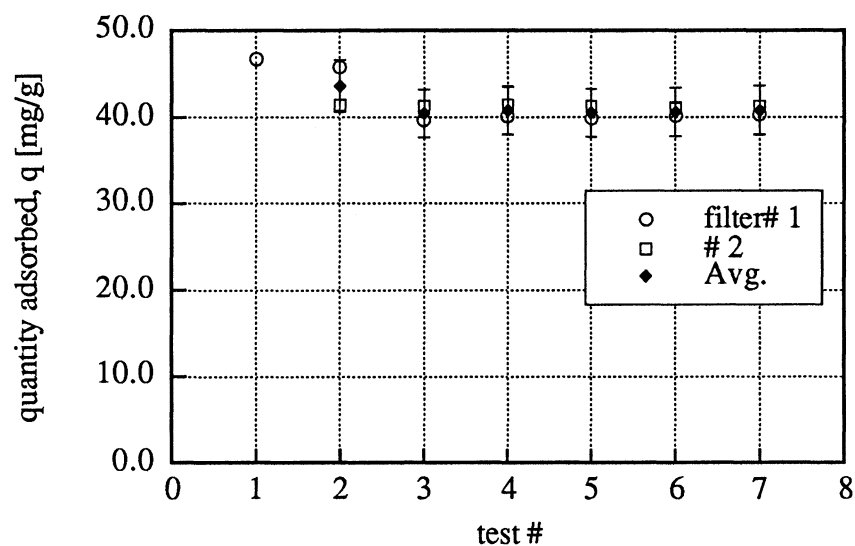
Figure 4.10 Duplication data of G65 50x150 with toluene (10.31 ppm) at 100°C.

4.2.3 Propane Tests

Results involving propane are shown in Figure 4.11. Only two carbons were tested with propane (G65 50x150 and G60 12x30) because the filters necessary for successful test runs were much larger than previously needed and the mesh size of the wood based carbon (LN100 325X) was too small. The large pressure drop that would have resulted from using LN 325X was unsuitable for this system. No degradation was observed for the two samples which were tested. There are multiple reasons for this result. First, the small size of the propane molecule results in low amounts being adsorbed. It would take a large number of tests to adsorb the same amount of propane onto the carbon sample as one test with toluene at the same test conditions; therefore, if loss in
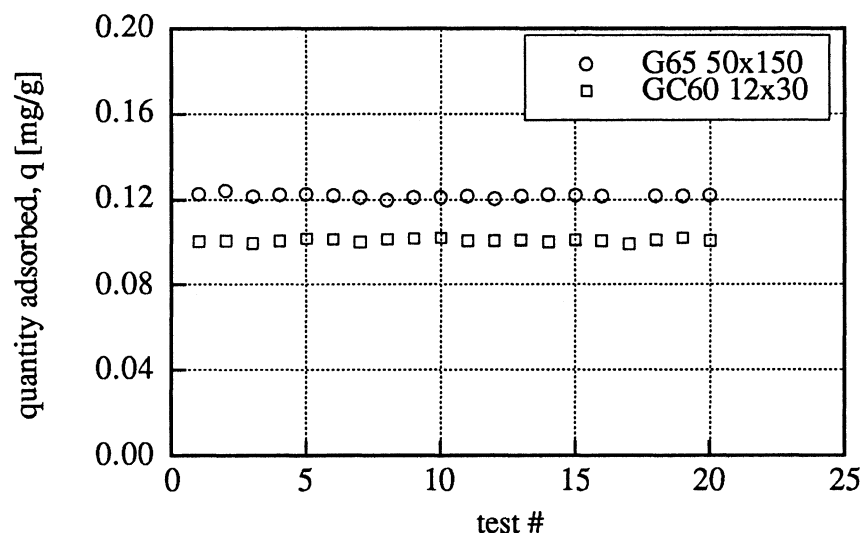
Figure 4.11 Consecutive tests with propane (43.9 ppm) at 100°C. Carbons tested are from NUCON International, Inc.

capacity is occurring, it may hardly be perceptible because of the small amount adsorbed. Second, like toluene, no oxygen is present in propane; thereby reducing the possibility of chemisorption. Third, the small molecules of propane are weakly held by physical adsorption and are easily driven off during regeneration.

To see if the results shown in Figure 4.11 could be duplicated, three more samples of carbon G65 50x150 were tested with propane under the same conditions stated previously. The data obtained are shown in Figure 4.12. Unlike the acetone duplication data (Figure 4.8) all data points obtained were within the bounds of the uncertainty analysis, possibly because the relatively large amount of carbon used in the filters for these tests (3 to 5 times larger than those used in acetone testing for carbon G65 50x150). The larger mass may result in a more homogeneous sample being extracted from the source.
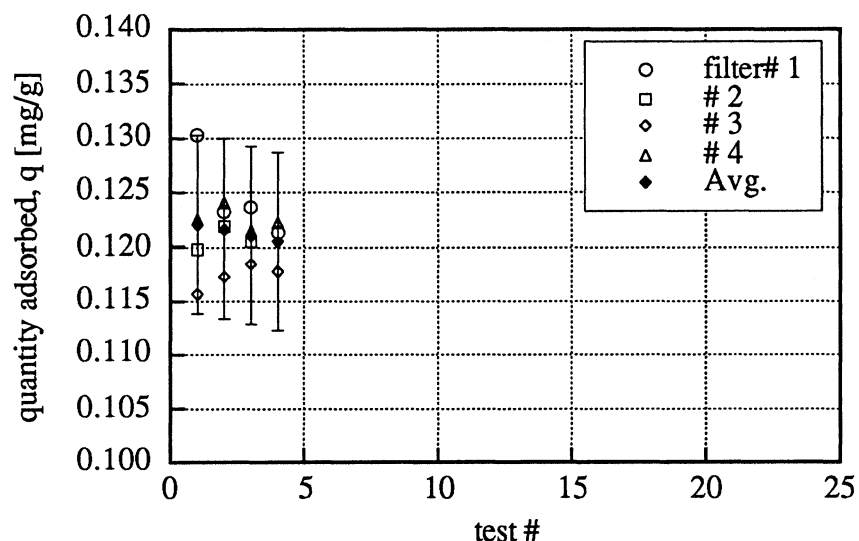
Figure 4.12   Duplication data of G65 50x150 with propane (43.9 ppm) at 100°C.

4.3   SUMMARY AND CONCLUSIONS

The first carbon tested was OL 20x50 manufactured by Calgon Carbon Corporation. Tests done with this carbon involved acetone as the contaminant. Because a loss in adsorptive capacity was occurring with acetone, an investigation took place to find the cause. The possible causes included: system uncertainty, thermal cycling, regeneration method and strong physical and/or chemical adsorption. Conclusions from the completed tests indicate that either strong physical adsorption, chemical adsorption or a combination of both were occurring.

Other carbons made for air filtration purposes were tested with the contaminants of acetone, toluene and propane. The carbons were each made of a different base material: coal, coconut and wood. Tests with acetone yielded a loss in capacity for each of the carbons. Tests involving toluene experienced a small amount of

degradation and the propane tests resulted in no loss in adsorptive capacity. It is believed that toluene and propane cause minimal degradation because no oxygen atom is present in their respective molecules to react with the carbon surface. Acetone should not be tested with the current method of analysis because the data would be virtually impossible to reproduce. The other two contaminants, toluene and propane caused a minimal amount loss in adsorptive capacity and it is thought that duplication of data is possible using current procedures. The cause for the data point in Figure 4.8 (acetone tests) to be outside of the uncertainty bars is thought to be due to either a nonhomogeneous carbon source from which the samples were drawn (which seems to be refuted by the toluene and propane duplication tests), or because the six hour desorb time before the first test was unable to purge some contaminant which was inserted into the carbon during the filter making process.

REFERENCES

ASTM D3467-88: Carbon Tetrachloride Activity of Activated Carbon.

Kovach, J. L., *Activated Carbon in Air Purification, Part I*, Nuclear Consulting Service Inc., P.O. Box 29151, Columbus, OH 43229, 1973.

Schaefer, M. *Measurements of Adsorption Isotherms by Means of Gas Chromatography,* M.S. Thesis in Chemical Engineering, University of Wisconsin-Madison, 1991.

Chapter 5

THEORY, ANALYSIS AND MODELING

It was found in Chapter 4 that carbon G65 50x150 had superior adsorptive capability over the other carbons when tested with the individual contaminants of acetone, toluene and propane. Carbon G65 50x150 also has a desirable mesh size which eliminates channeling and edge effects in the glass column [Kyle, et al. (1974)]. For these reasons, carbon G65 50x150 has been selected to be tested further. Testing will include investigating the equilibrium adsorptive capacity of the carbon and the dynamic behavior of the packed bed with contaminants toluene and propane. Toluene and propane were selected because testing done in Chapter 4 showed that it was possible to duplicate tests involving these contaminants. The dynamic equilibrium information will be used to generate isotherms which will then be modeled using the Henry [Smisek and Cerny (1970)], Langmuir (1918), Freundlich [Smisek and Cerny (1970)] Dubinin-Astakhov (1971a) equations. The kinetic behavior of the contaminants passing through the packed bed will be investigated using a modified version of the homogeneous-solid diffusion model [Forsythe (1988)]. The sources listed for the Henry, Freundlich and homogeneous-solid diffusion models are secondary.

5.1 DYNAMIC EQUILIBRIUM ANALYSIS

5.1.1 Equilibrium Theory

Isotherms, Isobars and Isosteres

Adsorption equilibrium data are used to generate what are called isotherms, isobars or isosteres. An isotherm is defined to be a plot of the amount of contaminant adsorbed q, versus the concentration or partial pressure of the contaminant at constant temperature. The amount adsorbed is usually represented in mass or mole units on a per mass or per mole of adsorbent basis. Isobars are similar to isotherms except in this case the partial pressure is held constant and the temperature is varied. Isosteres are obtained by holding q constant and plotting concentration or partial pressure against temperature. Figures 5.1, 5.2 and 5.3 show typical isotherms, isobars and isosteres, respectively.
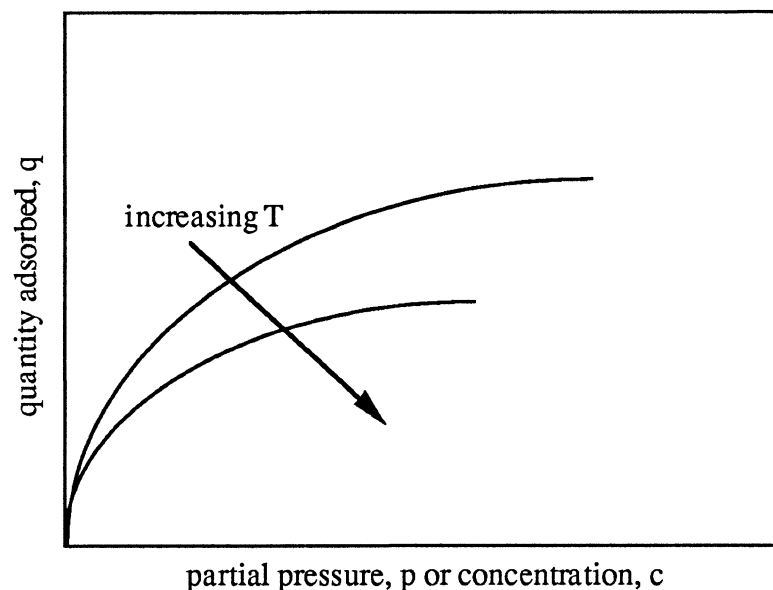
Figure 5.1   Adsorption isotherms.
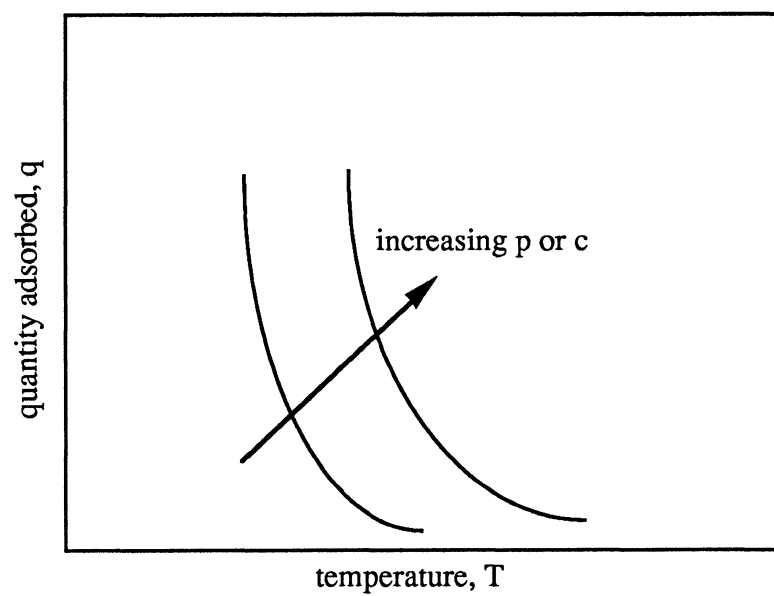
Figure 5.2   Adsorption isobars.
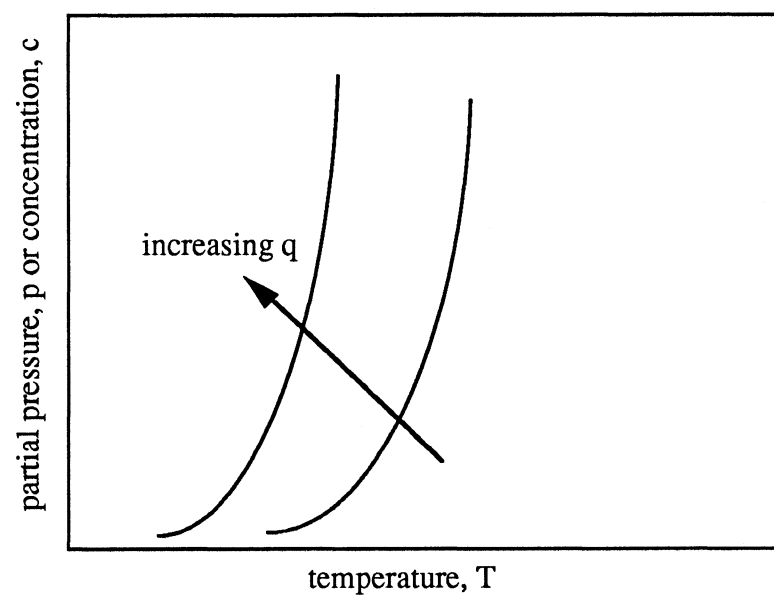
Figure 5.3   Adsorption isosteres.

Isotherms are the most common method of plotting equilibrium adsorption data; however, because the information obtained for these plots is taken when the system is at equilibrium, any one type of plot may be used to generate the other two.

Information From Isotherms

The main purpose of adsorption isotherms is to provide a basis for dynamic equilibrium modeling. Aside from this use, experimentally determined isotherms yield a significant amount of information about adsorbents and their behavior with different adsorbates. Both the heat of adsorption and the adsorbent surface area can be determined from isotherms. Also, the shape of the isotherm gives qualitative information concerning the adsorbent. Brunauer, et al. (1940) has classified five different isotherms (Figure 5.4). The qualitative information about each is listed below.

Type I isotherms display a system where only a monomolecular layer of particles is adsorbed onto the surface of the adsorbent.

Type II isotherms are representative of systems in which a monomolecular layer is first formed and then further multi-layer adsorption occurs.

Type III isotherms result when an unknown amount of molecular layering takes place.

Type IV isotherms experience multiple layers of molecules adsorbing on the surface and eventually reaches a limited quantity.

Type V isotherms occur when intermolecular forces between molecules are relatively large.

The class of isotherm worked with in this study is Type I.
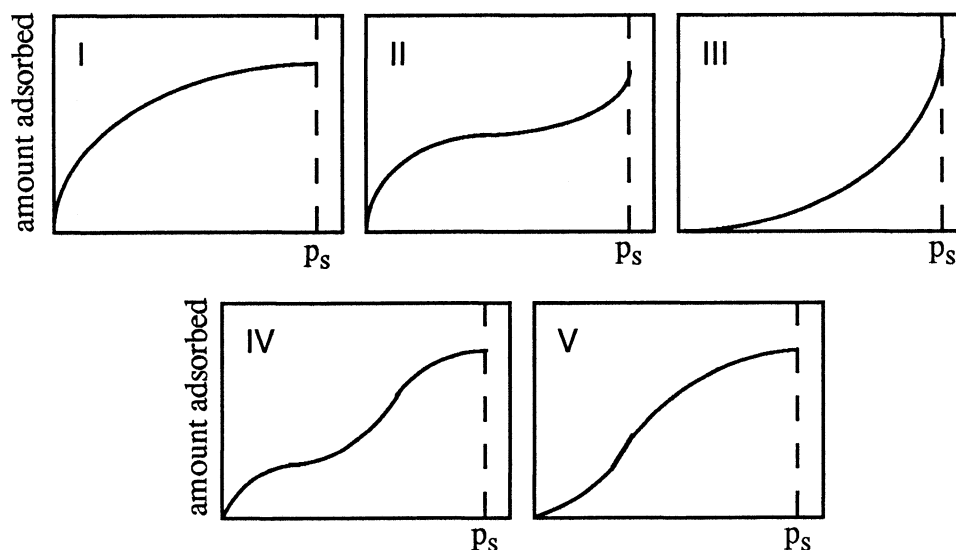
Figure 5.4 Display of the BET isotherms.

Isotherm Models

Several models have been derived in an effort to emulate experimentally determined isotherms. Some well known expressions include the Henry, Langmuir, Freundlich, Temkin, Brunauer-Emmett-Teller and Dubinin-Astakhov equations. The Temkin, Langmuir and Freundlich equations are generally applied to chemisorption, but the latter two models are sometimes fit to physical adsorption isotherms as well. The four types of isotherm models worked with in this analysis are the Henry, Langmuir, Freundlich and Dubinin-Astakhov types.

Henry's Isotherm

The simplest isotherm model that exists is Henry's Isotherm. This model states that the amount adsorbed (described as the volume V, of gas removed by adsorption from the vapor phase [Smisek and Cerny (1970)]) is directly proportional to the partial pressure

of the adsorbate in the solute. The constant k in Equation 5.1 is the slope of the isotherm.

$$V = kP \qquad\qquad (5.1)$$

The model is valid only where small amounts of contaminant are adsorbed, usually not covering more than fractions of one percent of the total surface area of the adsorbent. Theoretical derivations have been done [Young and Crowell (1962)] assuming that the gas and adsorbed phase is dispersed enough to warrant the use of ideal properties.

The Langmuir Isotherm

The Langmuir Isotherm model was the first to be developed in a theoretical manner. Smisek and Cerny (1970) mention there are three assumptions involved in this derivation. First, the adsorption is monomolecular. If a molecule contacts a position already occupied, it bounces off in a completely elastic manner. Second, the surface is homogeneous in the sense that the chance a molecule has of adsorbing on one position is the same as any other position on the surface. The third assumption is that the force of attraction between molecules is approximately zero. Initially derived from molecular-kinetic principles, the Langmuir Isotherm has since been determined by employing thermodynamical principles and many statistical procedures as well [Smisek and Cerny (1970)]. It will be discussed here using the molecular-kinetic approach.

Derivation begins by first assuming the rates of adsorption and desorption are equal when the system of adsorbate and adsorbent is in equilibrium (represented by either

Equation 5.2 or 5.3). The term $\nu\alpha$ is the rate of desorption and the term $\alpha\mu(1 - \theta)$ is the rate of adsorption.

$$\nu\alpha = \alpha\mu(1 - \theta) \tag{5.2}$$

or

$$\theta = \frac{\frac{\alpha}{\nu}\mu}{1 + \frac{\alpha}{\nu}\mu} \tag{5.3}$$

Variables in the equilibrium relation include

α: fraction of the surface covered by adsorbed particles

μ: total number of molecules striking a surface per unit time

ν: rate of desorbing when a monomolecular layer of adsorbate completely covers the surface in question

θ: fraction of the surface covered by adsorbed molecules

Noting that μ is proportional to the partial pressure p when μ is in the gas phase and θ is equal to the ratio of the quantity adsorbed q to the maximum amount q_m that could be adsorbed if a monomolecular layer was formed on the surface, Equation 5.3 can be rewritten as

$$q = q_m\frac{k_1P}{1 + k_1P} \tag{5.4}$$

At sufficiently small partial pressures or concentration, Equation 5.4 takes the approximate form

$$q = q_m k_1 P = kP \qquad (5.5)$$

which is Henry's Law.

Validity of Equation 5.4 is found by first rearranging it to the form of Equation 5.6.

$$\frac{P}{q} = \frac{1}{q_m k_1} + \frac{P}{q_m} \qquad (5.6)$$

If P/q versus P is a straight line, then the Langmuir equation is valid, although Smisek and Cerny (1970) point out that just because the isotherm fits the experimental data does not mean that the method of adsorption follows the three assumptions listed above. In fact, adsorption almost certainly does not follow these assumptions because they are too simplified when compared to the complex structure of typical adsorbents .

The Freundlich Isotherm

The Freundlich model is shown in Equation 5.7. It was first derived empirically but

$$q = k_2 P^{1/n} \qquad 5.7$$

has since been determined theoretically using both thermodynamical and statistical methods [Smisek and Cerny (1970)]. The constant k_2 is dependent on temperature, specific surface area of the adsorbent and other factors. The constant n is a function of temperature and is always greater than one [Smisek and Cerny (1970)]. This equation can also be shown in logarithmic form (as given by Equation 5.8).

$$\log q = \log k_2 + \frac{1}{n} \log P \qquad (5.8)$$

The significance here is that if log q versus log P is a straight line, then the equation is valid for the specific case being investigated. One major drawback of the Freundlich model is its inability to predict isotherms at temperatures other than those obtained experimentally. This undesirable feature is a result of the constants k_2 and n and limits the use of the equation to curve fitting experimental data and comparing the obtained coefficients [Smisek and Cerny (1970)].

The Dubinin-Astakhov Isotherm

Ideas from Polanyi and Berenyi [Suzuki (1990)] led to the Dubinin-Astakhov model. The goal of Polanyi and Berenyi was to establish an adsorption equilibrium relation which would be independent of temperature. The result of this work is Equation 5.9.

$$W = \frac{q}{\rho} = W(A) \tag{5.9}$$

where W is the volume of the adsorbent micropores which are filled with adsorbate. The term A is called the adsorption potential which is defined as the change in Gibbs free energy from the adsorbed phase to the saturated liquid phase [Suzuki (1990)].

$$A = -\Delta G = RT\ln\frac{P_{sat}}{P} = -RT\ln\frac{P}{P_{sat}} \tag{5.10}$$

Equation 5.9 was also stated by Dubinin (1975) as

$$\frac{W}{W_0} = f(\frac{A}{E}, n) \tag{5.11}$$

In Equation 5.11, the ratio of the amount adsorbed is a function of the adsorption potential divided by E, the characteristic energy of adsorption. The value of n represents the loss of degrees of freedom of the adsorbate. A value of n = 1 is associated with adsorption at the surface (loss of 1 degree of freedom), n = 2 indicates

adsorption in micropores (2 degrees of freedom lost) and n = 3 represents adsorption in ultramicroporous material (3 degrees of freedom lost). Note Equation 5.11 assumes that the E and n parameters are independent of temperature.

Dubinin and Astakhov (1971a) used Equation 5.11 in conjunction with a Weibull (1951) distribution and obtained an analytical form for the process of adsorption

$$F(A) = 1 - \exp\left[-\left(\frac{A}{E}\right)^n\right] \tag{5.12}$$

where the function F(A) is the fraction of the unfilled pore volume of the adsorbent. The term F(A) is equal to

$$F(A) = 1 - \theta = 1 - \frac{W}{W_0} \tag{5.13}$$

which implies that the equation for the quantity adsorbed W, is

$$1 - \theta = 1 - \exp\left[-\left(\frac{A}{E}\right)^n\right] \tag{5.14}$$

- or -

$$W = W_0\exp\left[-\left(\frac{A}{E}\right)^n\right] \tag{5.15}$$

Equation 5.15 is called the Dubinin-Astakhov (1971a) model. This model is used to fit what is called the "characteristic curve" which is a plot of the amount adsorbed q, vs the adsorption potential A. Equation 5.15 can also be slightly altered (Equation 5.16) (given the parameters of E and n from the characteristic curve) to yield isotherms at any desired temperature.

$$W = W_0\exp\left[-\left(\frac{-RT\ln(P/P_{sat})}{E}\right)^n\right] \tag{5.16}$$

The advantages of the D-A equation are twofold. First, only two parameters need to be found to fit the characteristic curve. Second, once the parameters are found, the equilibrium behavior of the adsorbent with whatever contaminant is being analyzed can be predicted quite easily. The disadvantage of the D-A equation is that it is bounded at the low range of adsorption capacity to ratios of 0.1 to 0.2 W/W_0 [Dubinin (1975)].

Heat of Adsorption

In Chapter 2, it was mentioned that physical adsorption from the gas phase is an exothermic process. The amount of thermal energy emitted during this process is called the heat of adsorption. Two heats of adsorption exist: the differential heat of adsorption and the isosteric heat of adsorption. The differential heat of adsorption Q_{diff} is defined as "heat evolution when unit adsorption takes place in an isolated system" [Suzuki (1990)]. This value can be found using a bomb calorimeter. The isosteric heat of adsorption is related to Q_{diff} by the following equation.

$$Q_{st} = Q_{diff} + RT \tag{5.17}$$

and can be found using adsorption isotherms via the vant Hoff equation.

$$Q_{st} = RT^2 \frac{d\ln P}{dT} \tag{5.18}$$

After manipulating isotherms into what are termed vant Hoff plots (Figure 5.15), Q_{st} can be easily calculated using the following relationship given by Suzuki (1990).

$$Q_{st} = R \frac{\ln P_1 - \ln P_2}{\frac{1}{T_1} - \frac{1}{T_2}} \tag{5.19}$$

which is the slope of the vant Hoff curve. If the slope of the vant Hoff plot is constant, the heat of adsorption is independent of temperature. Several vant Hoff plots that are

parallel to each other (varying quantities adsorbed) indicate that Q_{st} is also independent of surface coverage within the specified range tested. Independence results when the surface of the adsorbent is energetically homogeneous (all adsorption sites are the same) and small amounts of pollutant are adsorbed (low surface coverage) to prevent any interference between the adsorbed molecules.

5.1.2   Equilibrium Analysis and Modeling

Dynamic Equilibrium Results With Propane

Adsorption equilibrium data were taken with propane on carbon G65 50x150 at 35, 60, 80 and 100°C, respectively. The concentrations ranged from 1.8 to 43.9 ppm by volume. Six tests, each at a different propane concentration, were taken at each of the temperatures listed above to yield an isotherm. After a set of six tests were complete, a check test was done at 100°C, 43.9 ppm to investigate if any loss in adsorptive capacity had occurred. No noticeable loss in capacity was experienced during testing. The equilibrium data was then plotted as isotherms and are shown in Figure 5.5. The value of q is in units of milligram propane per gram of carbon and is plotted against the propane concentration (ppm). A point at zero concentration (partial pressure) was inserted for these isotherms because the experimental data indicate that the isotherm will pass through this location. All concentration and q data for these isotherms is given in Appendix E. The isotherms can also be plotted with the abscissa being in units of partial pressure (Pa) which can be obtained by multiplying the concentration of the propane by the total pressure (assumed to be one atmosphere - 98508 Pascals for Madison, WI as was found in Chapter 3). Figure 5.6 shows the isotherms plotted as a function of partial pressure. To be sure that the isotherms could be duplicated, two sets

of equilibrium data were taken at 100°C (one set at the start of testing and one at the end of testing). As can be seen in Figure 5.7, the line passing through the data points is well within the uncertainty bars, indicating that duplication was successful.
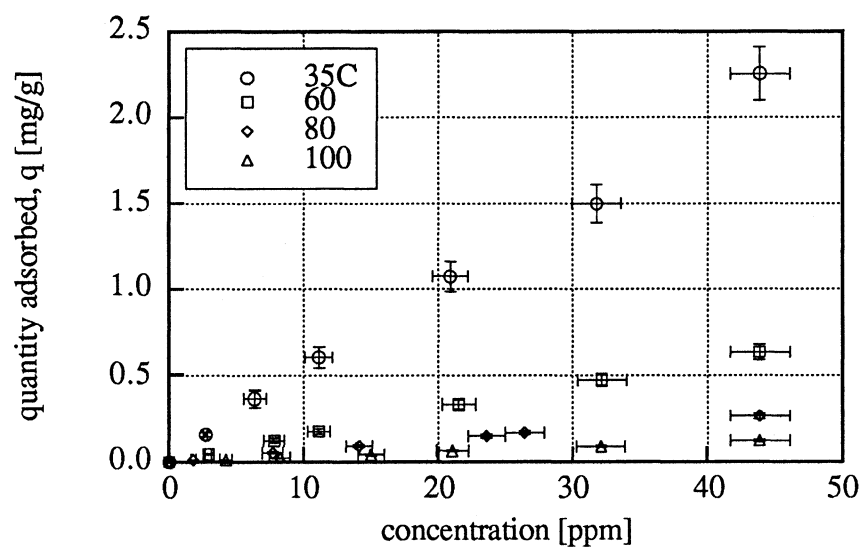

Figure 5.5   Experimental isotherms for propane on carbon G65 50x150. Total pressure is assumed to be 98508 Pa.
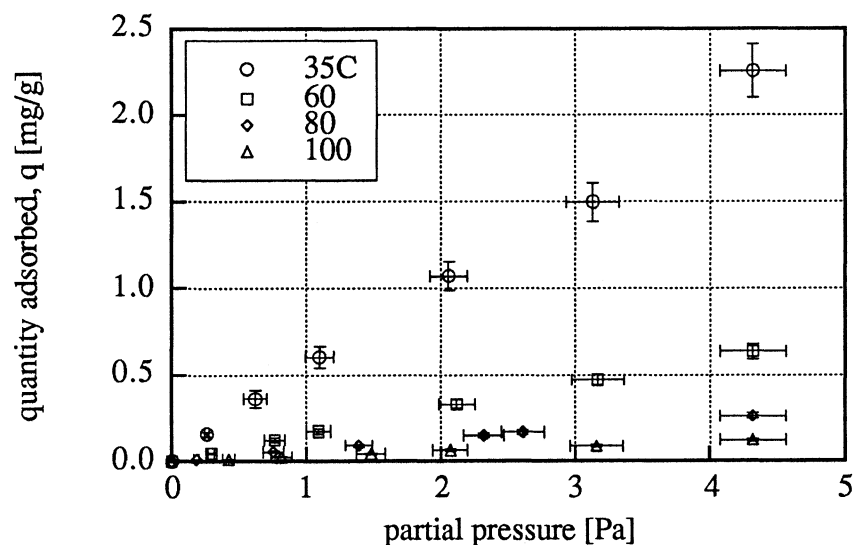
Figure 5.6   Experimental isotherms for propane on carbon G65 50x150. Total pressure is assumed to be 98508 Pa.
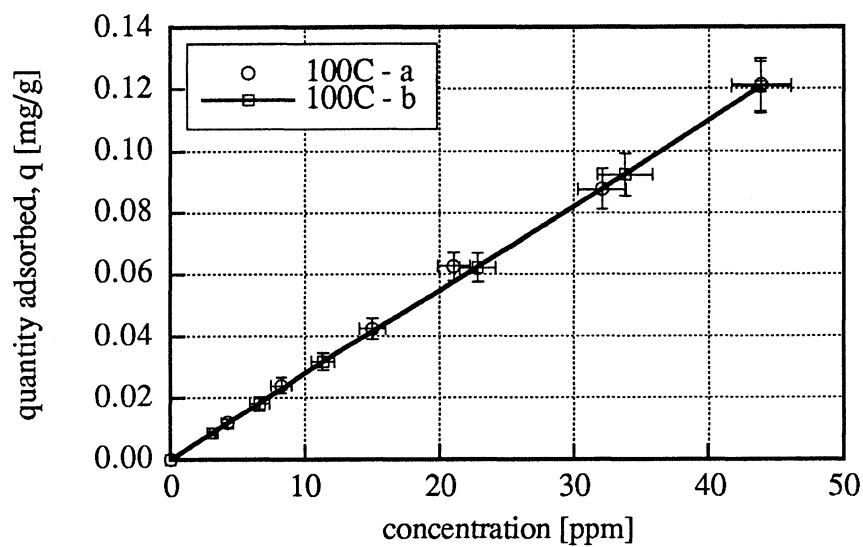
Figure 5.7   Duplication of experimental isotherms involving propane and carbon G65 50x150. Total pressure is assumed to be one atmosphere.

Modeling Using the Henry Equation

As can be seen in either Figure 5.5 or 5.6 the isotherms are linear, which indicates that the amount adsorbed is small relative to the total that could be adsorbed by the activated carbon. Because of this linearity, the isotherms conform to Henry's Law and can be curve fit using the Henry Isotherm. Coefficients for the Henry model were found using a least squares fit of the data. Figure 5.8 shows the curve fitting results with volume (m^3) adsorbed per gram of carbon vs the partial pressure (Pa). The amount adsorbed was converted from mass to volume by using the specific volume of propane at the respective isotherm temperatures and a pressure of 98508 Pa. The specific volumes are listed in Table 5.1 and were obtained from a software program called EES, which is an engineering equation solver program. All of the isotherm curve fits are within the predicted uncertainty of the data. The values of the Henry constants ranged from 2.92e-7 at 35°C to 1.98e-8 m^3/g Pa at 100°C. The Henry constants were then plotted against their respective temperature and fit with a curve of the following form.

$$k = c_1 \exp(-c_2) \tag{5.20}$$

Results are shown in Figure 5.9. The uncertainty of the Henry constants is a first order approximation based on the average errors of the quantity adsorbed V and the partial pressure. These mean values were calculated to be 9% for the volume and 7% for the partial pressure with the actual errors of the data varying from 7 - 14% for V and 5 - 13% for the partial pressure. The temperature uncertainty is ±0.5°C and is based on one-half the least significant digit provided by the gas chromatograph's alphanumeric display. Figure 5.9 shows that the curve fit is within the uncertainty that

has been established. With the equation for the value of k now known, the experimentally determined isotherms can be predicted as shown in Figure 5.10. All of the predicted curves are within the uncertainty bars of the isotherm data, indicating that this method of analysis was successful, although the generated isotherm at 35°C tends to be low of the data. The reason for this can be seen in Figure 5.9 where the exponential curve fitting the Henry constants below the actual data point.

Table 5.1 Specific volume of propane at isotherm temperatures. Pressure at which values were obtained was 98508 Pa. Data from EES.

temperature (°C)	specific volume (m3/kg)
35	0.582
60	0.631
80	0.670
100	0.709
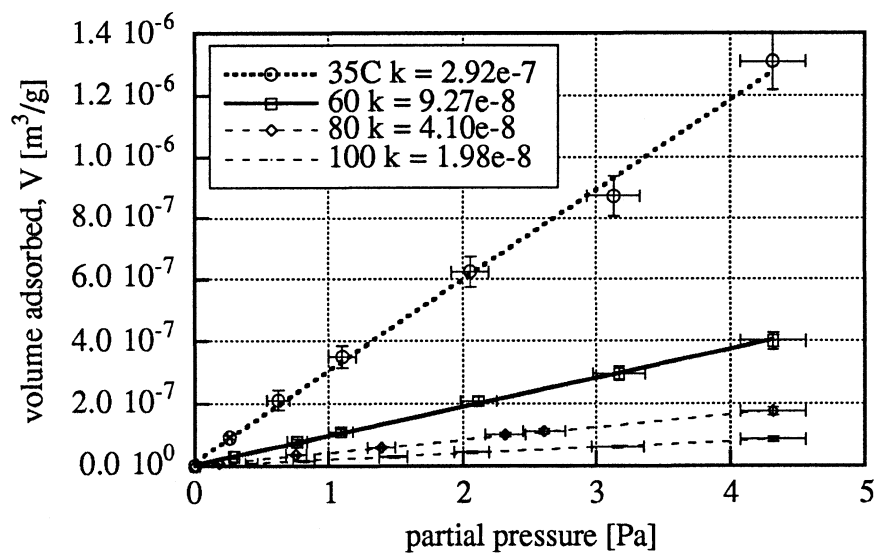
Figure 5.8 Curve fit of the propane isotherms using Henry's Isotherm model. The constant k has the units of (m3/g_carbon Pa).
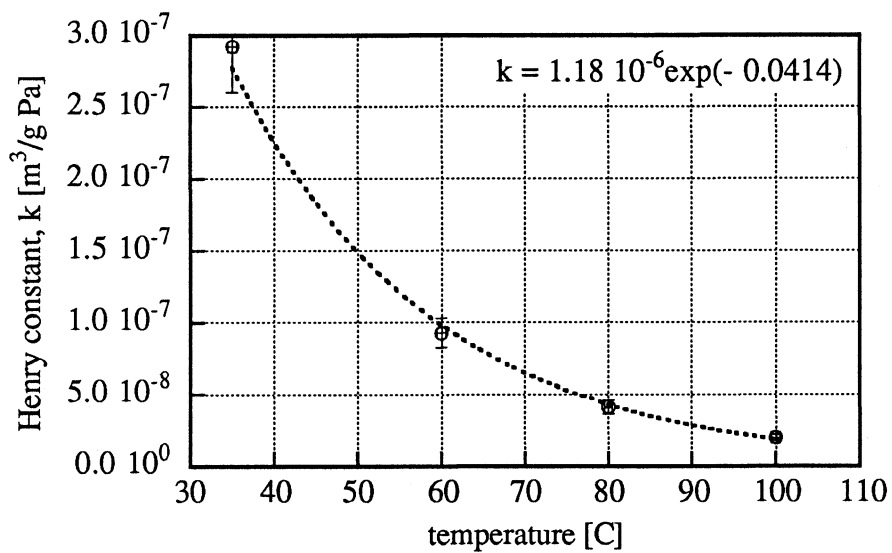
Figure 5.9 Curve fit of the Henry constants.
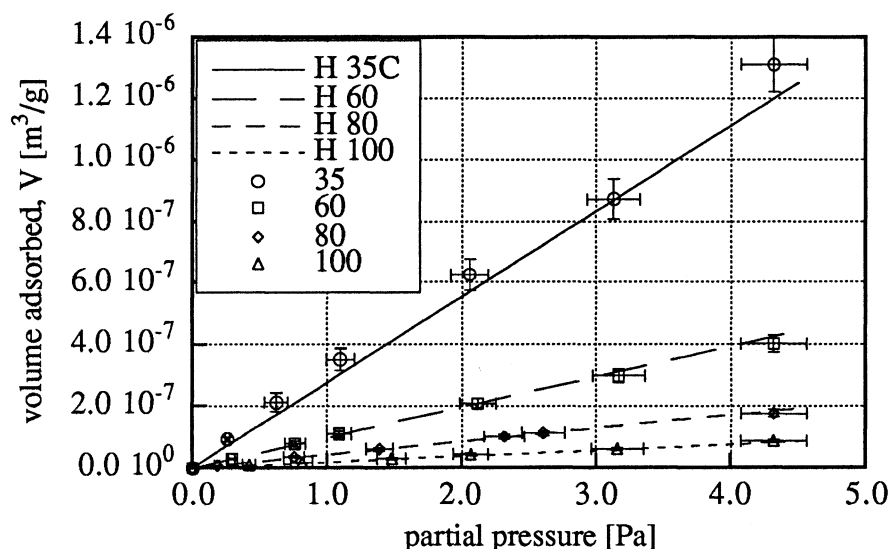
Figure 5.10 Estimation of the experimental isotherms using the Henry constants obtained from the curve fit shown in Figure 5.9.

Modeling Using the Dubinin-Astakhov Equation

The other model used to attempt to curve fit the data was the Dubinin-Astakhov model. Dubinin (1975) states that a drawback of this model is its inability to predict isotherms which involve small amounts adsorbed (low surface area coverage bound of 0.1 or 0.2). This potential limitation was investigated for the isotherms involving propane.

The first step of this analysis process was to develop a characteristic curve. The curve was obtained by first determining the adsorption potential A and then plotting q vs A. Calculating A requires the saturation pressure of the propane to be known. Unfortunately, at a temperature of 100°C the saturation pressure does not exist because this temperature is above the propane vapor dome. The solution to obtaining a "saturation pressure" when it does not exist is given by Balzhiser, et al. (1972) and

involves making a plot of saturation pressures (log scale) against inverse temperature and then extrapolating to the desired temperature. This method is illustrated in Figure 5.11. With the saturation pressures known, the adsorption potentials of the data were calculated and the characteristic curve was then plotted (Figure 5.12). The characteristic curve was then fit using the D-A model. Values of n were varied from one to three with the most realistic results being found when n = 2 (Figure 5.13). A value of n = 3 resulted in value of W_0 which was thought to be too low. When n = 1 was input into Equation 5.16, W_0 was extremely large. With the parameters of E and n now known, Equation 5.16 was implemented to determine the isotherms for propane at the temperatures used in the experiments. The curves from the D-A model
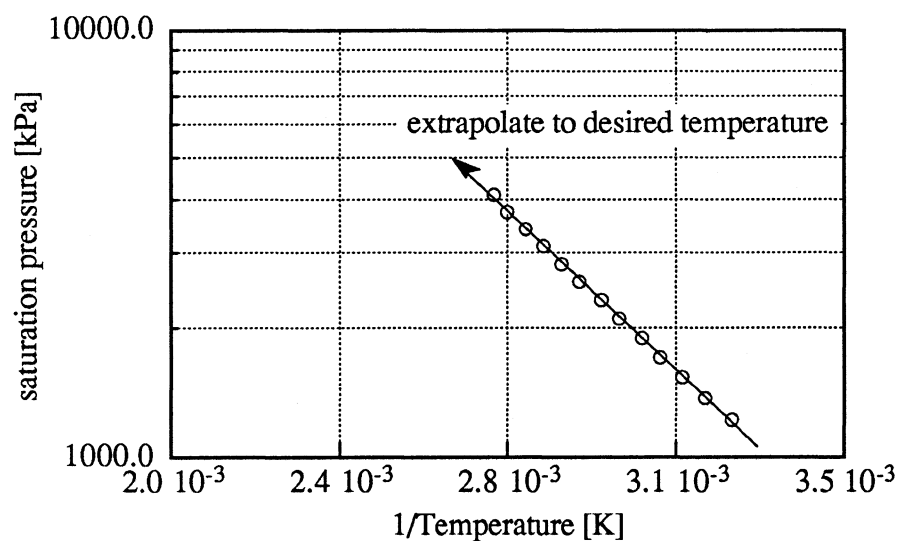
Figure 5.11   Method of obtaining saturation pressures of propane above the vapor dome. From Balzhiser, et al. (1972).
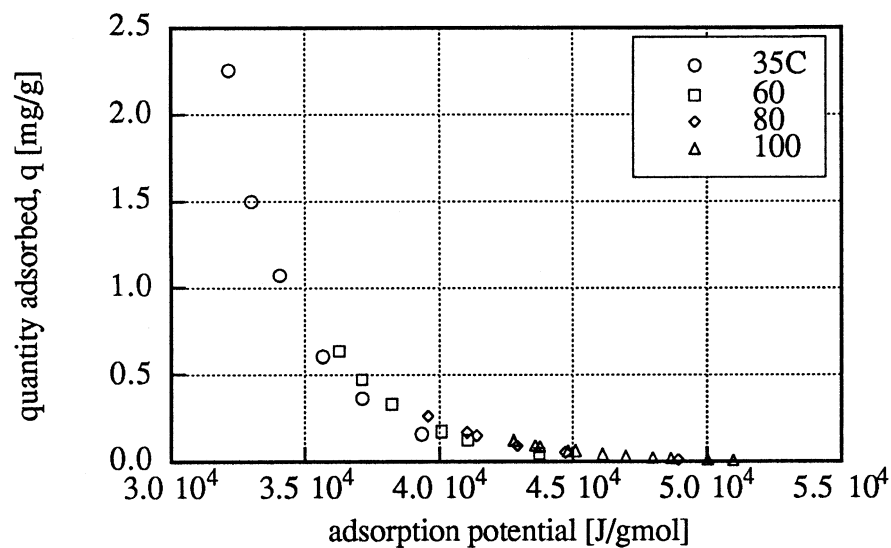
Figure 5.12 Characteristic curve for propane and carbon G65 50x150 under the conditions listed.
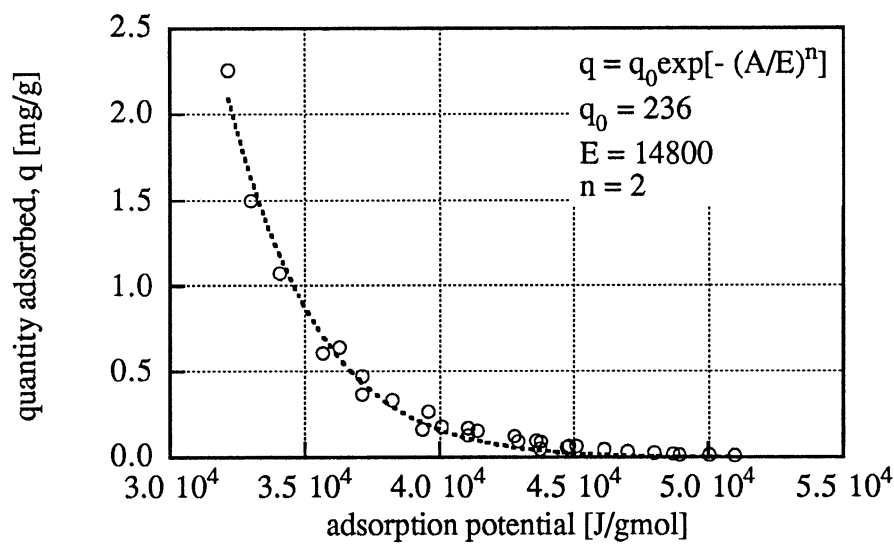
Figure 5.13 Dubinin-Astakhov curve fit.

and the experimentally obtained data are shown in Figure 5.14. Results indicate that the curve fits are very poor at high temperatures (D-A values are as much as 82% lower than the experimental values) and improve as more propane is adsorbed (occurring at low temperatures) At 35°C, the D-A curve is within the uncertainty bars. These results verify what Dubinin (1975) has stated - the model does not hold at low quantities adsorbed.
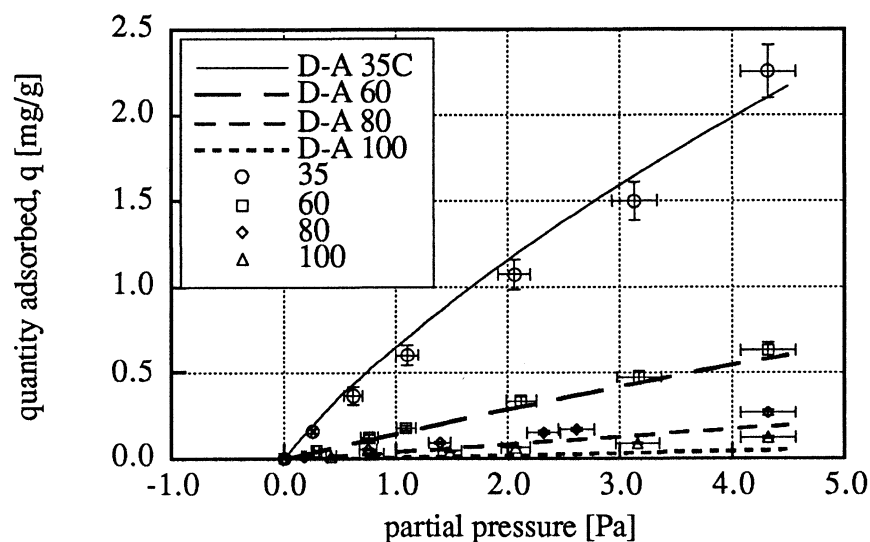
Figure 5.14 D-A generated isotherms compared to the experimental data.

Heat of Adsorption

The isoteric heat of adsorption Q_{st}, for propane on carbon G65 50x150 has been found to be 42.0 - 42.8 kJ/gmole (10.0 - 10.2 kcal/gmole) using the vant Hoff plots shown in Figure 5.15. These values agree to within ±3.0% of the value reported (10.3 kcal/gmole) in the literature [Czepirski and Jagiello (1989)]. Figure 5.15 also gives
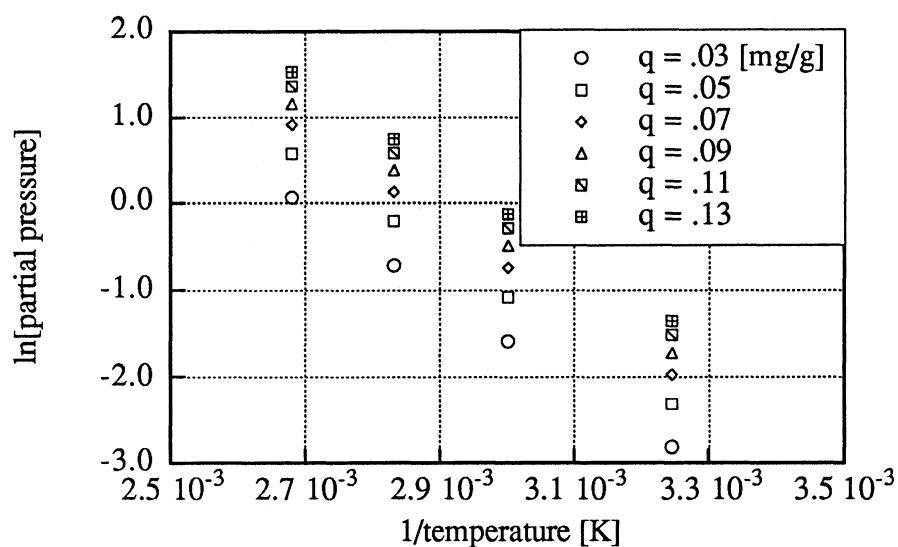
Figure 5.15   vant Hoff plots for propane on carbon G65 50x150.

two other pieces of information concerning the adsorption of propane onto carbon G65 50x150.

1.   The heats of adsorption are insensitive to temperature i.e., the slopes of the vant Hoff plots are relatively constant.

2. Q_{st} is independent of surface coverage within the range of q shown, i.e. the vant Hoff plots for different quantities adsorbed are parallel within the partial pressure and temperature shown.

Dynamic Equilibrium Results With Toluene

Adsorption equilibrium data were taken with toluene on carbon G65 50x150 at 100, 120 and 140°C, respectively. Testing was not done at the same temperatures as the propane tests because much more toluene is adsorbed than propane, which takes a longer period of time. The concentrations ranged from 1.06 to 10.31 ppm by volume. A minimum of four tests , each at a different concentration, were taken at the temperatures listed above to yield an isotherm. Two tests were completed throughout the testing process to determine if any loss in adsorptive capacity had occurred. After equilibrium testing, the total loss in adsorptive capacity of the activated carbon was 3.5%. The loss in adsorptive capacity is within the established uncertainty, indicating duplication of the tests was successful. Upon completion of the tests, the equilibrium data was plotted in the form of isotherms (Figure 5.16), which were found to be highly nonlinear. Because of this nonlinearity, the Henry isotherm model does not hold and therefore was not used to analyze the isotherms. Models which conform to the nonlinear profile are the Langmuir, Freundlich and Dubinin-Astakhov equations and they were used in this analysis.
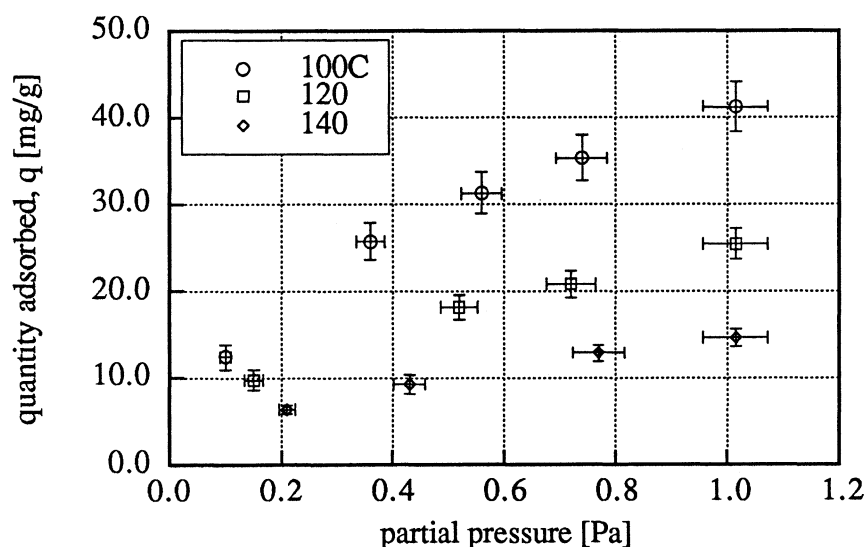
Figure 5.16 Experimental isotherms for toluene on carbon G65 50x150. Total pressure is assumed to be 98508 Pa.

Modeling Using the Langmuir Equation

Before the Langmuir Isotherm could be applied to the experimental isotherms involving toluene on carbon G65 50x150, the data was linearized and plotted (P/q vs P) to investigate if the Langmuir equation was valid (discussed previously). Figure 5.17 shows that the lines which have been fit through the linearized data pass well within the uncertainty, so it can be concluded from these results that validity has been established. The Langmuir (Equation 5.4) was then used to fit the adsorption isotherms with results shown in Figure 5.18. All of the curves pass within the uncertainty bars. The constants q_0 (maximum amount adsorbed for a given isotherm) and k_1, (Table 5.2) were taken from the Langmuir equation used to fit each isotherm and plotted against temperature. Figure 5.19 shows q_0 vs temperature. An exponential curve fit was done for the q_0 values, with the results also shown in Figure 5.19. Figure 5.20 shows the

equation used to fit the constant k_1 values vs inverse temperature. Although the curve fit did not pass directly through the data points like that for the q_0 values, the regression value obtained was R = 0.9 and this was considered to be acceptable (R is a measure of the goodness of a curve fit). The equations obtained by fitting the q_0 and k_1 constants were then used to generate q_0 and k_1 values for the temperatures at which the isotherms were taken. These coefficients were then inserted into the Langmuir equation and plotted. The results (Figure 5.21) were almost identical to the curves which were initially obtained previously in Figure 5.18, thus showing that the curve fits of the constants q_0 and k_1 were successful (between +7% and -12% of the experimental data). Predicting the adsorptive capacity of the activated carbon at temperatures between 100 and 140°C is now possible.

Table 5.2 Langmuir constants obtained from the curve fits of Figure 5.18.

temperature [C]	q_0 [mg/g]	k_1 [1/Pa]
100	56.5	2.4
120	35.1	2.2
140	23.0	1.7
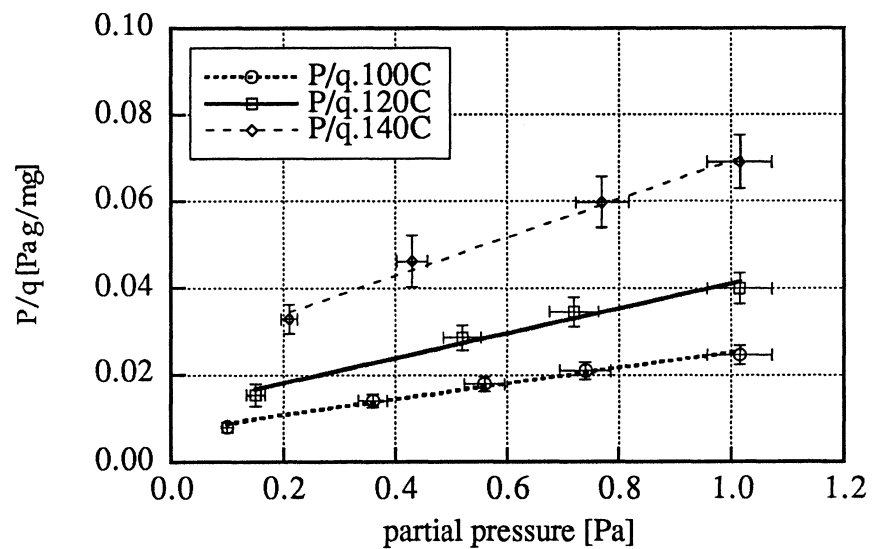
Figure 5.17 Linearized Langmuir plot for toluene on carbon G65 50x150. Total pressure is assumed to be 98508 Pa.
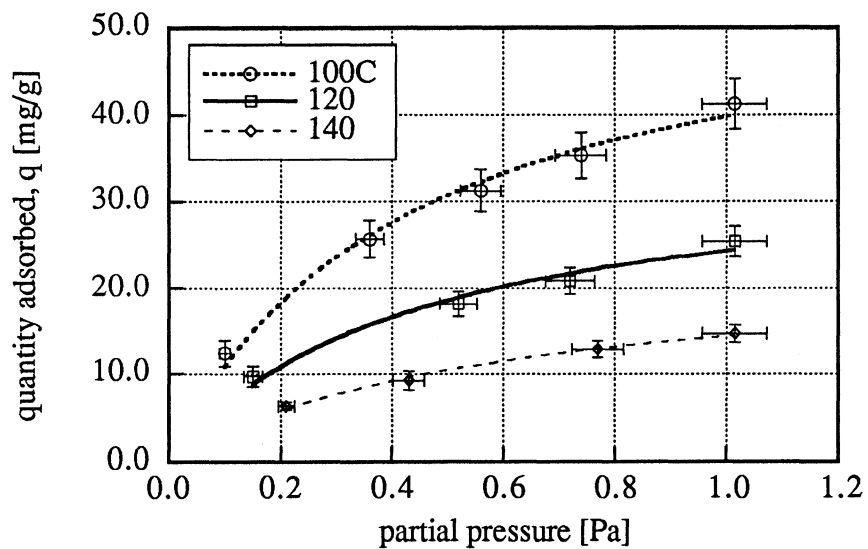
Figure 5.18 Langmuir isotherm model used to fit the experimental data.
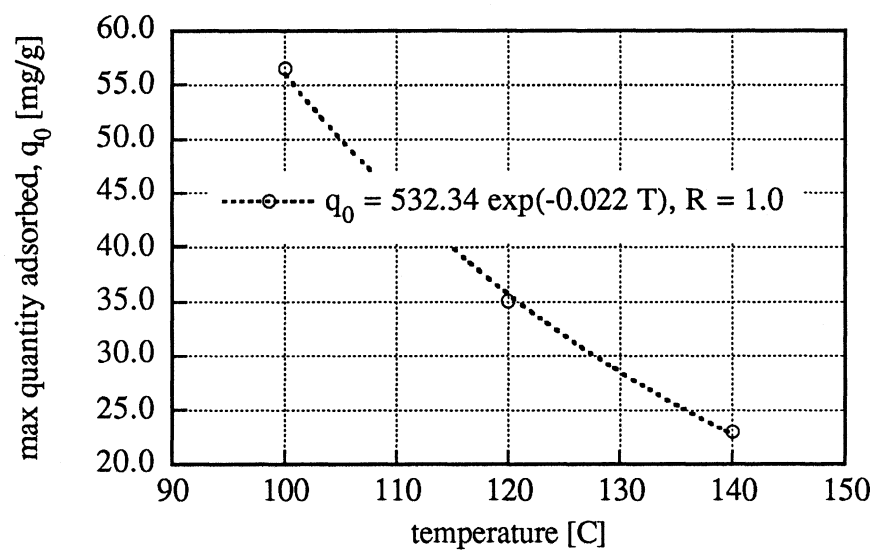
Figure 5.19   Langmuir constants q_0 plotted against temperature.
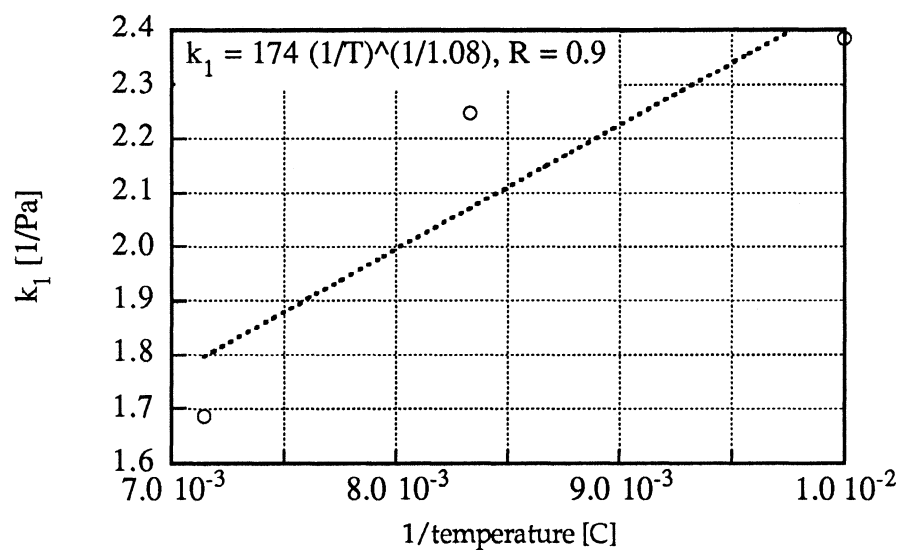
Figure 5.20   Langmuir constants k_1 plotted vs inverse temperature.
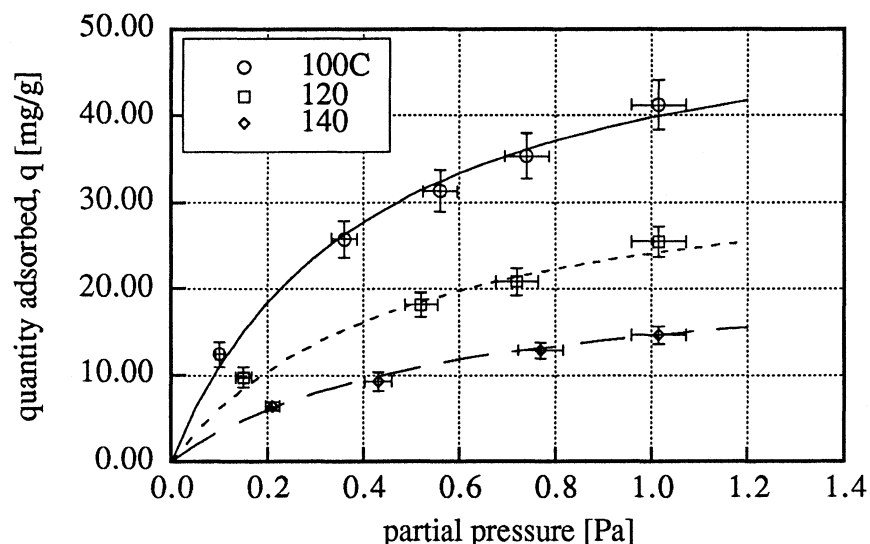
Figure 5.21 Langmuir isotherms generated using constants q_0 and k_1 obtained from curve fits (Figures 5.19 and 5.20).

Modeling Using the Freundlich Equation

The Freundlich equation [Smisek and Cerny (1970)] was the next model used to investigate the experimental isotherms. Similar to the Langmuir (1918) analysis, the data was first linearized by considering a log-log plot of q vs partial pressure. The curves obtained are shown in Figure 5.22. The data appears to be linear, thus validating the Freundlich model for this case. The curve fits obtained using the Freundlich model (Equation 5.7) are shown in Figure 5.23 and the constants k_2 and n for each of the isotherms are shown in Table 5.3. These constants were plotted against temperature and fit with equations (Figure 5.24). An exponential expression was used to fit the k_2 values and a linear expression was used to fit the n values. The respective equations are shown in Figure 5.24. All regression values were acceptable at levels greater than R = 0.9. The equations for k_2 and n were then used to generate values of

k_2 and n at isotherm temperatures consistent with the measured data. These constants were next inserted into the Freundlich equation to determine if the fitting process of the Freundlich constants was successful. The curves produced to compare against the experimental data are given in Figure 5.25. As can be seen Figure 5.25, the curves pass well within the uncertainty of the data (between +10% and -3% of the experimental data). It can be concluded from this analysis that, although Smisek and Cerny (1970) stated that the Freundlich model is only used to fit experimental data, it is possible to obtain equations for the Freundlich constants and then use these equations to obtain isotherms at temperatures other than was tested experimentally. Extrapolating significantly outside the range of temperature where isotherms were experimentally obtained is not recommended.

Table 5.3 Freundlich constants obtained from curve fitting data in Figure 5.23.

temperature [C]	k_2 [mg/g Pa]	n [unitless]
100	41.3	2.0
120	25.0	2.0
140	14.6	1.9
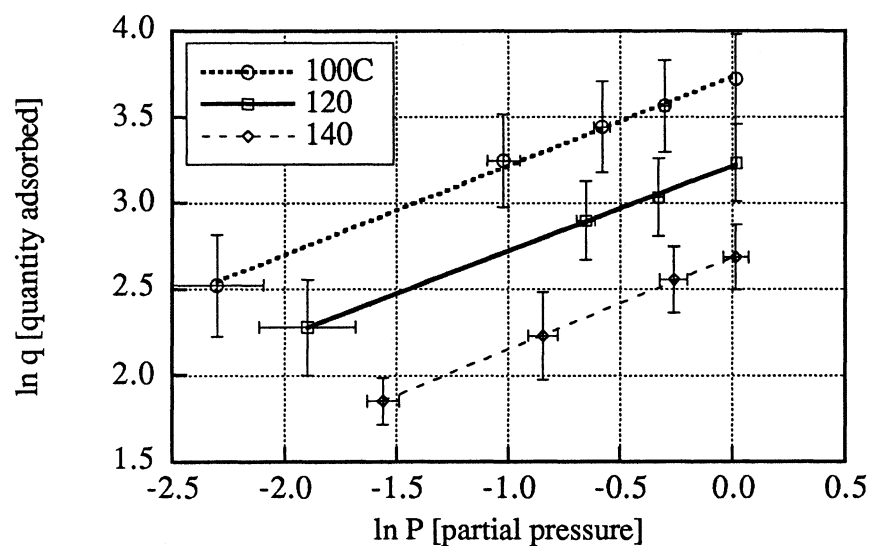
Figure 5.22   Linearized Freundlich plot for toluene on carbon G65 50x150. Total pressure is assumed to be 98508 Pa.
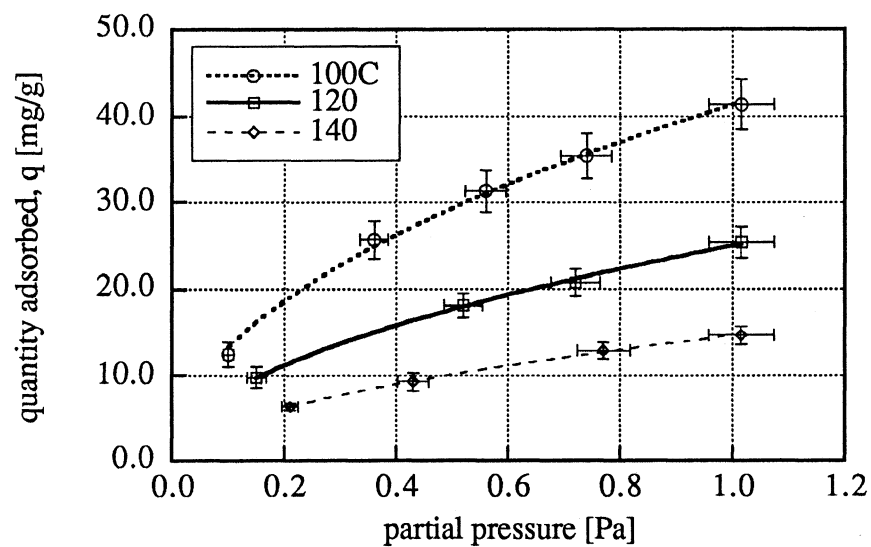
**Figure 5.23**   Freundlich isotherm model used to fit the experimental data.
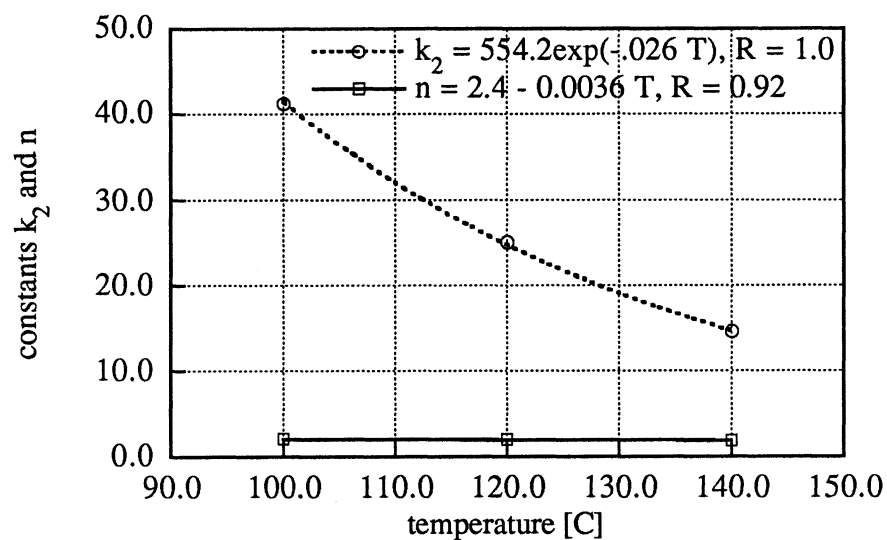
Figure 5.24 Freundlich constants k_2 and n vs temperature.
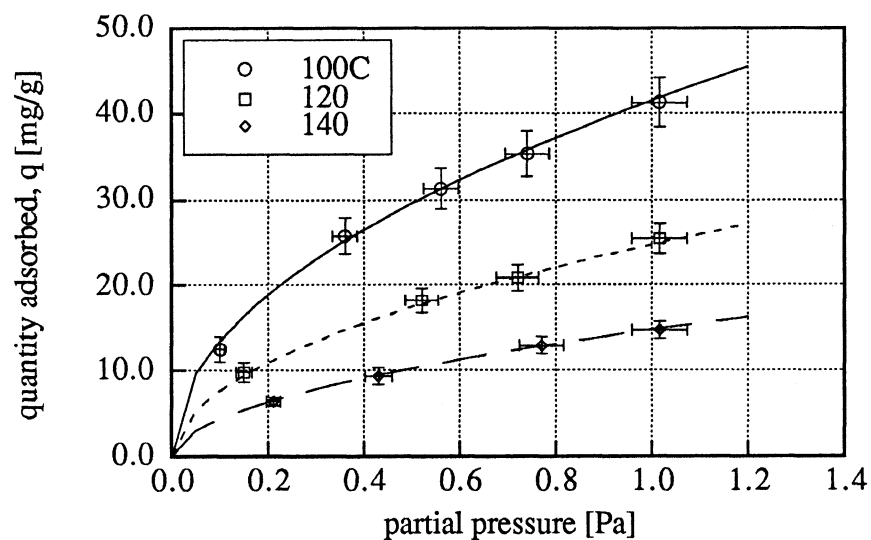
Figure 5.25 Freundlich isotherms generated using constants k_2 and n obtained from curve fits (Figures 24).

Modeling Using the Dubinin-Astakhov Equation

Before the Dubinin-Astakhov model can be used, the characteristic curve must first be obtained and this requires determining the adsorption potential of the equilibrium data. As with the propane on carbon G65 50x150 isotherm analysis, saturation pressure data for toluene was not available at all of the temperatures at which testing was done. The method of extrapolation [Balzhiser, et al. (1972)] from known values of the saturation pressure to the unknown values of saturation pressure was again employed (Figure 5.26). A source from Perry (1963) provided the saturation pressure data for toluene used to generate the $\ln P_{sat}$ vs $1/T$ plot. With the "saturation pressures" known, Equation 5.10 was used to calculate the adsorption potential for the data. The characteristic curve is shown in Figure 5.27 and the D-A curve fit of this data is shown in Figure 5.28. The value of n = 2 was chosen over n = 1 or 3 because n = 2 gave the most realistic results for q_0. With the constants of the D-A model acquired from the fit of the characteristic curve, Equation 5.16 was implemented to obtain isotherms at the respective experimental isotherm temperatures. These isotherms were then compared with the experimental data. The results are shown in Figure 5.29 and it is readily seen that the D-A isotherms do not fit the data as well as the Langmuir or Freundlich models (between +30% and -8% of the experimental data), although the curves do pass through all but one of the data uncertainty bars.
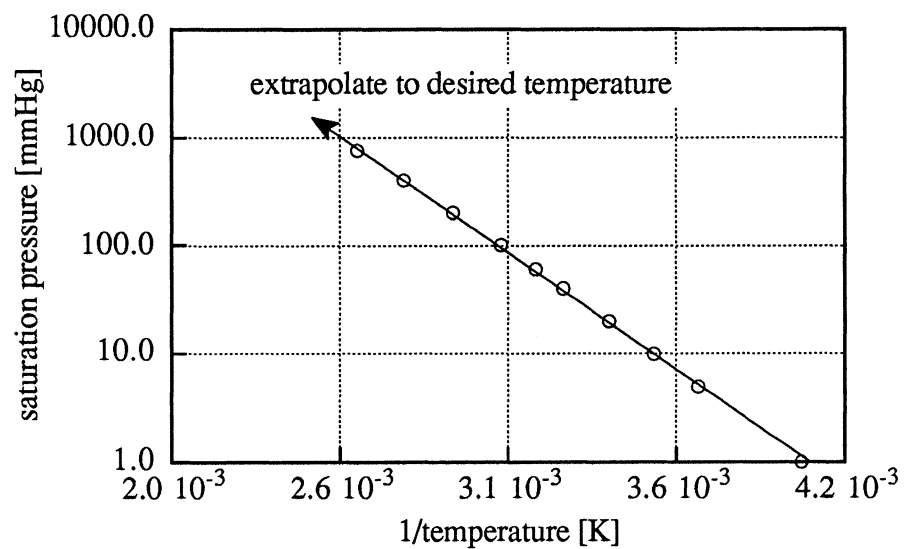
Figure 5.26 Method of obtaining saturation pressures of toluene above the vapor dome. From Balzhiser, et al. (1972).
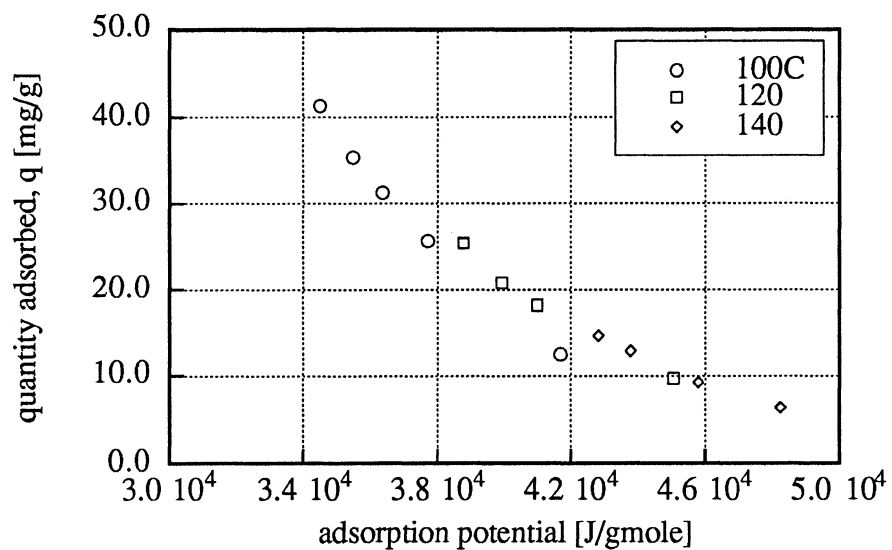
Figure 5.27 Characteristic curve for toluene on carbon G65 50x150.
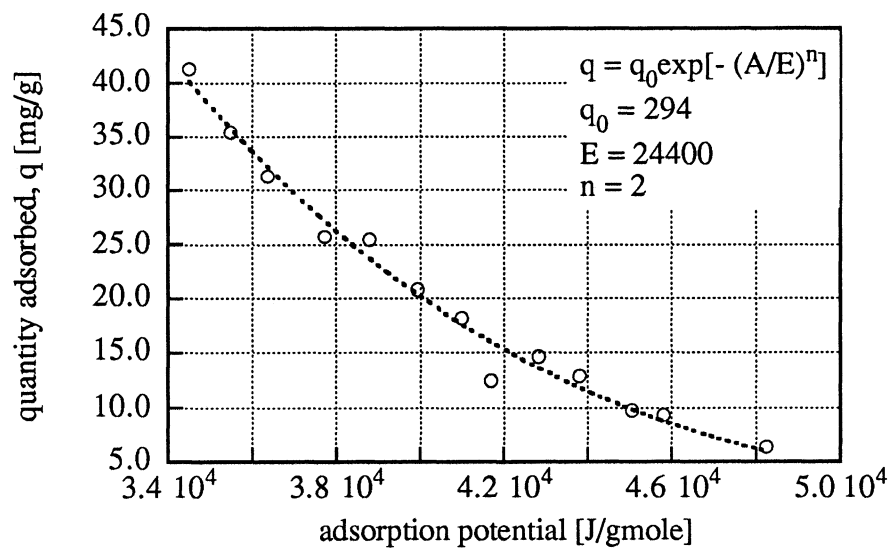
Figure 5.28 Dubinin-Astakhov fit of the characteristic curve.

The chart shows:
$$q = q_0 \exp[-(A/E)^n]$$
$$q_0 = 294$$
$$E = 24400$$
$$n = 2$$

X-axis: adsorption potential [J/gmole]

Y-axis: quantity adsorbed, q [mg/g]
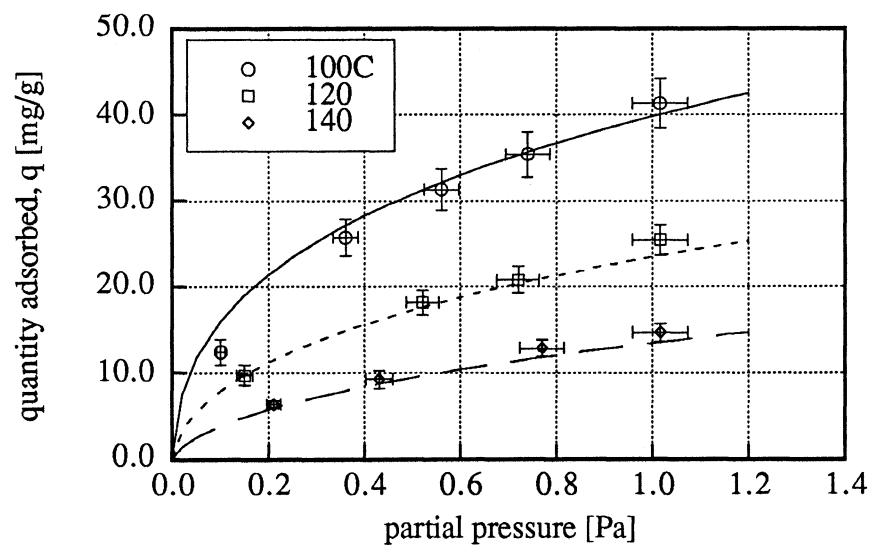
Figure 5.29 Dubinin-Astakhov isotherms compared to the experimental data.

Legend:
- ○ 100C
- □ 120
- ◇ 140

X-axis: partial pressure [Pa]

Y-axis: quantity adsorbed, q [mg/g]

Heat of Adsorption

The final step in the analysis of the equilibrium data with toluene on carbon G65 50x150 is the determination of the heat of adsorption. The vant Hoff plots showing q varying from 14 - 17 mg/g are given in Figure 5.30. From these plots and using Equation 5.19, the heat of adsorption was found to vary from 62.6 - 72.2 kJ/gmole (15.0 - 17.3 kcal/gmole). These results conform to within 2% of values given by Robell, et al. (1970). The nonlinearity of the vant Hoff plots caused the heat of adsorption to vary and indicates temperature dependency. The vant Hoff plots are approximately parallel to each other, showing that the heat of adsorption is unaffected by surface coverage of the carbon for this range of constant q.
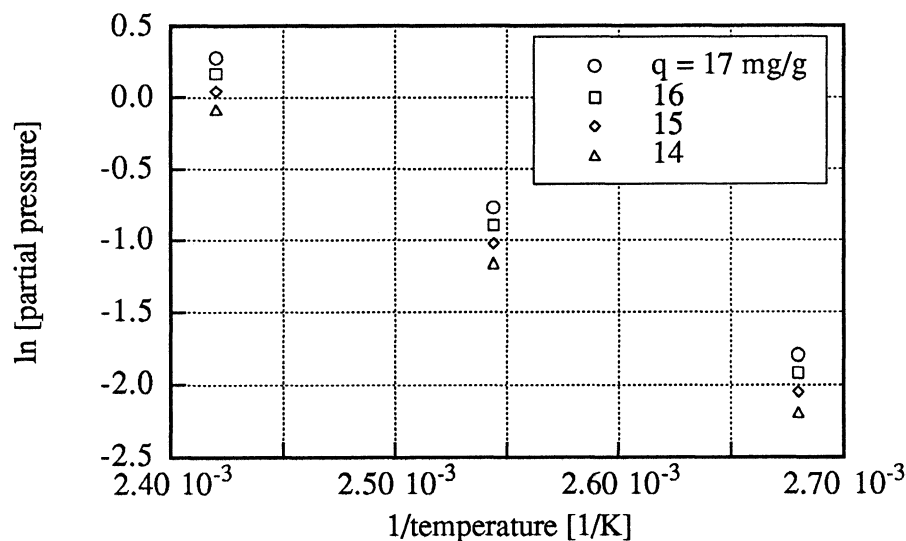
Figure 5.30 vant Hoff plots for toluene on carbon G65 50x150.

5.2   KINETICS OF ADSORPTION IN PACKED BEDS

5.2.1   Kinetic Theory

The kinetics of physical and chemical adsorption are quite different from one another. In this study, activated carbon is used to adsorb one component from gaseous solution and it is assumed that physical adsorption is occurring. For this reason, the kinetics of chemisorption will not be discussed; however, Hayward and Trapnell (1964) have written about this topic.

An analysis done by de Boer (1953) describes physical adsorption in the following manner. Given an adsorbate-adsorbent system, n molecules of adsorbate will be coming into contact with a unit area of adsorbent during a unit of time. The average time t which these molecules remain on the surface then provides the necessary information to calculate the number of molecules σ located on the surface (adsorbed) per unit area per unit time.

$$\sigma = nt \qquad\qquad\qquad (5.21)$$

de Boer's analysis is a simplification of real adsorption processes because it does not take into account the different types of mass transfer resistance present in a packed bed. There are three main types of resistance for adsorbate particles to overcome.

1.   external film resistance

2.   intraparticle diffusion - macropore

3.   intraparticle diffusion - micropore

External Film Resistance

The properties of the packed bed will determine whether one, two or all of these different resistances play a major role in the adsorption process. If a particle is to be adsorbed, it must first overcome the external film resistance. As molecules near the adsorbent surface are removed from the gaseous state a concentration gradient is produced. Particles must pass through this region to become adsorbed. If a dynamic condition exists, the flowing solute mixture over the adsorbent causes a convective flow term to come into play, which enhances the external diffusion process. Once on the outer surface of the adsorbent, the particle must overcome macropore and micropore resistances.

Macropore Diffusion

Macropore diffusion can be broken down into four separate mechanisms

1. molecular diffusion

2. Knudson diffusion

3. surface diffusion

4. Poiseuille flow

Molecular diffusion, also known as random molecular motion, is a major contributor to macropore diffusion when the average distance between colliding solute particles is small relative to the diameter of the pore. Ruthven (1984) states that the molecular diffusivity "may be estimated with confidence" using the Chapman-Enskog equation [Hirschfelder, Curtiss and Bird (1954)].

$$D_m = \frac{0.00158 T^{3/2} \left(\frac{1}{M_1} + \frac{1}{M_2}\right)^{1/2}}{P \sigma_{12} \Omega(\epsilon/kT)}$$ (5.22)

Equation 5.22 applies to binary mixtures where M_1 and M_2 are the molecular weights, P is the total pressure in atmospheres, σ_{12} is called the collision diameter and equals $1/2(\sigma_1 + \sigma_2)$ in units of angstroms, Ω is a function of ϵ/kT where $\epsilon = (\epsilon_1 \epsilon_2)^{1/2}$ (the Lennard-Jones force constant), and k is the Boltzman constant. Hirschfelder, Curtiss and Bird (1954) and Satterfield (1970) give values of the force constant.

If the pores have a small diameter and the pressure is low, the mean free path between the molecules will be greater than the path from the molecule to the pore wall. When this happens we have what is called Knudson diffusion. Representation of this diffusion type is given by Ruthven (1984) as

$$D_k = 9700 \kappa \left(\frac{T}{M}\right)^{1/2}$$ (5.23)

Molecules contacting the pore wall do not experience an elastic collision with the wall, rather the molecule is first adsorbed and then re-emitted in a direction not related to the one at which it came in. The phenomena of adsorption and re-emission is a distinctive feature of a diffusion process.

Surface diffusion of solute only occurs when a large concentration of particles is located on the surface. For this to happen, the temperature of the system must be low (usually not far above the boiling point of the contaminant). A flux results from the large solute concentrations, therefore forcing the particles to move further into the porous structure of the adsorbent. It is impossible to measure surface diffusion directly because diffusion in the gas phase is always occurring. Instead, the method used to

determine surface diffusivity is to first measure the diffusion at high temperatures (realizing that surface diffusion is negligible at these temperatures) and then extrapolating the gas diffusion value to low temperatures where surface diffusion exists. Surface diffusion is then found by subtracting the gas diffusion value from the value of diffusion measured at the low temperatures.

Poiseuille flow results when there is a pressure difference across a particle. The pressure difference causes flow to occur in the macropores which aids in adsorption. In a packed bed, the effect of Poiseuille flow can be represented by

$$D_{poiseuille} = \frac{P\kappa^2}{8\mu} \tag{5.24}$$

where P is the absolute pressure, κ is the viscosity and μ represents the mean pore radius. The diffusivity as a result of Poiseuille flow is almost always relatively small when compared with the other diffusivities.

Micropore Diffusion

Micropore diffusion occurs when the adsorbate is similar in diameter to the adsorbent pore in which it is entering. The mechanism for this type of diffusion is a chemical potential gradient [Suzuki (1990)] and the diffusion can be represented as

$$D_c = D_{c0}exp\left(-\frac{E}{RT}\right) \tag{5.25}$$

where E is the activation energy (see discussion of the Dubinin-Astakhov model above). With this information, the diffusivity can be found by using what are called Arrhenius plots [Suzuki (1990)] which is a plot of the micropore diffusivity vs inverse temperature, with the slope of the plot being the activation energy E.

Modeling the Kinetics of Packed Beds

It is apparent from the description concerning the various types of diffusivities that modeling the kinetic behavior of adsorbate traveling in packed beds can become quite involved from two points of view: first, much effort would be required to characterize all of the different diffusions listed above and second, mathematical complications arise when several diffusivities are included in kinetic models. For these reasons, several models make use of a so-called "lumped" diffusion coefficient which includes all of the types of diffusion present in a given system. Other models assume one diffusion is much larger than the others (based on certain system parameters), thus rendering the lesser diffusivities negligible. In many cases, the assumptions that make these models possible yield very good results and there is no point in using models which are more complicated [Ruthven (1984)]. The model used in this study to investigate the kinetic behavior of a solute passing through a packed bed uses only one diffusion coefficient based on the assumption that the other types of diffusion are negligible.

The Homogeneous-Solid Diffusion Model (H-S DM)

The model used in this study is based on the homogeneous-solid diffusion model. It has been discussed extensively by Forsythe (1988), Madey, et al. (1981), and Famularo, et al. (1980). This model is derived by assuming two mechanisms of diffusion are present: exterior diffusion and interior diffusion. Longitudinal (axial) diffusion takes place outside the adsorbent at the surface and intraparticle diffusion occurs inside the adsorbent and lumps all types of diffusion that appear in this region into one parameter.

By employing the following assumptions, the derivation of this model is made much easier.

1. The dynamic equilibrium isotherm is linear.

2. One adsorbable component is present in the gas stream which implies the existence of a single mass transfer zone.

3. The adsorbent bed is initially sorbate free.

4. The adsorbent bed will be subject to a step input of contaminant which then propagates through the bed over time.

5. The level of contaminant is at trace amounts.

6. Plug flow is assumed.

7. Low flowrates exist for the system.

Derivation of the H-S D model begins by considering an isolated element of the packed bed as shown in Figure 5.31. (The notation used here follows that of Forsythe (1988)). An analysis of the volume of gas in the selected element of the packed bed yields the differential equations which satisfy the law of continuity.

$$\frac{\partial C}{\partial t} = D_L \frac{\partial^2 C}{\partial z^2} - u \frac{\partial C}{\partial z} - \left(\frac{1-\varepsilon}{\varepsilon}\right) \frac{\partial q_{ave}}{\partial t} \tag{5.26}$$

$$\frac{\partial q}{\partial t} = D_s \left[\frac{\partial^2 q}{\partial r^2} + \frac{2}{r} \frac{\partial q}{\partial r}\right] \tag{5.27}$$

$$q_{ave} = \frac{3}{R^3} \int_0^R q R^2 dR \tag{5.28}$$

The interstitial void fraction ε is the fraction of cross sectional area of the column not occupied by adsorbent, z is the length of the packed bed at which the analysis is being done, r is the radial coordinate of an adsorbent particle, R is the radius of a typical adsorbent particle, D_L is the longitudinal diffusion coefficient and D_s is the intraparticle diffusion coefficient. The value u is called the interstitial flow velocity and is the average gas velocity passing through the packed bed. It is defined in Equation 5.29

$$u = Q/A\varepsilon \tag{5.29}$$

where Q is the volumetric flowrate and A is the cross-sectional area of the column.
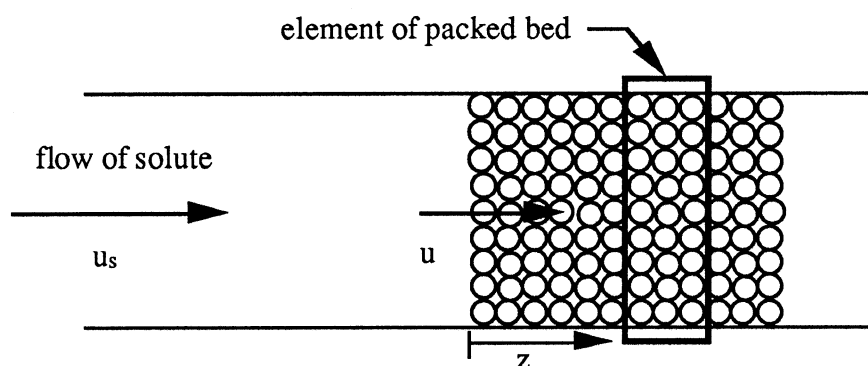
Figure 5.31   Schematic of a packed bed.

Equation 5.26 represents the change in concentration of the solute as it passes through the element. Equation 5.27 characterizes the change in the solid phase adsorbate concentration inside the adsorbent. Equation 5.28 portrays the average solid phase concentration.

If the system is subject to low flowrates, molecular diffusion will be the dominating resistance; therefore, axial diffusion becomes the major resistance of the adsorption process (D_L dominates). Also, the intraparticle diffusion coefficient disappears when only trace amounts of solute are present [Forsythe (1988)]. Because of this, there is no longer a concentration gradient within the particle, resulting in q_{ave} being equal to q. With these assumptions and the results which stem from them, the initial transport equations are now induced to

$$\frac{\partial C}{\partial t} = D_L \frac{\partial^2 C}{\partial z^2} + u \frac{\partial C}{\partial z} + \left(\frac{1-\varepsilon}{\varepsilon}\right) \frac{\partial q}{\partial t} \tag{5.30}$$

The variables C and q are correlated via Henry's Law. With a step input in concentration from 0 to C_0 at time t (Equation 5.31), the final solution for the breakthrough curve can be derived (Equation 5.32).

$$C(z,0) = 0 \qquad t = 0 \tag{5.31}$$

$$C(0,t) = C_0 \qquad t > 0$$

$$T(t) = \frac{C}{C_0} = \frac{1}{2}\exp(1/\Delta)\,\mathrm{erfc}(s_+) + \frac{1}{2}\mathrm{erfc}(s_-) \tag{5.32}$$

where

$$s_{\pm}(t) = \frac{1}{2\Delta^{1/2}}\left(\frac{t_p}{t}\right)^{1/2} \pm \left(\frac{t}{t_p}\right)^{1/2} \tag{5.33}$$

$$\Delta = \frac{D_L}{uL} \tag{5.34}$$

and

$$t_p = \int_0^\infty (1 - T)\,dt \tag{5.35}$$

In Equation 5.32, T is the transmission of the adsorbate through the column (normalized frontal chromatogram), Δ is a dimensionless dispersion number and t_p is the propagation time. It should be noticed that the propagation time is equal to an integral with a range from zero to infinity (Equation 5.35). However, because the frontal chromatograms in this analysis eventually reach equilibrium (solute entering equals solute leaving), the transmission T will eventually reach a value of one. At this point, t_p no longer changes and the integration can be truncated.

The advantages of this model is that it is relatively easy to derive and use. The only parameter which needs to be adjusted to fit an experimental transmission curve is D_L

(all others can be determined beforehand). The disadvantages of this model is that the specific types of diffusions present and their magnitudes are not known. Also, the model is restricted by the major assumptions of the contaminant having a linear equilibrium isotherm and low flowrates being present.

5.2.2 Kinetic Analysis and Modeling

The kinetic modeling of solute passing through packed beds thus far is only in the preliminary stages. All fitting of the transmission curves has been done visually, i.e. no program has been utilized to perform regression to obtain the best curve fit. The void fraction ε used to determine the interstitial flow velocity u is assumed to be 0.5 due to lack of data to better estimate this value. Also, no uncertainty has been calculated for the longitudinal diffusion coefficients; however, as the analysis will show, two trends involving the axial diffusion coefficients D_L and the system parameters are apparent.

Modeling Results with Propane Passing Through a Packed Bed

The first steps in determining D_L for a transmission curve include: measuring the bed length z, calculating the interstitial flow velocity u (Equation 5.29), and the propagation time t_p (Equation 5.35). With these parameters known, the next phase of the fitting procedure is to vary D_L until the theoretical transmission curve matches the experimental transmission curve. Examples of this curve fitting procedure are shown in Figures 5.32 and 5.33 for propane passing through carbon G65 50x150. The conditions for the transmission curves are given in the figure caption. Figures 5.32 and 5.33 are shown because they represent the maximum and minimum values of D_L obtained from the propane transmission curves. It is clear by observing the figures that

the model is fits the experimental transmission curves quite well. All other curve fits involving the theoretical and experimental transmission curves produced results similar to those shown in Figures 5.32 and 5.33.
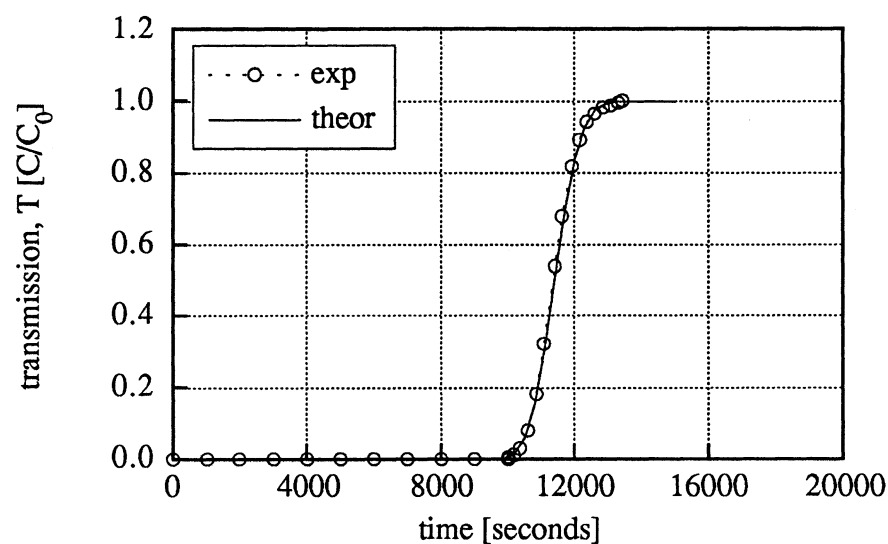
Figure 5.32 Transmission curve modeling using the modified H-S DM. $D_L = 1.8 \ 10^{-5} \ m^2/s$; $u = 0.23 \ m/s$; $t_p = 11402 \ s$; $T = 35C$, $C = 43.9 \ ppm$, $\varepsilon = 0.5$, $z = 0.057 \ m$.

Figure 5.33 Transmission curve modeling using the modified H-S DM.
$D_L = 1.5 \ 10^{-4} \ m^2/s$; $u = 0.34 \ m/s$; $t_p = 653 \ s$; $T = 100C$, $C = 21.0 \ ppm$, $\varepsilon = 0.5$, $z = 0.057 \ m$.

Values of D_L vs the interstitial flow velocity u are shown in Figure 5.34. Although the scatter for the D_L values appears large (due to the experimental curve fitting procedure), a trend in this graph is apparent - as the flow rate increases, D_L also increases. Forsythe (1988) states that D_L is a function of flow at higher velocities because intraparticle diffusion and forced convection around the adsorbent particles become significant. Forsythe (1988) found that D_L (for methane) no longer changed for flow velocities in the range of 1.0 - 1.5 cm/s. Although the adsorbate in this case is propane, it is clear from Forsythe's work that more than molecular diffusion is occurring for this system. Another factor which could have an effect on the D_L value is temperature. The transmission curves used to obtain D_L ranged from 35 - 100°C. The different flow rates and temperature values are intertwined in the data used to obtain

D_L and the possible effects on D_L that either factor may be causing cannot be separated from one another.
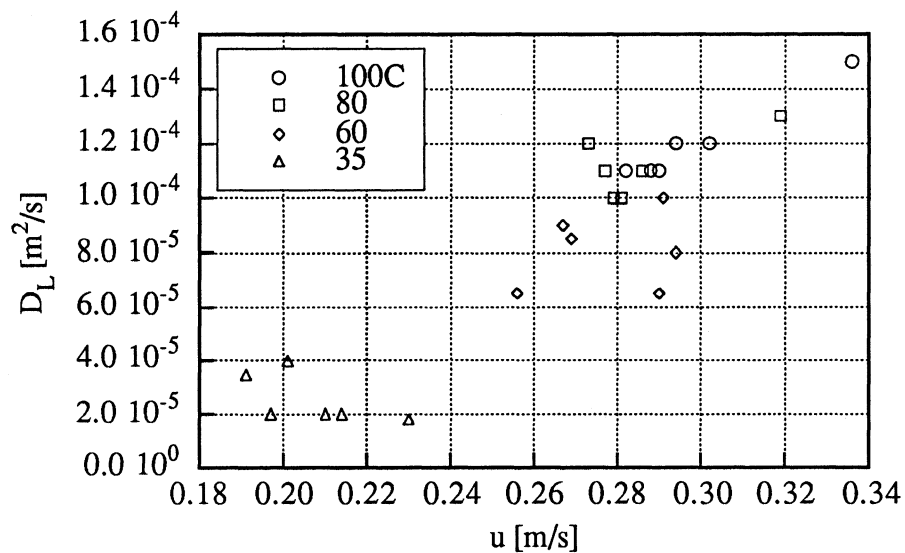
Figure 5.34 D_L vs u for propane passing through carbon G65 50x150.

Figure 5.35 is a plot of D_L vs concentration (ppm by volume). It appears that there is no correlation between D_L and the concentration within the range tested.
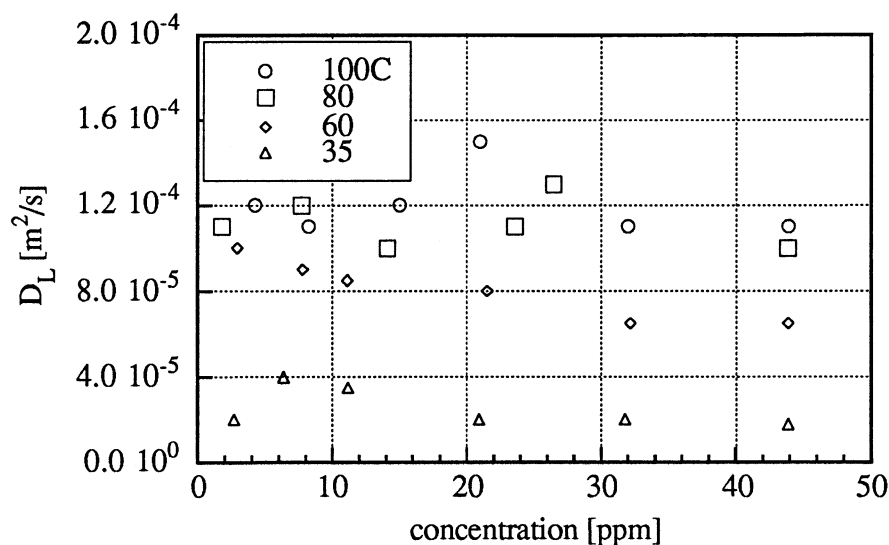
Figure 5.35 D_L vs concentration for propane passing through carbon G65 50x150.

Modeling Results with Toluene Passing Through a Packed Bed

Figures 5.36 and 5.37 display the theoretical and experimental transmission curves for toluene passing through carbon G65 50x150. Figures 5.36 and 5.37 are shown because they represent the curves which produced the maximum and minimum values of D_L. The theoretical transmission curves fit reasonably well, although not as well as the transmission curves involving propane. The curve fits are somewhat surprising because the assumption of the solute possessing a linear isotherm is no longer valid. The value of D_L has seemingly accounted for the kinetic effects which result from nonlinear isotherms [Ruthven (1984)].
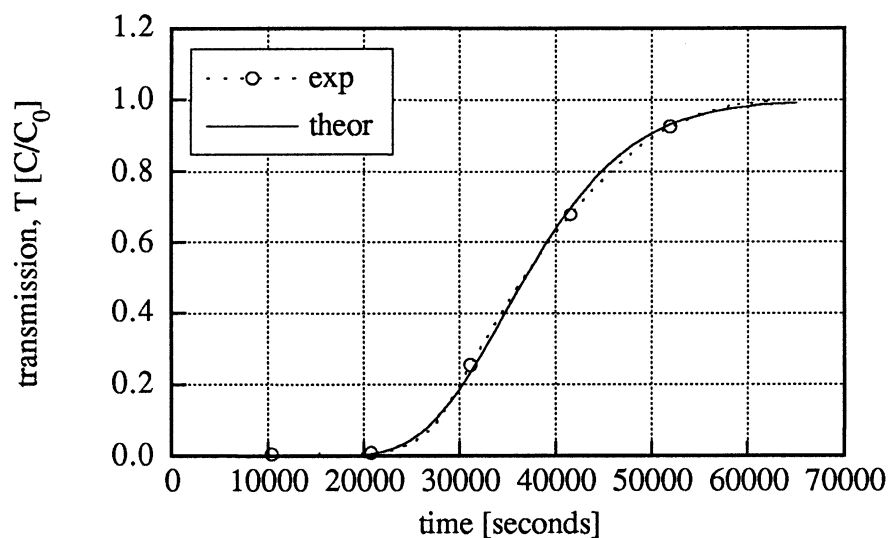
Figure 5.36 Transmission curve modeling using the modified H-S DM.
$D_L = 5.0 \; 10^{-5} \; m^2/s$; $u = 0.31 \; m/s$; $t_p = 37880 \; s$; $T = 100C$, $C = 7.6 \; ppm$, $\varepsilon = 0.5$, $z = 0.006 \; m$.

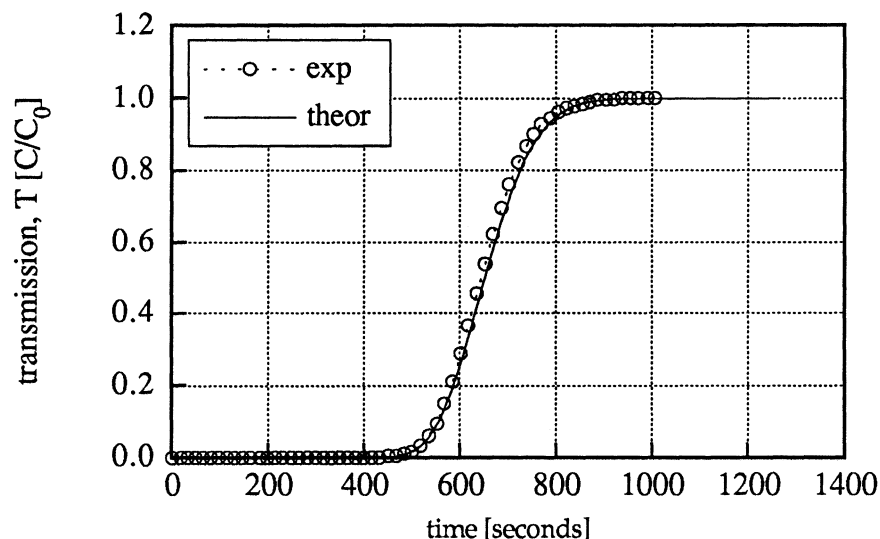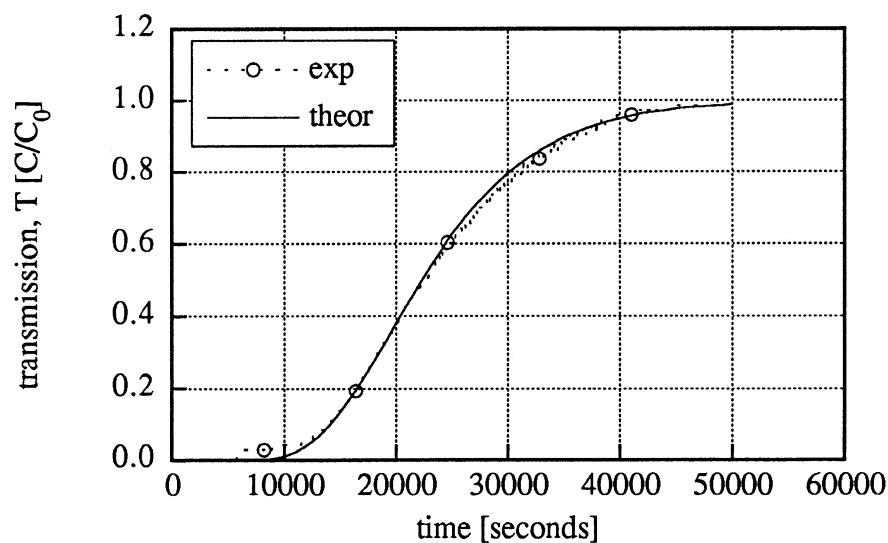**Figure 5.37** Transmission curve modeling using the modified H-S DM.
$D_L = 1.4 \; 10^{-4} \; m^2/s$; $u = 0.35 \; m/s$; $t_p = 23752 \; s$; $T = 140 \; C$, $C = 2.1 \; ppm$, $\varepsilon = 0.5$, $z = 0.006 \; m$.

Similar to the results from the kinetic behavior of propane passing through the activated carbon, D_L also increased with increasing u (Figure 5.38) The effect of temperature on D_L may also be present in the data used to obtain this figure but, as before, both the effects of interstitial flow velocity and temperature are confounded and cannot be separated.

Figure 5.39 shows that no relation exists between D_L and the range of concentrations tested.
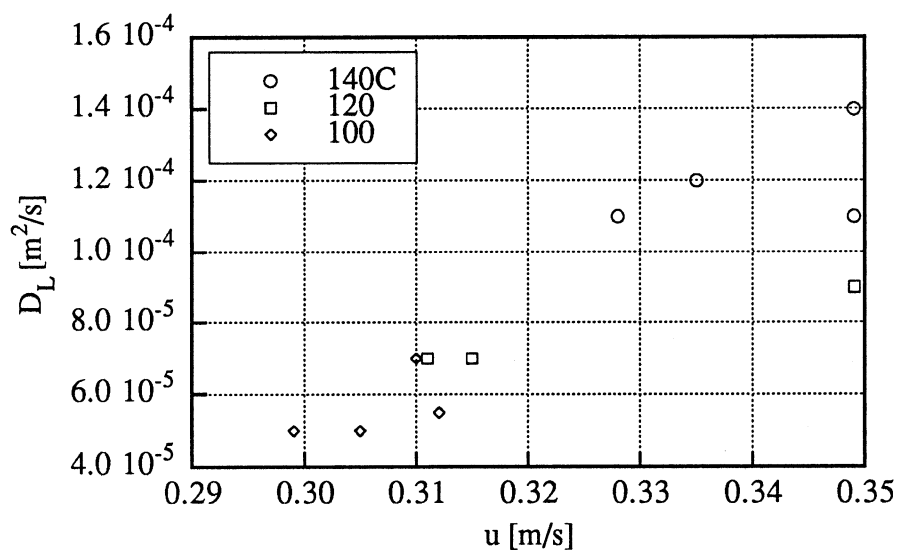
Figure 5.38 D_L vs u for toluene passing through carbon G65 50x150.
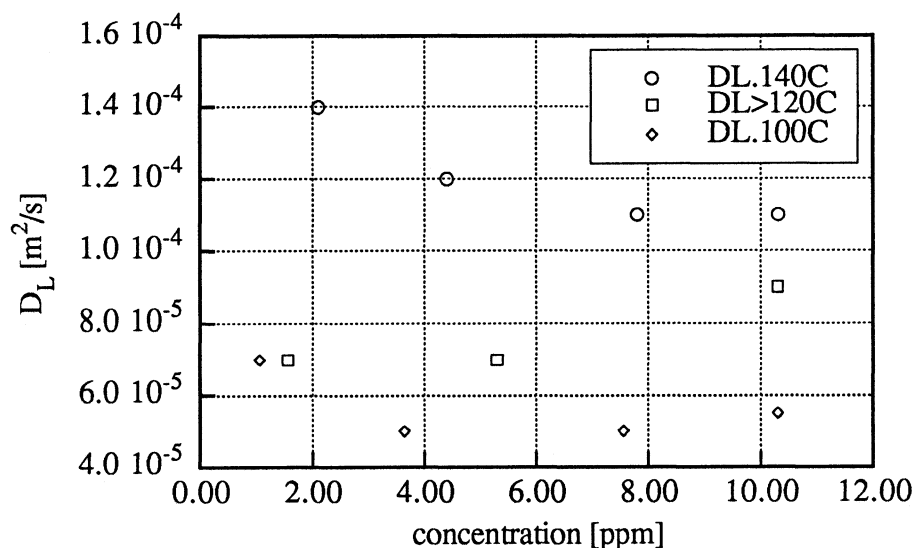
Figure 5.39 D_L vs concentration for toluene passing through carbon G65 50x150.

5.3   SUMMARY

The experimental isotherms obtained by passing propane through carbon G65 50x150 were found to be linear. These isotherms were modeled using the Henry equation and the Dubinin-Astakhov equation. Modeling of the isotherms was possible using the Henry model but poor results were obtained from the D-A model. The isotherms found by passing toluene through carbon G65 50x150 were highly nonlinear. Models used to simulate the experimental isotherms included the Langmuir, Freundlich and Dubinin-Astakhov equations. All modeling yielded results which were within the experimental uncertainty of the data except one point involving the D-A model. The model which yielded results that most closely matched the experimental data was the Freundlich model. Support of the equilibrium results has been obtained from the determination of the heats of adsorption for both propane and toluene, which deviated a maximum of

3% from the values in the literature. A comparison of the heats of adsorption obtained for propane and toluene indicate that the bond strength between the toluene and the activated carbon is significantly greater than the propane-carbon bond because the heat of adsorption for toluene is much greater than that of propane. The greater bond strength (and therefore larger heat of adsorption) is expected for toluene because it is a larger molecule than propane (Chapter 2).

The modified homogeneous-solid diffusion model is able to generate transmission curves which correlate quite well with the experimental transmission curves involving both propane (linear isotherms) and toluene (nonlinear isotherms). It appears that flow rates are great enough to make forced convection around the adsorbent particles and intraparticle diffusion significant, although temperature may also be having some effect on the D_L values. There is no correlation between between D_L and the concentrations of the contaminants.

REFERENCES

Balzhiser, R. E., Samuels, M. R., and Eliassen, J. D., *CHEMICAL ENGINEERING THERMODYNAMICS, The Study of Energy, Entropy, and Equilibrium,* Prentice-Hall Inc., 1972.

Brunauer, S., Deming, L. S., Deming, W. E., and Teller, E. J., J. Am. Chem. Soc. 62, 1723, 1940.

Czepirski, L., and Jagiello, J., *Virial-Type Thermal Eqaution of Gas-Solid Adsorption,* Chem. Eng. Sci. 44(4), 797-801, 1989.

de Boer, J. H., *The Dynamical Character of Adsorption,* Clarendon, Oxford. 1953.

Dubinin, M. M. and Astakhov, V. A., Izv. Akad. Navk. SSSR, Ser Khim. pg.5, 1971a.

Dubinin, M. M., *Physical Adsorption of Gases and Vapors in Micropores,* Progress in Surface and Membrane Science, Academic Press, 1975.

EES Engineering Equation Solver, Copyright 1989 - 1991 by Klein, S. A. and Alvarado, F. L., F-Chart Software, 4406 Fox Bluff Road, Middleton, WI 53562

Famularo, J., Mueller, J. A. and Pannu, A. S., *Prediction of Carbon Column Performance from Pure-Solute Data,* Journal of Water Pollution Control Federation, Vol 52, No. 7, pg 2019 - 2032, 1980.

Forsythe, R. K. Jr. *Adsorption and Dispersion of Selected Organic Gases Flowing Through Activated Carbon Adsorber Beds,* Ph.D. Thesis in Physics, Kent State University, 1988.

Hayward, D.C. and Trapnell, B. M. W., *Chemisorption,* Butterworths, London, 1964.

Madey, R., Huang, J. - C. and Pflumm, E., *Transmission of a Gaseous Radioactive Isotope Through an Adsorber Bed,* American Nuclear Society, **78**, 205 - 210,1981.

Hirschfelder, J. O., Curtiss, C. F., Bird, R. B., *Molecular Theory of Gases and Liquids,* Wiley, New York, 1954.

Kyle, B. G., and Eckhoff, N. D., *Odor Removal from Air by Adsorption on Charcoal,* EPA-650/2-74-084, PB-236-928, Kansas State University, 1974.

Langmuir, I, J. Chem. Soc., **40**, 1361, 1918.

Perry, R. H., Chilton, C. H. and Kirkpatrick, S. D., *Perry's Chemical Engineers Handbook, 4th Edition,* McGraw - Hill Book Company, 1963.

Ruthven, D. M., *Principles of Adsorption & Adsorption Processes*, John Wiley & Sons, Inc., 1984.

Satterfield, C. N., *Mass Transfer in Heterogeneous Catalysis.* MIT Press, Cambridge, Mass., 1970.

Smisek, M. and Cerny, S., *ACTIVE CARBON Manufacture, Properties and Applications ,* Elsevier Publishing Company, Inc., 1970

Suzuki, M., *Adsorption Engineering*, Elsevier Publishing Company, Inc., 1990

Weibull, W., J. Appl. Mech. 18, 293. (1951)

Young, D. M. and Crowell, A. D., *Physical Adsorption of Gases*, Butterworths, London, 1962.

Chapter 6

CONCLUSIONS AND RECOMMENDATIONS

6.1   CONCLUSIONS

Several conclusions can be drawn from the work that has been completed.

1. The experimental procedure used to run tests and analyze the data has relatively little precision error when a single stream of solute is used. This is apparent from the consecutive run tests involving acetone, propane and toluene on the various carbons used in this analysis. These tests (Figure 4.7, 4.9 and 4.11) show only a small amount of fluctuation from test to test, indicating a small amount of precision error is present.

2. The uncertainty analysis done in Chapter 3 has accomplished two things. First, it enables the total error for the quantity adsorbed to be estimated for both the single gas stream case (range of 6 - 8%) and the multiple gas stream case (range 7 - 15%). The analysis also provides the error estimates for the concentration of the contaminant (5 - 11%) and partial pressure (6 - 14%). Second, the analysis showed where the largest sources of error were occurring. The largest bias error is that of the solute (± 5%) and the two largest precision errors are the atmospheric pressure and (2.7%) and the combined multiple gas stream measurements (error

varies). If the total error is to be reduced from current levels, these are the errors which need to be addressed.

3. Precision error increases when two streams of gas (one solute and one carrier) are mixed to obtain a lower concentration than is available directly from the source tank. The larger overall error results from propagation of errors in the individual flow measurements and also the precision error introduced into the concentration of the contaminant as a result of this mixing. The uncertainty analysis done in Chapter 3 shows this in the multiple flow stream case analysis. The results from the increased precision error can be seen in the experimentally determined isotherm data where, at concentrations other than the source, the percent error increases.

4. The current system is unable to fully regenerate the carbon when acetone is the contaminant used in testing and is thought to be a result of either strong physical adsorption or chemisorption. This inability results in the adsorption capacity continually decreasing which means that duplication of the results is not possible. For this reason, isotherm data was not taken with acetone as the contaminant in this study. One way in which isotherm data could be taken using acetone is using one carbon sample for each test.

5. Multiple tests involving a single sample of carbon with toluene or propane experience little, if any, loss in adsorptive capacity. The particular sample used for the toluene isotherm tests lost 3.5% of its original adsorptive capacity over a period of 19 tests. Tests with propane showed virtually no change in adsorptive

capacity. Also, the carbon G65 50x150 sample used to obtain the isotherm data showed approximately no change in adsorptive capacity throughout testing.

6. Duplication of equilibrium data can be done with different samples of a particular carbon involving either toluene or propane. Testing was done with multiple samples of carbon G65 50x150 with both toluene (Figure 4.10) and propane (Figure 4.12). All of the tests were within the established uncertainty.

7. Carbon G65 50x150 has superior adsorptive capacity when compared to the other carbons tested. The low concentration contaminants used for testing included acetone, propane and toluene. No mixing of the different contaminants was done.

8. All of the dynamic equilibrium models (except the D-A model when applied to the propane isotherms) can be used to generate isotherms at temperatures other than those used during testing; however, significant extrapolation outside the temperature ranges tested could lead to large errors.

9. The heats of adsorption for propane and toluene tests with carbon G65 50x150 agree within 3% of those published in the literature. These results support the experimental testing which has been done.

10. The bond strength between the toluene and carbon is stronger than that of the propane-carbon bond (proven by the much larger heat of adsorption for toluene).

11. The modified homogeneous-solid diffusion model was used to successfully characterize transmission curves from both propane and toluene tests. Good agreement is found between the experimental transmission curves and the theoretical curves.

12. The longitudinal diffusion coefficient varies with the interstitial flow velocity and temperature. It is possible D_L is only a function of the flowrate but the data used to obtain values of D_L also varied with temperature and that conclusion cannot be drawn at this time.

13. The interstitial flowrates are large enough to cause forced convection around the adsorbent particles and dispersion in the adsorbent to become significant [Forsythe (1988)]. This conclusion is verified by observing that there is a noticeable increase in D_L as u increases. Forsythe (1988) states that D_L will not change with u when forced convection around a particle and intraparticle diffusion are negligible.

14. The longitudinal diffusion coefficient is independent of concentration. Random results were obtained when D_L was plotted against concentration. It is thought from these results that the concentrations are low enough so as to have no effect on the types of diffusion occurring in the packed bed.

6.2 RECOMMENDATIONS

Recommendations for future work include

1. A pressure transducer installed in the line in which the solute passes through shortly before the packed bed of carbon will enable the determination of the pressure drop across a given a packed bed. The assumption at this time is that the pressure drop is negligible and hence the conclusion that the equilibrium information obtained was done so at atmospheric pressure. Not only will knowledge of the pressure drop across the packed bed prove or disprove this

assumption, it will also enable the calculation of the void fraction ε, which is currently assumed to be 0.5.

2. The uncertainty analysis is currently somewhat conservative when multiple flowrates are used to lower the contaminant to some desired value because the precision errors in the flow measurements are conservative. This error could be reduced by taking sample populations of flow measurements at various flowrates and then determining the 95% confidence interval for the precision flow errors.

3. The transmission curves need to be fit using a program which will do some form of regression to obtain the best fit to the experimental transmission curves. The current method of curve fitting, although acceptable to acquire trends in the data, is inadequate to obtain precise results.

4. Measurements of the diffusion coefficient done at ranges of velocity which are typical for ventilation systems will provide information needed to model actual systems. It is hoped that a correlation between the diffusion and the flowrate could then be obtained. This information, combined with knowledge of the equilibrium capacity of the activated carbon comprising the packed bed, will enable the determination of when the carbon should be either replaced or regenerated.

5. Transmission curve modeling of frontal chromatograms obtained using different molecules will determine if size or other properties of the molecule affect the type of diffusion occurring within a packed bed.

6. Development of a device which will allow greater flows through the packed will enable tests to be done in a shorter period of time. The flow through the FID is limited because too high of a flowrate will blow out the flame. Some type of splitter device may be possible, with part of the sample passing through the FID and the rest passing directly to a hood.

7. Checking the plumbing on a regular basis will help to prevent any leaks in the system.

8. Mixing contaminants would probably yield interesting results concerning how the contaminants behave with one another. If mixing is done, the uncertainty analysis will need to be modified.

9. It is possible that multiple columns could be installed in the gas chromatograph with only one detector present. Accomplishing this task would require a valve located at the end of the columns which would switch from one column to the other during testing. Doing this would enable multiple tests to be run simultaneously.

REFERENCES

Forsythe, R. K. Jr. *Adsorption and Dispersion of Selected Organic Gases Flowing Through Activated Carbon Adsorber Beds,* Ph.D. Thesis in Physics, Kent State University, 1988.

Appendix A

CARBON MESH SIZE CLASSIFICATION

Appendix A gives the classifications of standard mesh sizes along with their corresponding openings in SI and English units. Sizing is done by passing the carbon through various sizes of mesh. Both the Tyler and U.S. mesh sizes are listed.

Table A.1 Activated Carbon Standard Mesh Sizes. From Barneby and Sutcliffe.

Standard Mesh		Opening	
Tyler	U.S.	mm	inches
4	4	4.70	0.185
6	6	3.33	0.131
8	8	2.36	0.094
10	12	1.65	0.065
12	14	1.40	0.056
14	16	1.17	0.047
16	18	0.991	0.039
20	20	0.833	0.033
24	25	0.701	0.028
28	30	0.589	0.023
32	35	0.495	0.020
35	40	0.417	0.016
42	45	0.351	0.014
48	50	0.295	0.012
60	60	0.246	0.0097
80	80	0.175	0.0069
100	100	0.147	0.0058
150	140	0.104	0.0041
200	200	0.074	0.0029
250	230	0.061	0.0024
325	325	0.043	0.0017
400	400	0.038	0.0015

Appendix B

SYSTEM COMPONENTS

The main components of the system are listed and explained in this appendix. Figure B.1 provides a visual reference for each of the components.

Figure B.1   Experimental System. Adapted from Schaefer (1991).

1. compressed air
2. carrier gas
3. nitrogen diluent
4. contaminant-N_2 mix
5. compressed air
6. hydrogen
7. pressure regulator
8. hydrocarbon trap

9. moisture trap
10. chemical trap
11. pressure gauge
12. flow controller
13. on/off valves
14. two-stream selection valve
15. vent to atmosphere

16. glass column and filter
17. flame ionization detector
18. detector exhaust
19. gas chromatograph
20. junction box
21. personal computer
22. electronic integrator

- **Item 1** is a cylinder containing compressed air and is used to operate a pneumatic valve (14).

- **Item 2** is a cylinder containing compressed nitrogen that is used as a carrier gas. Carrier gas is passed through the system when desorbing the activated carbon filter, (located in the oven compartment of the gas chromatograph (19)). The nitrogen carrier gas flows through the activated carbon filter located in the glass column (16) and carries the contaminant that was adsorbed on the carbon out to the atmosphere.

- **Item 3** is a cylinder that also contains compressed nitrogen but in this case the nitrogen is used as a diluent. A diluent is necessary when the contaminant concentration needs to be reduced from what is present at the source (4).

    All tanks of compressed nitrogen have a grade of Ultra High Purity which implies a purity of 99.999% . [Liquid Carbonic Specialty Gas Corporation catalog (1991)].

- **Item 4** is a cylinder which contains a contaminant, (acetone, propane or toluene for this system) with a makeup gas of nitrogen. These cylinders with the various contaminants were purchased from Matheson Gas Products. The mixtures are certified and are defined in the Matheson Gas Products catalog (1990) as being "calibration gas mixtures prepared by a variety of gravimetric, partial pressure and volumetric techniques. Component certification is provided through the use of NBS Standard Reference Materials, Matheson Primary Standards, certified weights, or wet chemical methods." The contaminant concentrations purchased have a ±5.0% bias error as stated in the Matheson Gas Products catalog (1990).

- **Item 5** is a cylinder containing compressed air. This air is used in conjunction with hydrogen (6) to sustain a flame in the flame ionization detector during testing.

- **Item 6** is a cylinder containing compressed hydrogen.

  All cylinders of compressed air, nitrogen, and hydrogen were purchased from Liquid Carbonic Specialty Gas Corporation.

- **Items 7** are the pressure regulators (either Hewlett-Packard or Matheson brand) and are used to set each cylinder outlet pressure to a desired value. These pressures correspond directly to the desired flowrates of the various gases.

- **Items 8** are Hewlett-Packard hydrocarbon traps (part # 5060-9096). They are used to remove any organic compounds that may be present in the compressed nitrogen tanks. Regenerating these filters is recommended by Hewlett-Packard every six months and can be done in the oven compartment of the gas chromatograph (19).

- **Items 9** are LABCLEAR indicating moisture traps (model # RGF 125 200). They are called "indicating" because the clear traps contain pellets that, once a given amount of moisture is present, will change color, hence indicating when replacement of the pellets is necessary. These traps ensure that no moisture or oil enters the system that may be present in the compressed nitrogen tanks and/or connecting lines.

- **Item 10** is a chemical trap purchased from Hewlett-Packard (part # 05890-61260). The trap is installed in the carrier gas line and removes impurities from the nitrogen stream. Because of this filter and the ones previously mentioned, the nitrogen stream is essentially free from impurities and does not contaminate the

activated carbon filter. As was the case with the hydrocarbon traps, the chemical trap can also be reconditioned in the oven compartment of the gas chromatograph (19).

• **Item 11** is a pressure gauge used to monitor the column head pressure of the carrier gas flow line.

• **Items 12** are adjustable flow controllers manufactured by Vici Condyne (model # A202-3(3) 1). These flow controllers have a measuring range of "a few cc/min to over 1000 cc/min", [Alltech Catalog #200, (1989)]. They have stainless steel diaphragms which provide a constant flowrate from the exit of the controller even when small pressure fluctuations occur on the inlet side of the controller. Since the diaphragms are stainless steel, no outgassing of contaminants occurs which is typical with diaphragms manufactured from polymers. The controllers are used to set the nitrogen diluent and the solute-nitrogen flowrates.

• **Items 13** are on/off valves for the air and hydrogen gas that is used to maintain a flame for the flame ionization detector (17). The valves are turned off when the nitrogen diluent and contaminant-nitrogen flowrates are being measured.

• **Item 14** is a two-stream pneumatic selection valve. This valve is used to switch between either the nitrogen carrier gas stream or the contaminant-nitrogen stream. The nitrogen carrier gas is passed through the system when desorbing the activated carbon filter while the solute-nitrogen gas is run through the filter during adsorption testing. Whichever gas stream is not being passed through the system is ejected into the atmosphere, (15) and should be turned off at the source to prevent pollution and also to avoid wasting gas.

Items 10, 11, 13, and 14 are located in the gas chromatograph. They are pictured outside the gas chromatograph in Figure B.1 for clarity purposes only.

- **Item 15** is the gas stream (either solute nitrogen or carrier gas) that is being passed directly to the atmosphere via the two-stream selection valve.

- **Item 16** is the glass column and activated carbon filter. Dimensions of the column are approximately 1/4 inch outside diameter and 1/8 inch inside diameter. The column is located inside the temperature controlled compartment of the gas chromatograph (19) to permit testing at temperatures ranging from 27 - 175 °C. As can be seen in Figure B.1, there are two connections (inlet and exit) for the glass column. The inlet is where the nitrogen or solute-nitrogen gas enters and the exit is the location where gases enter the flame ionization detector (17) and are ejected to the atmosphere. Figure B.2a shows how the glass column is connected to either the inlet or exit fitting. Ferrules are located between the fitting and the 1/4 inch nut to ensure a seal is made at the junction of the two components. The ferrules are made of teflon and are generally used only once because deformation occurs during attachment of the glass column to the fitting. Graphite ferrules were also initially used, but they have the undesirable quality of depositing graphite particles on the glass column upon attachment.

A schematic of the activated carbon filter is shown in Figure B.2b. Filters are made by first using acetone to eliminate contaminants from the inside of the glass

column. Once clean, the column is left to dry for several hours. Next, a glasswool plug is inserted into the column which will provide a relatively flat base for the carbon to be placed. The glasswool (purchased from Hewlett-Packard, part # 5080-8764) used in filter manufacturing has been treated with silane to prevent it from having any adsorptive capacity. With the lower glasswool plug in place, activated carbon is weighed and inserted into the column via a funnel. Care must be taken to avoid losing carbon in this transfer process, although some losses are inevitable due to carbon adhering to the side of the funnel and also to the weighing paper. The final step in constructing the filter is to place a glasswool plug on top of the activated carbon. The upper plug prevents activated carbon from being blown into the flame ionization detector (17) by flowing gases. Filter shape is to be kept as uniform as possible to thwart any channeling effects that might occur and Kyle, et al. (1974) recommend the bed to particle diameter ratio be greater than eight.

- **Item 17** is the flame ionization detector (FID). A schematic of the FID is shown in Figure B.3. The flame ionization detector was selected because of its large range of linearity. Signal response of the FID is typically linear from a minimum readable contaminant concentration to 10^6 or 10^7 the minimum contaminant concentration. Figure B.4 shows detector response in the range of contaminant concentration used during testing.

The FID functions by obtaining ions from burning organic contaminants in the column effluent. Initially, when no organic is present in the effluent, the flame is sustained by a hydrogen and air stream and very little signal is generated because
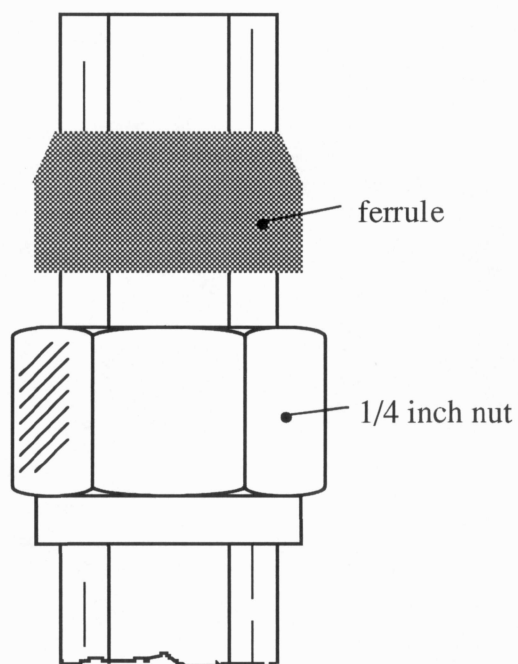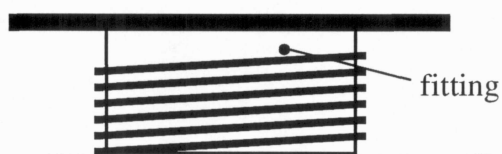
Figure B.2a   Connection of glass

Figure B.2b   Activated carbon filter.

column to fitting.

Adapted from Schaefer (1991).

of lack of ions. When organic compounds are present in the effluent many more ions are released upon combustion and are received in the collector where a polarizing voltage is present. Buffington and Wilson (1991) state that the ions are attracted by this voltage and produce current which is proportional to the amount of organic present in the flame. The current signal is run through a resistor and the

voltage drop across this resistor is measured. An electrometer then amplifies the voltage and sends it to the personal computer (21) where the signal is converted to digital form and logged. An electronic integrator (22) also receives the FID signal and plots the results.

The FID sensitivity is dependent on the flame shape, position of the flame relative to the detection zone, hydrogen and air flowrates and the organic being burned [Buffington and Wilson (1991)]. The flame shape can be adjusted by the jet size. A smaller jet inside diameter generally yields a greater sensitivity than large diameter
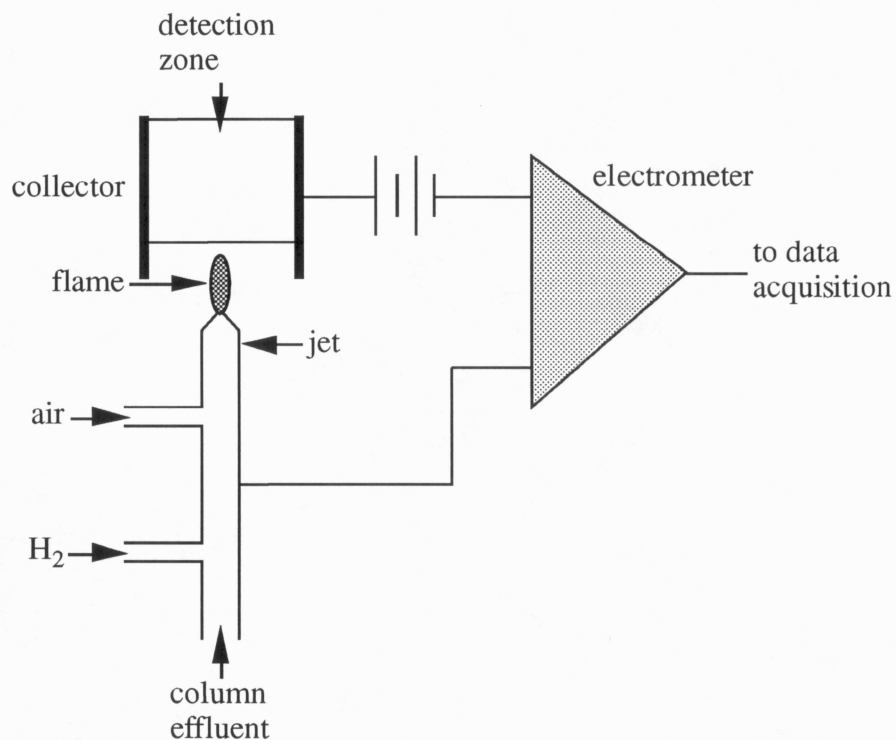
Figure B.3   Schematic of flame ionization detector. Adapted from Buffington and Wilson (1991).

jets, but tend to clog more easily. Given a certain jet inside diameter, FID sensitivity can be maximized by adjusting the hydrogen and air flowrates. The hydrogen flow has been optimized for the FID in this system and was found to be approximately 57 ml/min. See Figure B.5 for graphic results. The air flowrate has less of an effect on the sensitivity than the hydrogen flowrate. However, a minimum flowrate of 300 ml/min is required as shown by McNair and Bonelli (1968). Flame ionization detectors function well with most organic compounds except those that do not burn or ionize. A list of the compounds that give little or no response when processed by a FID is given in Table B.1

Water is formed from the combustion process in the FID. To avoid corrosion and loss of sensitivity, temperatures inside the FID must be greater than 100 °C. FID
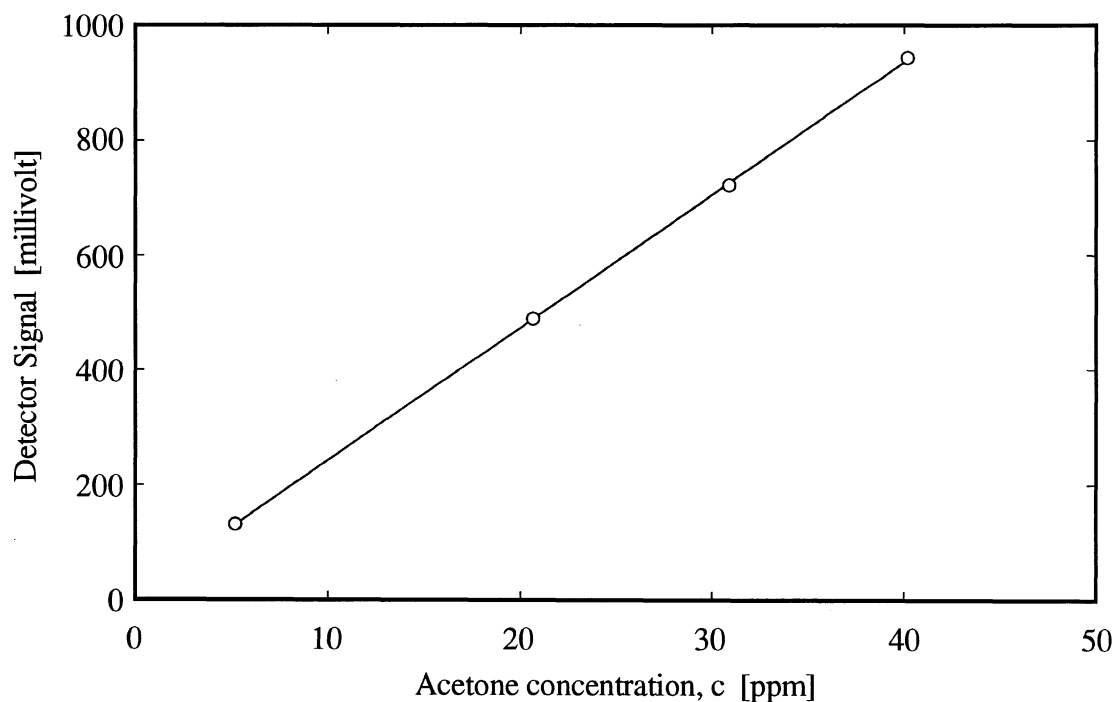
Figure B.4   Flame ionization detector linearity. From Schaefer (1991).

temperature for this system has been set to 200 °C using the keyboard present on the gas chromatograph (19).
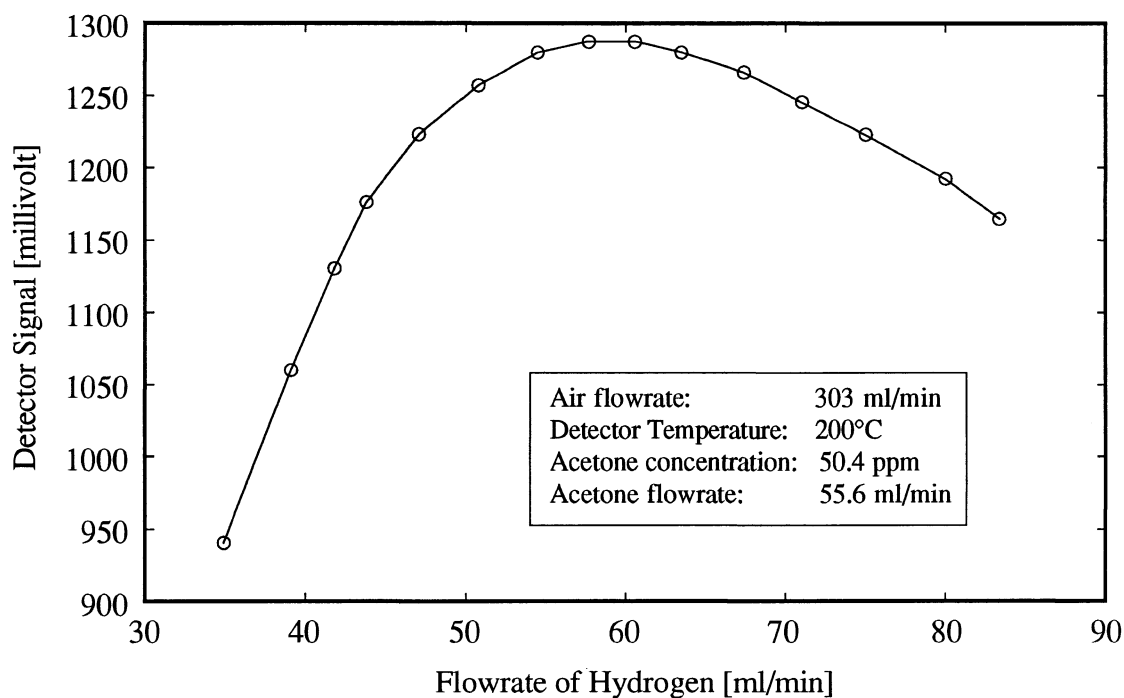
Figure B.5   FID sensitivity optimization. From Schaefer (1991).

Table B.1 Compounds which give little or no response when processed by a FID. Information obtained from Buffington and Wilson (1991).

H_2O	N_2	all inert gases
CO_2	O_2	formaldehyde
CO	CS_2	heavily halogenated compounds

- **Item 18** is the exhaust gas from the flame ionization detector. Once the gas is processed in the FID, it is ejected directly to the atmosphere.

• **Item 19** is a Hewlett-Packard 5890 Series II gas chromatograph. The HP 5890 (seen in detail in Figure B.6) has several features that are necessary for system operation. One of the most important is the oven compartment. This portion of the HP 5890 contains the glass column (16) in which the activated carbon filter is located. The oven permits tests to be run at temperatures ranging from 27 - 175 °C in 1 °C increments. An optional cryogenic coolant attachment can be installed to make it possible for lower temperatures to be reached. The HP 5890 in this system was not fitted with this attachment. The upper level oven temperature is 450 °C, but for this system is limited to 175 °C because of a valve located in the oven compartment. Temperatures above 175 °C could destroy the valve.

One other main feature of the HP 5890 is a keyboard and alphanumeric display panel from which temperature, FID signal, valve position, time and other functions can be set and/or monitored.

The temperature of the oven can either be set manually or can be programmed for a period up to 650 minutes. The HP 5890 reference manual (1990) states that during the desired run time, up to three temperature ramps can be programmed, in any arrangement of heating or cooling.

FID output signal can be monitored via the display panel and can be manipulated using the keyboard. The FID in this system sends an analog signal that varies between 0 and 1 volt. Before testing begins, the FID registers a steady reference signal, which can be eliminated by the ZERO command. The ZERO command subtracts a constant value from the initial signal to set it equal to zero. Since the FID signal does not always have the same initial value, this command is not used.

Instead, the information obtained from testing is zeroed later in the data analysis process. With the FID sensitivity optimized as discussed previously, the magnitude of the FID signal is dependent on the type and concentration of organic compound being burned. Too large a signal can result in information to be truncated because of the one volt maximum stated earlier. To prevent this from happening, the RANGE 2↑ ( ) command is used to attenuate the output. Equation B.1 displays the RANGE 2↑ ( ) command and the effect it has on the FID output signal.

$$1 \text{ volt} = \frac{\text{FID signal}}{2^{\text{RANGE 2↑ ( )}}} \tag{B.1}$$

two stream selection
valve (14)

flame ionization detector (17)

t = 10.7 s   F = 56.1

oven compartment

glass column (16)

packed bed and
glasswool plugs

keyboard and alpha-
numeric display
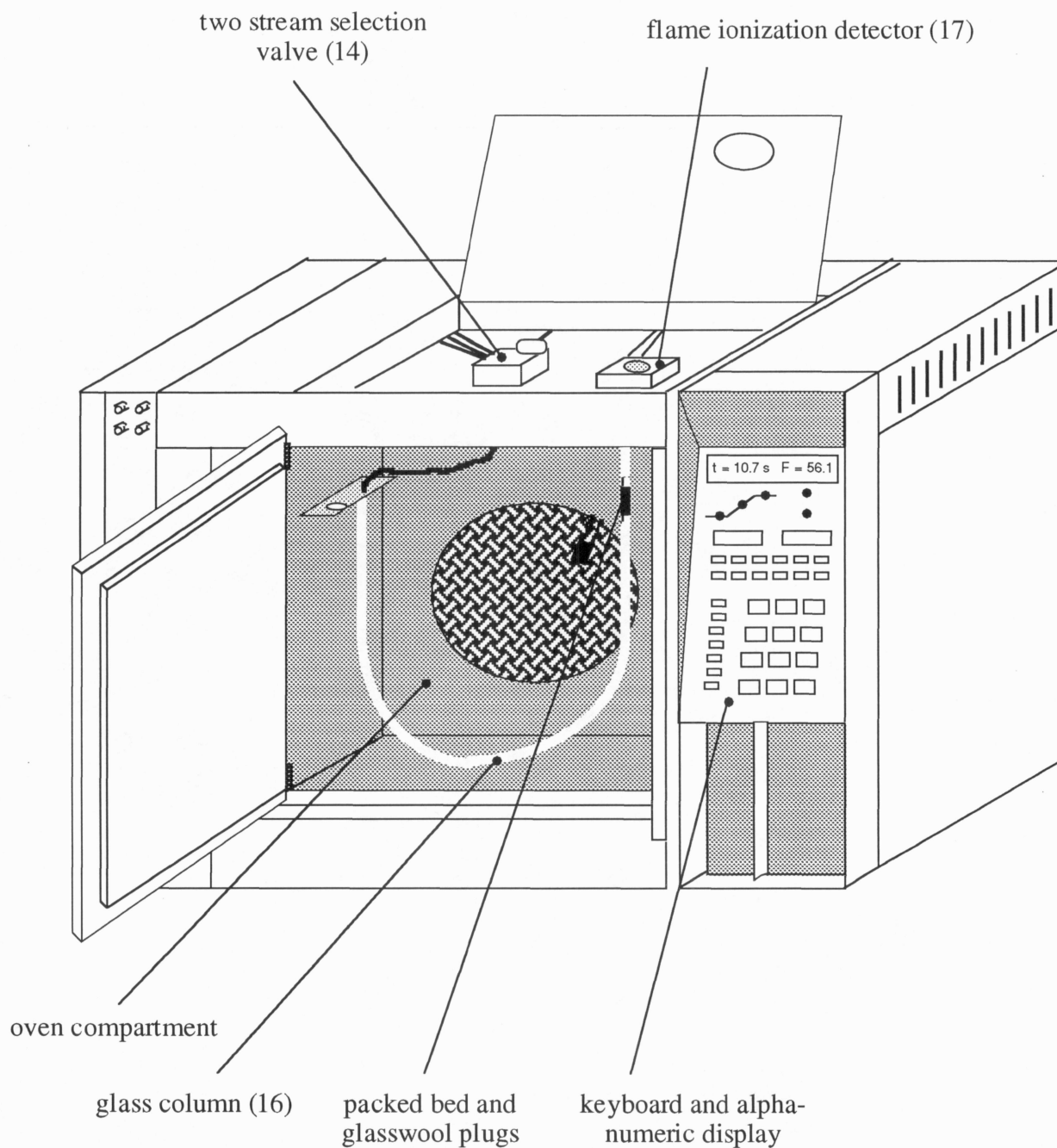
Figure B.6   Schematic of the HP 5890 gas chromatograph. Adapted from Schaefer
(1991).

As an example, consider a signal that registers 1.2 volts. A RANGE 2↑ ( ) command setting of 1 would be required to eliminate truncation of the data with the output result being 0.6 volts.

The pneumatic valve, (14) is set to either ON or OFF using the keyboard. In this system, the valve is used to switch from the nitrogen carrier gas stream to the solute-nitrogen gas stream, depending on the phase of a given test.

The timing feature is used in conjunction with a soap film flowmeter to measure the flowrates of the gas streams (discussed in section 2.2.2).

- **Item 20** is a junction box used to connect the circuit which transmits the FID output voltage signal from the HP 5890 to the personal computer (21).

- **Item 21** is an Apple IIe personal computer and is used to log the information sent from the FID. The Apple IIe contains an analog-to-digital card that converts the FID signal into digital data. The program used to record this data was manufactured by Strawberry Tree Computers. All information is stored on either 5 1/4 floppy disks or on a Sider hard disk (manufactured by First Class Peripherals).

- **Item 22** is a Hewlett-Packard 3396A Integrator. In this system the HP 3396A is used as a plotter to give a visual record of a test while it is in progress and also to have a hard copy for later use.

REFERENCES

Alltech Catalog #200, 1989.

Buffington, R. and Wilson, M. K., *Detectors for Gas Chromatography - A Practical Primer*, Hewlett Packard part number 5958-9433, Printed in U.S.A. 1991.

Hewlett-Packard 5890 Series II Reference Manual, Third Edition, Printed in U.S.A., 1990.

Hewlett Packard 1992 Chromatography Users Catalog, Printed in U.S.A., 1992.

Kyle, B. G. and Eckoff, N. D., *Odor Removal from Air by Adsorption on Charcoal*, EPA-650/2-74-084, PB-236-928, Kansas State University, 1974.

Liquid Carbonic Specialty Gas Corp Catalog, Form 6466 R90, Printed in U.S.A., 1991.

Matheson Gas Products Catalog, Printed in U.S.A., 1990

McNair, H. M. and Bonelli, E. J., *Basic Gas Chromatography*, Printed in U.S.A., 1968.

Schaefer, M., *Measurement of Adsorption Isotherms by Means of Gas Chromatography*, M.S. Thesis in Chemical Engineering, University of Wisconsin-Madison, 1991.

Appendix C

UNCERTAINTY DERIVATION FOR AREA BIAS

This appendix displays the methods used to obtain the final form of Equation 3.28 (shown below). The partial derivatives for each of the terms are derived in a step by step manner.

The uncertainty equation for the area bias error is

$$U_{BA}^2 = \left(\frac{\partial A}{\partial \overline{V}_{max}}U_{BV_{max}}\right)^2 + \left(\frac{\partial A}{\partial V(t)}U_{BV(t)}\right)^2 + \left(\frac{\partial A}{\partial t_{end}}U_{Bt_{end}}\right)^2 \tag{3.28}$$

$$+ \left(\frac{\partial A}{\partial t}U_{Bt}\right)^2 + \left(\frac{\partial A}{\partial C}U_{BC}\right)^2 + 2\left(\frac{\partial A}{\partial \overline{V}_{max}}\right)\left(\frac{\partial A}{\partial V(t)}\right)\rho_{\overline{V}_{max}V(t)}B_{\overline{V}_{max}}B_{V(t)}$$

$$+ 2\left(\frac{\partial A}{\partial t_{end}}\right)\left(\frac{\partial A}{\partial t}\right)\rho_{t_{end}t}B_{t_{end}}B_t$$

The final two terms of Equation 3.28 are present because the voltage values ($\overline{V}_{max}$ and $V(t)$) and the time values (t_{end} and t) are correlated.

The partial derivative of A with respect to $\overline{V}_{max}$ is

$$\frac{\partial A}{\partial \overline{V}_{max}} = + \frac{C}{\overline{V}_{max}^2}\int_0^{t_{end}} V(t)dt \tag{C.1}$$

The partial derivative of A with respect to $V(t)$ is

$$\frac{\partial A}{\partial V(t)} = -\frac{C}{\overline{V}_{max}}\frac{\partial}{\partial V(t)}\left[\int_0^{t_{end}} V(t)dt\right] \tag{C.2}$$

$$= -\frac{C}{\overline{V}_{max}}\int_0^{t_{end}} \frac{\partial}{\partial V(t)}[V(t)dt] \tag{C.3}$$

$$= -\frac{C}{\overline{V}_{max}}\int_0^{t_{end}} dt\frac{\partial V(t)}{\partial V(t)} + V(t)\frac{\partial dt}{\partial V(t)} \tag{C.4}$$

$$= -\frac{C}{\overline{V}_{max}}\int_0^{t_{end}} dt \tag{C.5}$$

$$= -\frac{C}{\overline{V}_{max}}(t_{end} - 0) \tag{C.6}$$

$$= -\frac{C}{\overline{V}_{max}}(t_{end}) \tag{C.7}$$

The partial derivative of A with respect to t_{end} is

$$\frac{\partial A}{\partial t_{end}} = C - 0 \tag{C.8}$$

The partial derivative of A with respect to t is

$$\frac{\partial A}{\partial t} = 0 - \frac{C}{\overline{V}_{max}}\frac{\partial}{\partial t}\left[\int_{t0}^{t_{end}} V(\tau)d\tau\right] \tag{C.9}$$

Manipulation of this equation requires the use of Leibnitz's Rule.

$$= -\frac{C}{\overline{V}_{max}} \left[\int_{t_0}^{t_{end}} \left(\frac{\partial V(t)}{\partial t}\right)(d\tau) + V(t_{end})\frac{dt_{end}}{dt} - V(t_0)\frac{dt_0}{dt} \right]$$

(C.10)

The latter two terms of Equation C.10 are zero because the derivative of time at the end of the tests is zero and the voltage signal at the beginning of the tests is also zero.

$$= -\frac{C}{\overline{V}_{max}} \int_{t_0}^{t_{end}} \left(\frac{\partial V(t)}{\partial t}\right)(d\tau)$$

(C.11)

$$= -\frac{C}{\overline{V}_{max}} V(t_{end}) - V(t_0)$$

(C.12)

Because $V(t_{end}) = \overline{V}_{max}$ the equation simplifies to

$$\frac{\partial A}{\partial t} = -C$$

(C.13)

The partial derivative of A with respect to C is

$$\frac{\partial A}{\partial C} = t_{end} - \frac{1}{\overline{V}_{max}} \int_0^t V(t)dt$$

(C.14)

All of the partial derivatives have now been derived. The final form is Equation 3.29 and is shown below for convenience.

$$U^2_{BA} = \left(\frac{C}{\overline{V}_{max}^2} \int_{t_o}^{t_{end}} V(t)dt \, U_{B\overline{V}_{max}} \right)^2 + \left(\frac{-C}{\overline{V}_{max}} t_{end} U_{BV(t)} \right)^2 \tag{3.29}$$

$$+ \left(CU_{Bt_{end}} \right)^2 + \left(-CU_{Bt} \right)^2 + \left(\left(t_{end} - \frac{1}{\overline{V}_{max}} \int_{t_o}^{t_{end}} V(t)dt \right) U_{BC} \right)^2$$

$$+ 2 \left(\frac{C}{\overline{V}_{max}^2} \int_{t_o}^{t_{end}} V(t)dt \right) \left(\frac{-C \, t_{end}}{\overline{V}_{max}} \right) U_{B\overline{V}_{max}} U_{BV(t)} + 2(C)(-C)U_{Bt_{end}} U_{Bt}$$

Appendix D

TECHNICAL DATA FOR ACTIVATED CARBON

Appendix D contains the technical data sheets for the carbons used in this analysis. The information was obtained from NUCON International, Inc. and Calgon Carbon Corporation.

NUSORB® GC60-12X30 TECHNICAL DATA SHEET

RAW MATERIAL: Coal
ACTIVATION METHOD: High Temperature Steam
PARTICLE TYPE: Granule
PHYSICAL PROPERTIES:

APPARENT DENSITY (g/ml)(ASTM D2854)	0.45 Typical
SURFACE AREA (m^2/g)(BET)	1000 Typical
HARDNESS (ASTM D3802)	95 Typical
ASH (% by Wt.)(ASTM D2866)	12 Typical
PARTICLE SIZE US SIEVE (ASTM D2862)	on 12 - 3% max. on 30 - 90-100% Thru 30 - 7% max.
PORE VOLUME (ml/g)	0.9 Total

CHEMICAL PROPERTIES

CARBON TETRACHLORIDE ACTIVITY (% by Wt.) (ASTM D3467)	60 Typical
IODINE NUMBER	950 Typical

Information herein is accurate to the best of our knowledge. User should determine the suitability of the product for the intended use; liability consists of replacing product. NUCON International, Inc., does not suggest violation of any existing patents or give permission to practice any patented invention without a license.

IMPORTANT SAFETY INFORMATION

CAUTION: OXYGEN IS REMOVED FROM AIR BY WET ACTIVATED CARBON.

Oxygen may be rapidly reduced to a hazardous level in closed or partially closed tanks, receptacles or other enclosed spaces containing carbon. When entering any enclosed space regardless of its contents, follow recommended safety procedures (See MCA Safety Guide SG-10, "Recommended Safe Practices and Procedures, Entering Tanks and Other Enclosed Spaces", Mfgr. Chem. Assoc., 1825 Connecticut Ave., N.W., Washington, D.C., 20009).

NUSORB® LN100-325X ACTIVATED POWDERED CARBON
TECHNICAL DATA SHEET

RAW MATERIAL: Wood

PHYSICAL PROPERTIES: 1.0% Max. on 100 Mesh
      20.0% Max. on 100X325 Mesh
      75.0% Min. Thru 325 Mesh

PARTICLE SIZE US SIEVE (ASTM D2854)   0.35 - 0.40 g/ml

SURFACE AREA (BET)   1350 m^2/g Min.

AVERAGE PARTICLE SIZE (FISHER)   1.5 Micron

ASH (ASTM D2866)   4.0% Wt. Max.

IODINE NUMBER (EPA)   980 mg/g Min.

MOISTURE CONTENT (ASTM D2867)   6.0% Wt. Max.

CHEMICAL PROPERTIES:

CARBON TETRACHLORIDE ACTIVITY (% by Wt.)   100.0% Wt. Min.
 (ASTM D3467)

pH (ASTM D3838)   8.0 Typical

Information herein is accurate to the best of our knowledge. User should determine the suitability of the product for the intended use; liability consists of replacing product. NUCON International, Inc., does not suggest violation of any existing patents or give permission to practice any patented invention without a license.

IMPORTANT SAFETY INFORMATION

CAUTION: OXYGEN IS REMOVED FROM AIR BY WET ACTIVATED CARBON.

Oxygen may be rapidly reduced to a hazardous level in closed or partially closed tanks, receptacles or other enclosed spaces containing carbon. When entering any enclosed space regardless of its contents, follow recommended safety procedures (See MCA Safety Guide SG-10, "Recommended Safe Practices and Procedures, Entering Tanks and Other Enclosed Spaces", Mfgr. Chem. Assoc., 1825 Connecticut Ave., N.W., Washington, D.C., 20009).

NUSORB® G65-50X150 TECHNICAL DATA SHEET

RAW MATERIAL: Coconut Shell
ACTIVATION METHOD: High Temperature Steam
PARTICLE TYPE: Fine Granular

PHYSICAL PROPERTIES:

PARTICLE SIZE US SIEVE (ASTM D2862)	10% Maximum Retention on 50 mesh 90-100% 150 mesh 0-10% thru 150 mesh
APPARENT DENSITY (ASTM D2854)	0.43 - 0.47 g/ml
ASH CONTENT (ASTM D2867)	as packed 5.0% Maximum
SURFACE AREA	1000 m^2/g Minimum

CHEMICAL PROPERTIES

CARBON TETRACHLORIDE ACTIVITY (ASTM D3467)	65% Minimum
pH (ASTM D3838)	8.5 - 9.5
Iodine Number	1100

Information herein is accurate to the best of our knowledge. User should determine the suitability of the product for the intended use; liability consists of replacing product. NUCON International, Inc., does not suggest violation of any existing patents or give permission to practice any patented invention without a license.

IMPORTANT SAFETY INFORMATION

CAUTION: OXYGEN IS REMOVED FROM AIR BY WET ACTIVATED CARBON.

Oxygen may be rapidly reduced to a hazardous level in closed or partially closed tanks, receptacles or other enclosed spaces containing carbon. When entering any enclosed space regardless of its contents, follow recommended safety procedures (See MCA Safety Guide SG-10, "Recommended Safe Practices and Procedures, Entering Tanks and Other Enclosed Spaces", Mfgr. Chem. Assoc., 1825 Connecticut Ave., N.W., Washington, D.C., 20009).

CALGON CARBON: TYPE OL GRANULAR CARBON

Calgon Carbon Type OL is a granular carbon designed for efficient use in fixed beds for the purification and decolorization of many aqueous and organic liquids. Its particle size of 20 x 50 mesh has been selected to give maximum adsorption rates and reasonable pressure drop characteristics with liquors of relatively low viscosity. These properties often permit higher flow rates and shorter columns than those required for coarser mesh carbons.

Type OL Carbon is made from selected grades of bituminous coal combined with suitable hardness and long life. Produced under rigidly controlled conditions by high temperature steam activation, this carbon provides high surface area, large pore volume and high density. Its pore structure has been carefully designed for the adsorption of both high and low molecular weight impurities from solutions.

PHYSICAL PROPERTIES

Total Surface Area
  (N2, BET Method*), m^2/g   1000-1100
Apparent Density (Bulk Density,
  dense packing), g/cc   0.48
                    lb/ft   330.0
Particle Density (Hg Displacement), g/cc   0.75
Real Density (Hg Displacement), g/cc   2.2
Pore Volume (Within Particle), cc/g 0.88
Voids in Dense Packed Column, %   40
Specific Heat at 100°C   0.25
*Brunaur, Emmett and Teller, J. Am. Chem. Soc. 309 (1936)

SPECIFICATIONS

Mesh Size, U.S. Sieve Series 20 x 50

      Larger than 20 mesh, Maximum, % 3

      Smaller than 50 mesh, Maximum, % 1

Iodine Number, Minimum 1050

Molasses Number, Minimum 200

Ash, Maximum, %

Moisture as packed, Maximum, %

Abrasion Number, Minimum 70

Appendix E

ISOTHERM DATA FOR PROPANE ON CARBON G65 50x150

Included in this appendix is a colplete list of the equilbrium amounts adsorbed and their corrosponding concentrations. Also included is the uncertainty for each of these values. Note: partial pressure can be calculated by multiplying the concentration by atmospheric pressure (98508 Pa).

Table E.1 Isotherm data for propane on carbon G65 50x150.

	conc [ppm]	% uncrty	q [mg/g]	% uncrty
35°C	43.9	5.0	2.55	6.9
	31.8	5.8	1.50	7.5
	20.9	6.3	1.07	10.2
	11.1	9.0	0.61	10.3
	6.3	10.5	0.36	11.6
	2.7	11.7	0.16	12.8
60°C	43.9	5.0	0.64	6.9
	32.2	5.6	0.47	7.3
	21.5	5.8	0.33	7.4
	11.1	7.6	0.17	9.0
	7.7	9.6	0.12	10.7
	2.9	7.1	0.05	8.6
80°C	43.9	5.0	0.26	6.9
	26.5	5.6	0.17	7.3
	236	5.8	0.15	7.5
	14.1	6.7	0.090	8.3
	7.7	9.9	0.053	11.1
	1.8	10.3	0.011	11.6

Table E.1 (continued) Isotherm data for propane on carbon G65 50x150.

	conc [ppm]	% uncrty	q [mg/g]	% uncrty
100°C_a	43.9	5.0	0.12	6.9
	32.1	5.6	0.088	7.4
	21.0	5.8	0.063	7.5
	15.0	6.6	0.042	8.2
	8.2	9.5	0.024	10.7
	4.2	10.8	0.012	11.8
100°C_b	43.9	5.0	0.12	6.9
	33.8	6.0	0.092	7.3
	22.9	5.9	0.062	7.6
	11.3	7.5	0.032	8.9
	6.6	9.0	0.018	10.2
	3.1	9.1	0.0085	10.3

Appendix F

ISOTHERM DATA FOR TOLUENE ON CARBON G65 50x150

Included in this appendix is a complete list of the equilbrium amounts adsorbed and their corrosponding concentrations. Also included is the uncertainty for each of these values. Note: partial pressure can be calculated by multiplying the concentration by atmospheric pressure (98508 Pa).

Table F.1 Isotherm data for toluene on carbon G65 50x150.

	conc. [ppm]	% uncrty	q [mg/g]	% uncrty
100°C	10.31	5.0	41.3	7.0
	7.56	5.5	35.4	7.5
	5.73	5.7	31.3	7.7
	3.64	6.6	25.7	8.3
	1.06	10.3	12.5	11.7
120°C	10.31	5.0	25.4	7.0
	7.26	5.5	20.8	7.5
	5.30	6.0	18.2	7.8
	1.56	10.8	9.8	12.1
140°C	10.31	5.0	14.7	7.0
	7.8	5.5	12.9	7.5
	4.4	6.2	9.3	8.0
	2.1	8.4	6.4	10.1